Horizontal and Vertical Eye Movements in Gaze Tracking Tasks

A novel tool to classify neurodegeneration

V.P.A. de Jonckheere

Technische Universiteit Delft

TU Delft

Horizontal and Vertical Eye Movements in Gaze Tracking Tasks

A novel tool to classify neurodegeneration

by

V.P.A. de Jonckheere

to obtain the degree of Master of Science at the Delft University of Technology.

Student number:	4135482	
Project duration:	September 1, 2018 – December 9, 2019	
Thesis committee:	prof. dr. ir. M. Mulder,	TU Delft
	dr. ir. D. M. Pool,	TU Delft, supervisor
	dr. ir. J. J. M. Pel,	Erasmus MC, supervisor
	dr. O. A. Sharpanskykh	TU Delft, examiner

An electronic version of this thesis is available at http://repository.tudelft.nl/.

TU Delft

Preface

The start of the last chapters before completing the Aerospace Engineering master at the TU Delft. A long journey at the TU Delft almost coming to an end. I would like to thank Johan Pel and Daan Pool for their guidance during these last steps, I could not have achieved this without their support. I really enjoyed my time at the Erasmus MC as well, where I have met some lovely new people. I am really looking forward to collaborate on the development on the contact lens. Lastly, I want to express my gratitude towards my family for their unconditional love and support, and in special to my mother, who will always be in our hearts.

V.P.A. de Jonckheere
Delft, November 2019

Contents

List of Figures 1

List of Tables 4

List of Abbreviations 5

List of Symbols 7

1 Introduction 9

Part I: Paper 11

Part II: Preliminary report 29

2 Introduction 31

3 Eye movements 33
3.1 Why study eye movements? . . . 33
3.2 Extra-ocular eye muscles . . . 34
3.3 Classification of eye movements . . . 36
3.3.1 Gaze stabilizing eye movements . . . 36
3.3.2 Gaze shifting eye movements . . . 37
3.3.3 Voluntary eye movements . . . 37
3.3.4 Relevant eye movements . . . 38
3.4 From stimulus to eye movement . . . 38
3.4.1 Visual pathways . . . 38
3.4.2 Neuronal activity . . . 39
3.4.3 Saccades . . . 39
3.4.4 Smooth pursuit . . . 40
3.5 Eye movement analysis . . . 42
3.5.1 Stimulus . . . 42
3.5.2 The visual field . . . 44
3.5.3 Visual processing issues . . . 45
3.5.4 Eye trackers . . . 46
3.5.5 Eye tracking devices . . . 47
3.6 Conclusion . . . 48

4 Frequency domain analysis: The cybernetic approach 49
4.1 The human controller . . . 50
4.1.1 Successive Organization of Perception . . . 50
4.2 Tracking task: display design . . . 51
4.3 System identification . . . 52
4.4 Input signal: the forcing function . . . 52
4.5 Parameter estimation . . . 53

4.6 Gaze analysis . . . 54
4.6.1 Oculomotor models . . . 54
4.6.2 Dual-axis analysis . . . 55
4.7 Conclusion . . . 56

5 Time domain analysis: Pattern recognition 57
5.1 Principles . . . 57
5.2 Pattern recognition in gaze data . . . 58
5.2.1 Sensor . . . 58
5.2.2 Feature generation & selection . . . 58
5.2.3 Classifier design . . . 59
5.2.4 System evaluation . . . 59
5.3 Learning . . . 61
5.4 Conclusion . . . 61

6 Research experiments 63
6.1 Main experiment . . . 63
6.1.1 Task description . . . 63
6.1.2 Apparatus . . . 64
6.1.3 Subjects . . . 64
6.1.4 Experiment procedures . . . 65
6.1.5 Input signal . . . 66
6.1.6 Hypotheses . . . 67
6.2 Verification experiment . . . 69
6.2.1 Task description & apparatus . . . 69
6.2.2 Input signal . . . 69
6.2.3 Hypotheses . . . 69
6.3 Conclusion . . . 70

7 Conclusions 71

Part III: Paper appendices 73

A Briefing 75

B Informed consent form 79

C Binocular EyeSeeCam validation 81
C.1 Introduction . . . 81
C.2 Methods . . . 81
C.3 Results . . . 81
C.4 Conclusions . . . 81

D Torsional eye movements 83
D.1 Introduction . . . 83
D.2 Methods . . . 83
D.3 Results . . . 83
D.4 Conclusion . . . 83

E Right gaze 85

F Saccades 89

G Model parameters 97

H Bode plots 99

I Error compositions **111**

Bibliography **117**

List of Figures

2.1 The CNS consists of the brain and the spinal chord (Kandel et al. 2000). 32

3.1 Six extra-ocular eye muscles are divided in three antagonistic pairs, shown here in a cutaway view of the (left) eye in its socket, or orbit (Squire et al. 2008). 34
3.2 Schematic view of the locations of the oculomotor, trochlear and abducens nuclei (Remington 2012). 35
3.3 The eye with a detailed view of the region around the fovea. Light passes trough the cornea and optic disc to reach the fovea, where it proceeds through different nerve cells, after which is its processed by photoreceptor cells (Kandel et al. 2000). 36
3.4 Schematic overview of neuronal activity for saccadic eye movements. On the left, the fire rates of the tonic neurons (TN), burst neurons (BN) and omnipause neurons (OPN) together form an oculomotor neuronal (OMN) command. The long-lead burst neurons (LLBN) 'announce' a saccadic burst. On the right, the resulting eye position and velocity profiles are shown as a result from the OMN activity. 40
3.5 Schematic overview of important structures for generating saccadic eye movements after a local stimulus on the retina. Neuronal commands from the PPRF (paramedian pontine reticular formation), riMLF (rostral insterstitial nucleus of the medial longitudinal fasciculus) and RIP (nucleus raphe interpositus) form a oculomotor command for the CN (cranial nerves) to stimulate eye muscles. Constructed by combining work from Munoz & Fecteau (2002), Munoz (2002), Enderle (2002) and Harting & Updyke (2006). 41
3.6 Schematic and simplified outline of smooth pursuit and saccadic pathways in the monkey brain. Indicated are the CN (caudate nucleus), FEF (frontal eye field), LIP (lateral intraparietal area) MT (middle temporal area), MST (medial superior temporal area), PMN (brain stem premotor nuclei), PON, (precerebellar pontine nuclei), SC (superior colliculus), SEF (supplementary eye field), SNr (substantia nigra pars reticulate), Verm (oculomotor vermis), VN (verstibular nuclei) and VPF (ventral paraflocculus) (Krauzlis 2005). 42
3.7 Schematic overview of important structures for generating smooth pursuit eye movements. Constructed from work from Fukushima et al. (2013) 43
3.8 Distribution of rods and cones on the retina (Purves et al. 2004). 44
3.9 Spectral sensitivity of the three receptor primary systems: blue (B), green (G) and red (R) (Vos 1979). 44
3.10 The parallax effect (1&1 IONOS Products 2017). 45
3.11 EOG for vertical eye movements (Mind Media 2019). 47
3.12 Scleral search coil (Chronos Vision 2017). 47
3.13 VOG: EyeSeeCam Sci eye tracker device. 47
3.14 The corneal reflections produced by different eye-head positions. The corneal reflection appears as a bright white dot, just to the right of the pupil (A). The relative positions of the pupil and the corneal reflection change when the eye rotates around its vertical (B) and horizontal (C) axes. This relationship does not change, however, when the head moves and the eye is stable (D) (Richardson & Spivey 2008). 47
3.15 The Tobii Pro X3 (left) in use (right), Tobii AB (2019). 48

4.1 Design variables affecting the tracking task (McRuer & Jex 1967). 49
4.2 Systematic representation of the human controller in a compensatory control task. . . . 50

4.3 Systematic representation of the human controller in a pursuit tracking task. 51
4.4 Systematic representation of the human controller in a gaze pursuit task. 54
4.5 Example Bode plot of FRF (red asterisks) and fitted pilot model (blue line), obtained from Büskens (2018). 55
4.7 Control signal variance composition Barendswaard et al. (2016). 55
4.8 Example PSD for dual-axis task Barendswaard et al. (2016). 55
4.6 Gaze parameters as obtained by Büskens (2018) for an eye-hand (EH) and eye-only (EO) tracking task for different input signal bandwidths (‘2’ or ‘3’), for old (O) and young (Y) adults. 56

5.1 The basic stages of a pattern recognition classification system (Theodoridis & Koutroumbas 2006). 58
5.2 Saccade detection based on gaze acceleration (Büskens et al. 2019). 59
5.3 Boxplot with gaze performance scores for each trial of each condition from gaze records by Büskens (2018). EO is an eye only tracking task, EH is a eye-hand tracking task, 2 denotes the lower bandwidth, 3 denotes the higher bandwidth. 62
5.4 Running average performance (red plots, left vertical axis) for the first four trials of the practise phase with the target signal value (black plot, right vertical axis). 62

6.1 Snapshot of experiment display during a trial. 64
6.2 Snapshot of EyeSeeCam software of binocular tracking. 65
6.3 Experiment procedure, blocks highlighted in blue contain sub procedures. 65
6.4 Time series of the horizontal component of one trial. 67
6.5 Verification experiment procedure, blocks highlighted in blue contain sub procedures. . 69

C.1 Example time delay including both monocular and binocular recorded gaze. L-M, L-B and R-B correspond to left monocular, left binocular and right binocular gaze, respectively. 82

D.1 Example of torsional eye movements of Subject 1, raw signal. 84
D.2 Example power spectra for both subjects in both conditions. 84
D.3 Examples cumulative performance at each frequency for both subjects in both conditions. 84

E.1 Performance (right gaze) per trial per condition; short breaks are indicated with light gray dashed lines, longer breaks are indicated with black dashed lines. 85
E.2 VAF scores of different estimated gaze models ($H_{g_{H,V}}(s)$) for each condition for the right eye. 86
E.3 Relative remnant of right gaze in all conditions. 87

F.1 Number of saccades per second r_{sac} per trial for the left eye. 89
F.2 Subject 1 90
F.3 Subject 2 90
F.4 Subject 3 90
F.5 Subject 4 90
F.6 Subject 5 91
F.7 Subject 7 91
F.8 Subject 8 91
F.9 Subject 9 91
F.10 Subject 10 92
F.11 Subject 11 92
F.12 Subject 12 92
F.13 Subject 13 92
F.14 Subject 14 93
F.15 Subject 16 93
F.16 Subject 17 93
F.17 Subject 18 93
F.18 Subject 19 94
F.19 Subject 20 94

F.20 Subject 21 . . . 94
F.21 Subject 22 . . . 94
F.22 Subject 23 . . . 95
F.23 Subject 24 . . . 95

G.1 Fitted gaze parameter for different horizontal gaze models in the 1D-H condition, for the right eye. . . . 97
G.2 Fitted gaze parameter for different vertical gaze models in the 1D-V condition, for both left and right eye. . . . 97
G.3 Fitted gaze parameters for horizontal and vertical gaze models for the 2D condition, for both left and right eye. . . . 98

H.1 Subject 1 . . . 99
H.2 Subject 2 . . . 100
H.3 Subject 3 . . . 100
H.4 Subject 4 . . . 101
H.5 Subject 5 . . . 101
H.6 Subject 7 . . . 102
H.7 Subject 8 . . . 102
H.8 Subject 9 . . . 103
H.9 Subject 10 . . . 103
H.10 Subject 11 . . . 104
H.11 Subject 12 . . . 104
H.12 Subject 13 . . . 105
H.13 Subject 14 . . . 105
H.14 Subject 16 . . . 106
H.15 Subject 17 . . . 106
H.16 Subject 18 . . . 107
H.17 Subject 19 . . . 107
H.18 Subject 20 . . . 108
H.19 Subject 21 . . . 108
H.20 Subject 22 . . . 109
H.21 Subject 23 . . . 109
H.22 Subject 24 . . . 110

I.1 Subject 1 . . . 111
I.2 Subject 2 . . . 111
I.3 Subject 3 . . . 112
I.4 Subject 4 . . . 112
I.5 Subject 5 . . . 112
I.6 Subject 7 . . . 112
I.7 Subject 8 . . . 113
I.8 Subject 9 . . . 113
I.9 Subject 10 . . . 113
I.10 Subject 11 . . . 113
I.11 Subject 12 . . . 114
I.12 Subject 13 . . . 114
I.13 Subject 14 . . . 114
I.14 Subject 16 . . . 114
I.15 Subject 17 . . . 115
I.16 Subject 18 . . . 115
I.17 Subject 19 . . . 115
I.18 Subject 20 . . . 115
I.19 Subject 21 . . . 116
I.20 Subject 22 . . . 116
I.21 Subject 23 . . . 116
I.22 Subject 24 . . . 116

List of Tables

5.1 Monocular EyeSeeCam output variables of left eye, and their availability. 60

6.1 Latin square diagram. H = horizontal condition, V = vertical condition 66
6.2 Input signal parameters. 67
6.3 Forcing function sign conventions for different trials per condition. 68

E.1 ω_g statistics ($\mu \pm \sigma$ rad/s , N = 21) for the M4-models in every condition, for the right eye. For the 2D condition, the horizontal (2D(-H)) and vertical (2D(-V)) directions are separated. 87

F.1 Saccade pattern inclination ($\mu + \sigma$) $\alpha = \text{atan}(\frac{y_{sac}}{x_{sac}})$ in degrees. 95

List of Abbreviations

2	Lower bandwidth condition
3	Higher bandwidth condition
2D	Two-dimensional condition
B	Blue
BN	Medium-lead burst neurons
CF	Crest factor
CN	Cranial nerve
CN	Caudate Nucleus
CNS	Central nervous system
CVS	Computer Vision Syndrome
D	Dual axis task
DLPN	Dorsolateral Pontine Nuclei
EBN	Excitatory burst neurons
EH	Eye-hand condition
EO	Eye-only condition
EOG	Elektro-oculography
FEF	Frontal Eye Field
FRF	Frequency response function
G	Green
H	Horizontal condition
HC	Human controller
IBN	Inhibitory burst neurons
IMU	Inertial measurement unit
INoC	Interstitial Nucleus of Cajal
LASIK	Laser-assisted in situ keratomileusis
LGN	Lateral Geniculate Nucleus
LIP	Lateral Intraparietal Cortex
LLBN	Long-lead burst neurons
LSTM	Long short-term memory
LTI	Linear, time-invariant
MST	Medial superior temporal area
MT	Middle temporal area
NPH	Nucleus Prepositus Hyperglossi
NRTP	Nucleus Reticularis Tegmenti Pontis
O	Older age group

OKR	Optokinetic reflex
OMN	Oculomotor neurons
ON	Omnipause neurons
POG	Photo-oculography
PMN	Brain stem Premotor Nuclei
PON	Precerebellar Pontine Nuclei
PSD	Power spectral density
PPRF	Paramedian Pontine Reticular Formation
R	Red
riMLF	Rostral interstitial nucleus of the Medial Longitudinal Fasciculus
RIP	Nucleus Raphe Interpositus
S	Single axis task
SC	Superior Colliculus
SEF	Supplemental eye field
SNr	Substantia Nigra Pars Reticulate]
SOP	Successive Organization of Perception
SP	Smooth pursuit
TN	Tonic neurons
V	Vertical condition
VN	Vestibular Nuclei
VOG	Video-oculography
VOR	Vestibulo-ocular reflex
VPF	Ventral Paraflocculus
Vx	Visual area x
Y	Younger age group

List of Symbols

Roman

A_t, A_x, A_y	Input signal amplitude	pixels
d_{pup}	Pupil diameter	pixels
e	Error signal	
f_t, f_x, f_y, F_t	Input signal	pixels
H_A	Filter dynamics	
H_p	Pilot dynamics	
$\hat{H}_p$	Approximated pilot dynamics	
H_g	Gaze dynamics	
H_c	Controlled element dynamics	
i	Input signal	
j	Imaginary number	-
J	Cost function value	-
k	Sinusoid index	-
K_g	Gaze gain	-
K_p	Pilot gain	-
n, n_x, n_y	Input signal prime numbers	-
n, N	Remnant signal	pixels
N_t	Number of sinusoids	-
s	Laplace complex variable	rad/s
t	Time	s
T_m	Measurement time	s
T_{A_1}, T_{A_2}	Filter time constant	s
u, U	Human output signal	
y	System output signal	

Greek

ζ_g	Gaze system damping ratio	-
ζ_{nm}	Neuromuscular system damping ratio	-
θ	Parameter vector	
σ_e^2	Error signal variance (performance)	
$\sigma_{f_t}^2$	Input signal variance	pixels

σ_u^2	Control signal variance (activity)	
$\sigma_{xx}^2, \sigma_{xy}^2, \sigma_{yy}^2$	Pupil diameter (co)variances	pixels
τ	Time delay	s
τ_c	Crossover time delay	s
τ_g	Gaze time delay	s
ϕ_t, ϕ_x, ϕ_y	Input signal phases	rad
ξ	Excited frequencies	rad/s
$\omega, \omega_x, \omega_y$	Frequency	rad/s
ω_0	Base frequency	rad/s
ω_c	Crossover frequency	rad/s
ω_{nm}	Natural frequency of the gaze system	rad/s
ω_{nm}	Natural frequency of the neuromuscular system	rad/s
ω_t	Input signal frequencies	rad/s

1

Introduction

This research is concerned with horizontal and vertical eye movements in gaze tracking tasks, to obtain the degree of Master of Science at the Delft University of Technology, at the faculty of Aerospace Engineering. At the department of Control & Simulation of this faculty, research is conducted on the interaction of man-machine systems, by analyzing mathematical models describing human control behavior, using a cybernetic approach. These mathematical models of humans can also be applied to other domains than aerospace engineering, such as the automotive or healthcare industry. This research will focus on the latter, and contributes to developing new tools to be used in a clinical setting. This research will focus on a tool to investigate neurodegeneration in humans.

The origin of neurodegeneration is unknown, and its classification is covered by neurodegenerative disorders, such as Alzheimer's disease, Parkinson's disease or amyotropic lateral sclerosis (ALS) (Przedborski et al. 2003). Neurodegenerative disease progress silently before symptoms are noticed, which are mostly used to classify its type (Castillo et al. 2019). Therefore, novel tools are required to catch neurodegeneration at an earlier stage, to help classifying and quantifying this process. Several years ago, the Department of Neuroscience of the Erasmus Medical Center of Rotterdam and the department of Control & Simulation mentioned earlier started a collaboration to use a cybernetic approach to develop new paradigms to achieve this. At first, manual control tasks were used (De Vries 2016, Haartsen 2017), and later gaze was analyzed as well (Büskens 2018), as the motor signals for the oculomotor system are the result of complex interactions between cortical and sub-cortical regions, spread over various regions in brain (Purves et al. 2004). Büskens (2018) concluded that gaze dynamics should be further investigated, as differences in gaze dynamics were obtained for younger and older healthy subjects.

However, aforementioned research was optimized for manual control tasks, and included a horizontal tracking task. As eye movements are the result of one and two extra-ocular muscle pairs for horizontal and vertical eye movements, respectively, vertical gaze should be addressed as well. This research focuses on gaze control behavior, and examines a new tool to be used in a clinical setting, which could be used to detect neurodegeneration at an earlier stage, and help to classify and quantify its state.

The structure of this thesis is as follows. In the first part, an experiment is conducted and its results are discussed. The experiment focuses on horizontal and vertical eye movements in one- and two-dimensional gaze tracking tasks. The second part includes a preliminary study for aforementioned experiment, including a discussion on the generation of eye movements, the cybernetic approach and pattern recognition, which could be applied to gaze data as well. Furthermore, the experiment performed in Part I was proposed. In Part III, the paper appendices from Part I can be found.

Part I:

Paper

Horizontal and Vertical Eye Movements of Normal Human Subjects in 1D and 2D Gaze Pursuit Tracking Tasks

Viktor P. A. de Jonckheere

***Abstract*—Eye movements are the result of complex interactions between cortical and sub-cortical regions. Consequently, they are considered as an important bio-marker for neurological function. Attempts to construct an oculomotor model rely on classic paradigms. In this research, a cybernetic approach was used to construct and examine a novel paradigm, which can be used as a new tool to quantify and classify neurodegeneration. Young, healthy adults (N = 24) participated in a quasi-random gaze pursuit tracking task to investigate horizontal and vertical gaze behavior in one- and two-dimensional tracking. Results indicate different horizontal gaze in terms of performance (13% and 23% better) and model parameters (5.6% and 10.2% higher K_g, 6.6% and 7.6% lower τ_g), comparing the 1D conditions and horizontal and vertical direction in the 2D condition, respectively. Vertical gaze due to cross-feed was observed up to 3 rad/s in presence of a horizontally moving target stimulus, varying in magnitude between subjects. For the proposed paradigm, an increased target signal bandwidth should be used, such that neuromuscular gaze dynamics can be captured as well, as these parameters are known to relate to neurodegeneration.**

***Index Terms*—Smooth pursuit, saccades, cross-feed, cybernetic approach, neurodegeneration**

I. Introduction

In daily life, a human performs myriads of eye movements per day, both voluntarily and reflexive, to track objects of interest. Visual tracking consists of smooth pursuit and saccadic eye movements, which should bring the target into the fovea for high acuity vision [1]. Different types of eye movements show different neurological paths, but share features as well [2]. The end of these pathways are the six extra-ocular muscles, which receive oculomotor signals to move the eye. The lateral and medial recti form antagonistic pairs, enabling horizontal gaze, while the superior and inferior recti and superior and inferior oblique control both vertical and torsional eye movements.

Motor commands are sent via several nerves to the extra-ocular muscles, see Fig. 1. The oculomotor nerve, or cranial nerve (CN) III, contains signals for the superior rectus, inferior oblique, inferior rectus, and medial rectus, while the abducens nerve (CN VI) contains signals for the lateral rectus inducing abductive eye movement. The trochlear nerve (CN IV) has a contra-lateral connection, controlling the superior oblique. For conjugate gaze, inter-nuclei motor-neurons are sent to the contra-lateral part of the oculomotor nerve, via the medial longitudinal fasciculus [3], [4]. As different brain regions are involved in this process, eye movement quality, in terms of precision and delay, of different types of eye movements is regarded as an important bio-marker for neurological diseases [5], [6], such as schizophrenia [7]. Mathematical models of gaze can assist to understand the origin of neurological disorders and help to classify and quantify impairments, which can result in more efficient diagnosis and medical treatment, which improve life quality for patients. In this research, a novel paradigm is proposed and examined based on a cybernetic modeling approach.

To model the eye, and construct a gaze path, its properties and behavior should be identified. The 19$^{\text{th}}$ century physiologists Donders, Listing and Helmholtz were intrigued by the question in which way the eye rotates to other orientations [8]. This resulted in Listing's law [9], a mode of gaze control, valid for stationary head position [10], [11]. Later, control theory was applied to model the five subsystems of the eye (smooth pursuit, vergence, saccadic, optokinetic reflex (OKR), and vestibulo-ocular reflex (VOR) [4]) [12], [13], commonly using Rashbass' step-ramp paradigm [14], or pro- and anti-saccade tasks [15], to investigate neurodegeneration [16].

However, a shift from time-domain to frequency-domain analysis can provide more insight into gaze dynamics, which is rarely performed [17], [18]. McRuer and Jex [19] introduced a cybernetic approach to understand and model manual control behavior using mathematical functions and quasi-random tracking tasks [20]. Several years ago, the Technical University of Delft and the Department of Neuroscience of the Erasmus Medical Center of Rotterdam started a collaboration to apply this cybernetic approach to develop clinical tools to quantify and classify neurodegeneration. First, only manual tracking tasks were examined [21], [22]. Later [23], gaze analysis was included as well. De Vries [21] and Haartsen [22] concluded that loss of motor skill can be determined using these tracking tasks, and Büskens [23] concluded that gaze dynamics should be further investigated, as differences in gaze dynamics were obtained for younger and older subjects. However, De Vries [21], Haartsen [22] and Büskens [23] considered only horizontal movements, using monocular gaze records. Furthermore, applied experiment procedures were optimized for manual control tasks.

This research includes both horizontal and vertical tracking and investigates gaze behavior in one- (1D) and two-dimensional (2D) gaze tracking tasks to identify gaze behavior. Contrary to previous research including this analysis, quasi-random target signals were used [24], and with increased bandwidth [17], [18]. Twenty-four subjects participated in the experiment. Cross-feed effects were detectable using two independent sets of target signal frequencies, similar to the dual-axis manual control tasks described by Barendswaard [25]. Binocular gaze was obtained using a video-oculography method, which includes challenges in signal filtering [26] and the identification of events [27].

This paper is organized as follows. In Section II, the design of the quasi-random tracking task is discussed, including

experiment procedures. Experiment results are shown and elaborated in Section III, and discussed in Section IV. Concluding remarks are stated in Section V.

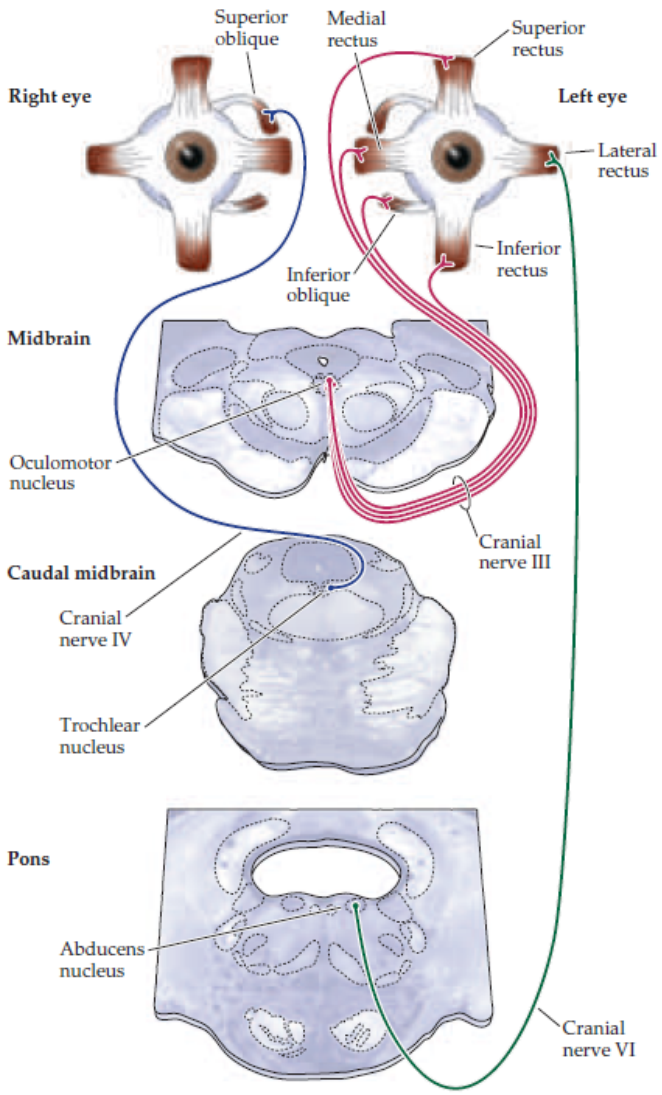

Fig. 1: Cranial nerves innervating the extra-ocular eye muscles from various brain regions and nuclei [4].

II. Methodology

A. TASK

The experiment involved a gaze pursuit tracking task, in which the participant had to track a moving stimulus on a display with their gaze. Similar to quasi-linear models of manual control dynamics [20], here the gaze control dynamics were considered as shown in Fig. 2. A subdivision was made between horizontal and vertical gaze ($H_{g_H}(s)$, $H_{g_V}(s)$), and cross-feed components ($H_{g_{c_H}}(s)$, $H_{g_{c_V}}(s)$), similar as visualized by Barendswaard [25].

A visual stimulus moved on a display in horizontal (f_H) and vertical (f_V) screen direction, and should be tracked by the participant's eyes while maintaining a fixed head position. Three conditions were tested, where the moving stimulus was restricted to either horizontal (1D-H) or vertical (1D-V) movements, or was free to move in both screen directions (2D). No secondary tasks had to be performed.

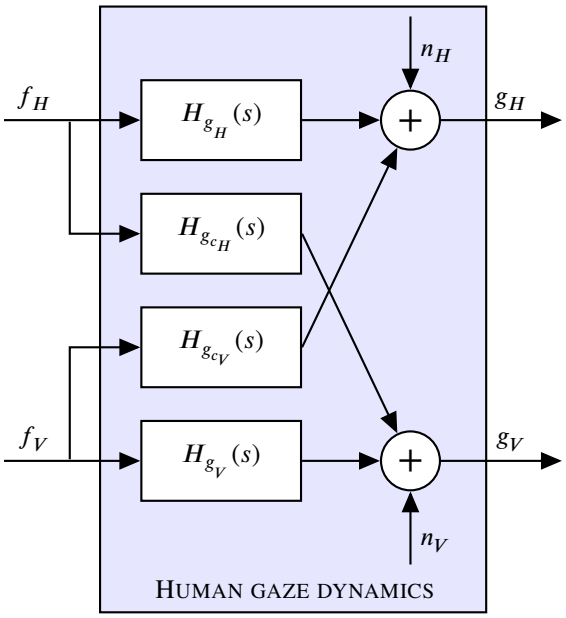

Fig. 2: Schematic representation of human gaze dynamics in a gaze pursuit tracking task.

B. TARGET FORCING FUNCTION

The target signal function $f_{H,V}$ was designed as a quasi-random multi-sine signal ($\mu = 0$ px, $\sigma = 40$ px), as defined in Equation (1), sampled at 50 Hz. The amplitudes $A_{H,V}$ of the $N_f = 11$ sinusoids were shaped with a second-order low-pass filter $H_A(s)$, as defined in Equation (3), with $T_{A_1} = 0.1$ and $T_{A_2} = 0.8$ [28]. Two different sets of frequencies were considered for the horizontal and vertical stimulus motion to be able to detect cross-talk [25]. f_H and f_V defined stimulus position in horizontal and vertical direction, respectively, see Fig. 3. The frequency components were chosen as a multiple of the base frequency, see Equation (2), with measurement time $T_m = 40.96$ s. They covered a domain of approximately 0.5 to 25 rad/s as identical primes $n_{f_{H,V}}$ and T_m were used with respect to earlier research [22]. Different phases were selected for the horizontal and vertical target forcing functions, both inducing a signal with average crest factor (CF), which is defined in Equation (4) [29]. The target signal properties are presented in Table I.

$$f_{H,V}(t) = \sum_{k=1}^{N_f} A_{H,V}[k] \sin(\omega_{H,V}[k]t + \phi_{H,V}[k]) \quad (1)$$

$$\omega_{H,V}[k] = \frac{2\pi n_{f_{H,V}}[k]}{T_m} \quad (2)$$

$$H_A(s) = \frac{(1 + T_{A_1}s)^2}{(1 + T_{A_2}s)^2} \quad (3)$$

$$\mathrm{CF} = \frac{\max(|f_{H,V}(t)|)}{\mathrm{rms}(f_{H,V}(t))} \quad (4)$$

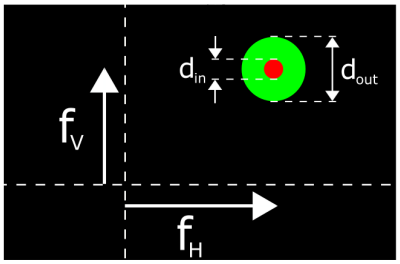

Fig. 3: Stimulus shape (d_{in} = 3 px, d_{out} = 10 px) and color with position functions f_H and f_V on the black display background. The white dashed lines represent the horizontal and vertical display center lines and stimulus diameters, and are, together with the white arrows and symbols, not displayed during the experiment.

C. APPARATUS

The experiment was performed at the vestibular and oculomotor research laboratory of the Department of Neuroscience of the Erasmus Medical Center in Rotterdam, The Netherlands. The visual stimulus was displayed at 50 Hz on a 32-inch touch screen (ELO Touch Solutions, Milpitas, California) using the Cogent graphics toolbox of MATLAB (2010, version 7.11.0 (R2010b), The MathWorks Inc., Natick, Massachusetts), ran on a Dell desktop (Windows 7 Enterprise). A head-mounted non-intrusive infrared binocular eye tracker, the EyeSeeCam (EyeSeeCam Sci, München, Germany), shown in Fig. 4, was used to record gaze at 220 Hz using video-oculography, connected to a MacBook Air (Sierra OS, version 10.12.2). An Arduino Mega 2560 created a 220 Hz pulse-train to synchronize data acquisition. A chin-rest ensured fixed head position and orientation, at approximately 0.5 m from the display, over consecutive trials. A schematic overview is shown in Fig. 5.

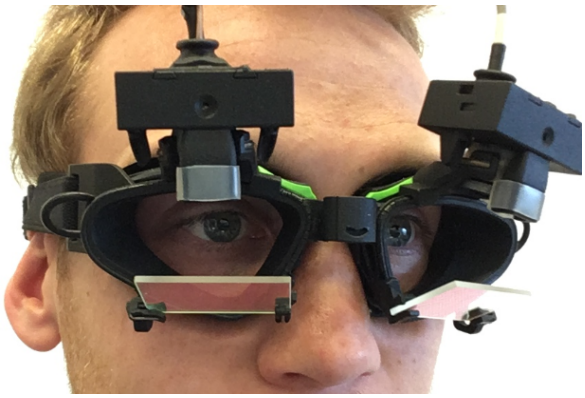

Fig. 4: Binocular EyeSeeCam; two infrared cameras make eye records via infrared mirrors.

D. EXPERIMENT PROCEDURES

In total, 12 females and 12 males (aged 24.6 ± 1.1), all young adults with no known neurological disorders participated in the experiment after giving written consent. All subjects were able to see the target stimulus and its colors clearly. The experiment design had a within-subject design, meaning that all subjects performed all conditions. The experiment was introduced by a familiarization phase, which consisted of one

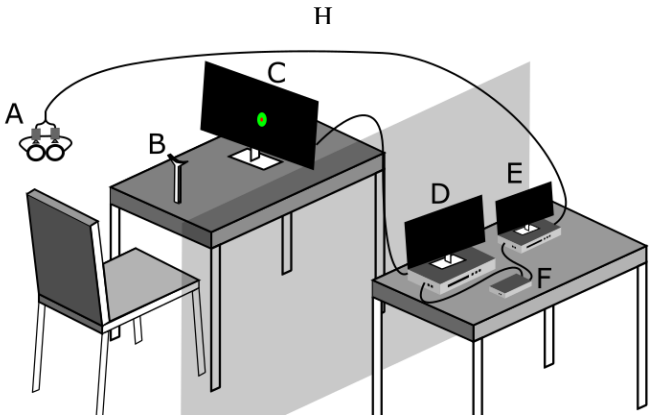

Fig. 5: Schematic representation of the experiment setup, with eye tracker (A), chin-rest (B) and display (C). In a separate control room, the Arduino (F) was used for synchronizing data acquisition in MATLAB (D) and eye tracker software (E).

trial of the 2D condition. Next, each condition was performed according to the Latin square design from Table II. After each set of four consecutive trials, a short break was taken. Each trial was constructed by a five-point calibration phase of 20 s, a run-in phase of 4 s where f_t was faded-in gradually according to Equation (5), and a measurement phase of 40.96 s. The target signal orientation was varied, as listed in Table III, to mitigate learning effects. An example of a time trial of the 2D condition is shown in Fig. 6.

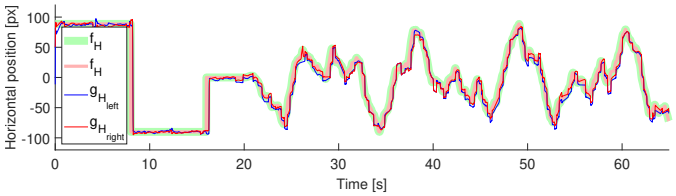

(a) Horizontal direction, f_H and g_H.

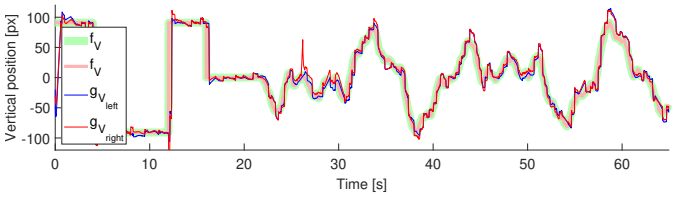

(b) Vertical direction, f_V and g_V.

Fig. 6: Example time traces for the 2D condition for horizontal and vertical screen directions, including target position and gaze position of both left and right eye.

$$f_{H,V}(t) = f_{H,V}(t) \cdot \cos^2\left(\frac{2\pi}{16}t\right) \quad \text{for} \quad 20 < t \leq 24 \qquad (5)$$

E. HYPOTHESES

The hypotheses regarding this gaze pursuit tracking task are as follows.

Learning effects have little influence on gaze tracking performance. In a manual tracking task, where the subject has to familiarize itself with both the control task and the manual control device, a training phase is induced to achieve

TABLE I: Target signal properties

	Horizontal f_H				Vertical f_V			
k	n_{f_H}	ω_H rad/s	A_H px	ϕ_H rad	n_{f_V}	ω_V rad/s	A_V px	ϕ_V rad
1	4	0.6136	43.1532	5.6627	3	0.4602	40.5878	2.0544
2	7	1.0738	31.0516	4.7021	5	0.7670	33.6087	3.1758
3	13	1.9942	15.6475	5.1108	11	1.6874	16.7602	5.1314
4	19	2.9146	8.9927	1.8137	17	2.6078	9.1773	2.7613
5	29	4.4485	4.6767	1.1288	23	3.5282	5.7677	4.3078
6	37	5.6757	3.2630	3.0070	31	4.7553	3.6447	4.4454
7	43	6.5961	2.6542	0.5584	41	6.2893	2.4390	3.6304
8	53	8.1301	2.0464	4.5919	59	9.0505	1.5661	1.5693
9	79	12.1184	1.3865	4.8193	83	12.7320	1.1508	4.9037
10	109	16.7204	1.1255	1.5588	107	16.4136	0.9797	1.3798
11	157	24.0835	0.9747	0.5004	151	23.1631	0.8501	5.4368

TABLE II: Latin square diagram

Subject ID		Condition per trial		
♀	♂	1 - 8	9 - 16	17 - 24
01, 07	13, 19	1D-H	1D-V	2D
02, 08	14, 20	2D	1D-H	1D-V
03, 09	15, 21	1D-V	2D	1D-H
04, 10	16, 22	1D-H	2D	1D-V
05, 11	17, 23	1D-V	1D-H	2D
06, 12	18, 24	2D	1D-V	1D-H

TABLE III: Target signal factors

Trial	Factor per condition					
	1D-H		1D-V		2D	
	f_H	f_V	f_H	f_V	f_H	f_V
1, 5	+1	0	0	+1	+1	+1
2, 6	-1	0	0	-1	+1	-1
3, 7	+1	0	0	+1	-1	+1
4, 8	-1	0	0	-1	-1	-1

a level of stable performance for reliable measurement data. Here, performance is defined as the standard deviation of the error signal normalized by the standard deviation of the target signal ($\sigma^2_{e_{H,V}}/\sigma^2_{H,V}$), where a lower value indicates better performance. The error is defined as $e_{H,V} = f_{H,V} - g_{H,V}$. In this eye-tracking task, a manual control device is absent. The task is comparable to daily visual tracking tasks, such as tracking a fly. It was therefore expected that the subject quickly familiarizes with the task, and no learning curve should be visible, i.e, constant values of $\sigma^2_{e_{H,V}}/\sigma^2_{f_{H,V}}$ over consecutive trials were expected.

Fatigue effects have significant effect on gaze tracking performance. Performance was expected to drop over consecutive trials as the eyes and brain, due to visual processing, are challenged, inducing fatigue effects. These effects could be to ignore high frequency components of the target signal (low ρ^2_g at high frequencies, see Equation (17)), increased time delays (larger τ_g), or difficulty to focus on the target (larger spread in saccades), causing the stimulus to appear as two different stimuli (diplopia). All aforementioned effects result in worse performance (higher $\sigma^2_{e_{H,V}}/\sigma^2_{f_{H,V}}$). This effect was expected to be more significant in 1D conditions, as these pure movements are less natural compared to the 2D condition, in which the eyes are 'free' to move. As performance degrades and smooth pursuit fails, the number of catch-up saccades should increase to keep up with the target stimulus. Therefore, it was expected that the number of saccades shows an opposite trend to performance, i.e., if performance decreases, the amount of saccades increases.

Gaze dynamics for the 1D conditions is identical to gaze dynamics for the 2D condition. Collewijn and Tamminga [17] concluded that horizontal smooth pursuit is "slightly smoother and more precise than vertical pursuit", but were not able to find any differences in horizontal or vertical eye movements for quasi-random tracking tasks, meaning similar values for gain K_g and time delay τ_g, although a lower bandwidth was applied in this research. At the high frequency components however, which were not covered by Collewijn and Tamminga [17], vertical gaze performance was expected to be worse, and vertical gaze dynamics was expected to have a lower bandwidth compared to horizontal gaze dynamics, as two muscle pairs should be controlled for these movements, instead of one for horizontal gaze. This could increase the complexity for the brain to generate correct motor inputs, which was expected to lead to increased time delays (higher τ_g), and/or simply wrong input, resulting in less precise movements and a degradation in performance.

Horizontal and vertical eye movements are independent. As the muscle pairs for horizontal eye movements are different than those for vertical eye movements [4], these movements were expected to be controlled independently. This implied that no cross-feed effects should be present, i.e., $H_{g_{c_{H,V}}} = 0$.

F. DATA SELECTION

Two output variables were used from the eye tracker gaze records; the pupil position with respect to the eye-tracker and the pupil diameter. Assuming a fixed head position and orientation, a gaze signal was constructed from the pupil position. This signal was manually calibrated using MATLAB's 'ginput' algorithm. The pupil diameter was monitored to extract blinks and events of incorrect tracking caused by eyelid and eyelash disturbances or the curvature of the eyeball. These discrepancies were filtered out, and the remaining gaps were linearly interpolated. 79 trials were removed after visual inspection of the time trials, due to significant head movements (Fig. 7a), incorrect calibration (Fig. 7b), or significant time delays (Fig. 7c). Furthermore, the data of Subject 6 and Subject 15 were discarded due to very noisy gaze records and unexpected oculomotor pathology, respectively. In total, 127 of 576 trials were discarded.

G. DATA ANALYSIS

Once the stimulus position data and eye-tracking records were synchronized, data analysis could be performed. Performance and saccades were derived from the time traces.

Saccades were detected based on an acceleration threshold of 6250 px/s², marking the start and end of a saccadic eye movement. The maximum target acceleration was approximately 1500 px/s². Gaze velocity and acceleration were obtained by differentiating absolute gaze position using MATLAB's 'diff' algorithm. An example of a time trace with detected saccades is shown in Fig. 8. The threshold was larger than applied in earlier research [30], where 1000 px/s² was used. This difference can be explained by the fact that the 2D gaze position was used in this research, instead of 1D position. A saccade was detected based on a positive and negative acceleration threshold, where both criteria should be met. This method is more strict in detecting saccades than the algorithm from Büskens et al. [30]. More advanced methods exist to detect saccades [27], mostly based on velocity thresholds [31], [32], but this was outside the scope of this research project.

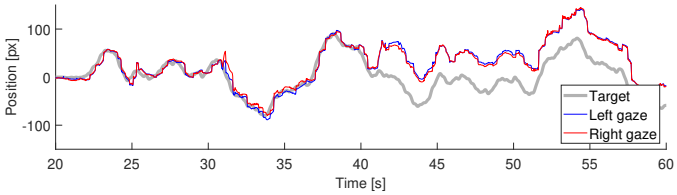

(a) Trial discarded due to head movement.

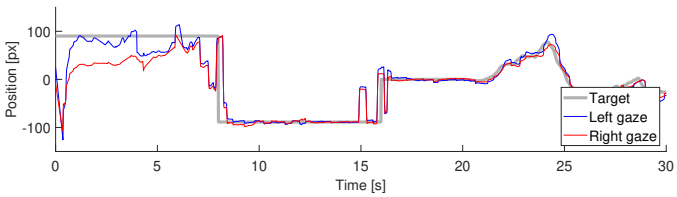

(b) Trial discarded due to calibration uncertainty.

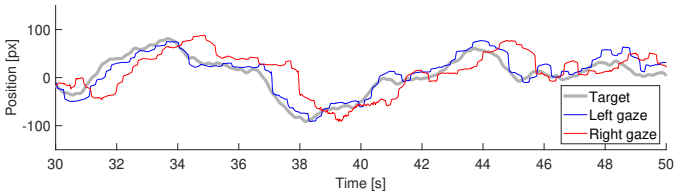

(c) Trial discarded due to tracking delay of right gaze.

Fig. 7: Examples of time traces from discarded trials for various reasons.

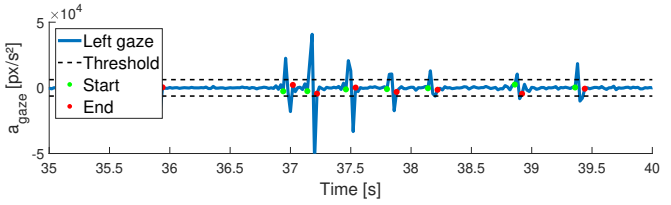

Fig. 8: Example of time trace of gaze acceleration a_{gaze} with identified saccades, with the start and end of a saccade indicated with green and red nodes, respectively. Detection thresholds are indicated with dashed black lines. Only left gaze is shown for clarity.

Using frequency-domain analysis, by applying the fast Fourier transform (MATLAB: 'FFT' algorithm), gaze dynamics were investigated. Human gaze dynamics are modeled with a quasi-linear model, with a linear part which responds to target motion, and remnant $n_{H,V}$ [20]. The linear part consists of direct ($H_{g_{H,V}}(s)$) and cross-feed components ($H_{g_{c_{H,V}}}(s)$), as defined in Equations (6) and (7), where $\cdot$ represents $j\omega$ for the sake of brevity. A schematic representation is shown in Fig. 2. The remnant accounts for non-linear effects in gaze control behavior [33]. By comparing the input $F_{H,V}(j\omega) = \text{FFT}(f_{H,V}(t))$ and gaze $G(j\omega) = \text{FFT}(g(t))$ at the excited frequencies $\omega_{H,V}$, the linear transfer functions can be estimated, see Equations (8) to (11). As the forcing functions are independent, $F_H(j\omega_V) = 0$ and $F_V(j\omega_H) = 0$. Moreover, the contribution of the relative remnant is relatively small at the excited frequencies, see (12). Therefore, some terms are dropped in Equations (8) to (11), such that of the right hand sides, only the first term remains, and estimates of the transfer functions were simply obtained by comparing input and output at $\omega_{H,V}$.

$$G_H(\cdot) = F_H(\cdot)H_{g_H}(\cdot) + F_V(\cdot)H_{g_{c_V}}(\cdot) + N_H(\cdot) \tag{6}$$

$$G_V(\cdot) = F_V(\cdot)H_{g_V}(\cdot) + F_H(\cdot)H_{g_{c_H}}(\cdot) + N_V(\cdot) \tag{7}$$

$$H_{g_H}(j\omega_H) = \frac{G_H(j\omega_H)}{F_H(j\omega_H)} - \frac{F_V(j\omega_H)}{F_H(j\omega_H)}H_{g_{c_V}}(j\omega_H) - \frac{N_H(j\omega_H)}{F_H(j\omega_H)} \tag{8}$$

$$H_{g_V}(j\omega_V) = \frac{G_V(j\omega_V)}{F_V(j\omega_V)} - \frac{F_H(j\omega_V)}{F_V(j\omega_V)}H_{g_{c_H}}(j\omega_V) - \frac{N_V(j\omega_V)}{F_V(j\omega_V)} \tag{9}$$

$$H_{g_{c_V}}(j\omega_V) = \frac{G_H(j\omega_V)}{F_V(j\omega_V)} - \frac{F_H(j\omega_V)}{F_V(j\omega_V)}H_{g_H}(j\omega_V) - \frac{N_H(j\omega_V)}{F_V(j\omega_V)} \tag{10}$$

$$H_{g_{c_H}}(j\omega_H) = \frac{G_V(j\omega_H)}{F_H(j\omega_H)} - \frac{F_V(j\omega_H)}{F_H(j\omega_H)}H_{g_V}(j\omega_H) - \frac{N_V(j\omega_H)}{F_H(j\omega_H)} \tag{11}$$

$$\frac{N_{H,V}(j\omega_{H,V})}{F_{H,V}(j\omega_{H,V})} \approx 0 \tag{12}$$

Büskens [23] modeled horizontal gaze dynamics using a gain (K_g), time delay (τ_g) and neuromuscular dynamics (with damping ratio ζ_g and natural frequency ω_g), as defined in (14), assuming to be equal to human arm dynamics. Contrary to the arm however, the eye is an almost perfectly round object, located in its orbit, and the extra-ocular muscles allow rotations in all directions, whereas translations are negligible [3]. Furthermore, a different fiber composition is present compared to skeletal muscles [34]. Thus, the neuromuscular dynamics of the eye could have different system properties. To investigate this, system identification was performed using two different models, one represented by Equation (13) excluding

the neuromuscular dynamics, the other by Equation (14), in which the neuromuscular dynamics is included. These models were compared to determine which one represents gaze dynamics best for the given pursuit tracking task.

$$H_{g_{M2}}(s) = K_g e^{-s\tau_g} \tag{13}$$

$$H_{g_{M4}}(s) = K_g e^{-s\tau_g} \frac{\omega_g^2}{\omega_g^2 + 2\zeta_g \omega_g s + s^2} \tag{14}$$

MATLAB's 'minsearch' algorithm was used to find a set of model parameters θ, which represents human gaze dynamics best. The cost function value $J(\theta)$ was minimized to achieve this, defined by a normalized squared cost function, see Equation (15), where $\cdot_{H,V} = j\omega_{H,V}$ for the sake of brevity. The Variance Accounted For (VAF) was used to quantify the model fitting by comparing simulated human gaze, $g_{s_{H,V}}(\theta)$, using MATLAB's 'lsim' algorithm [35], to the measured gaze $g_{H,V}$, see Equation (16). By applying variations of weights at components of $\omega_{H,V}$ during fitting, different models were obtained. Six models were used to fit the model parameters for $H_{g_{H,V}}(s)$, see Table IV. Cross-feed dynamics were not fitted with a particular model, as its origin was unknown if present. For the M2 and M4 models, separate equations were used to fit the model, which are Equations (13) and (14), respectively. For the WR models, each excited frequency was weighted with the relative remnant ρ_g^2. For the WB models, the weights applied by Büskens [23] were used, where a weight factor of 100 was applied at the first two and last three frequency components of ω_H. The weights of the W1 models were unity. The relative remnant, Equation (17), validates the assumption made in Equations (8) to (11) by comparing gaze signal power at the $\omega_{H,V}$, $S_{g_{H,V}g_{H,V}}(\omega_{H,V})$, with the estimated noise at these frequencies, $\hat{S}_{g_{H,V}g_{H,V_n}}(\omega_{H,V})$ [33]. In this case, the latter was obtained by interpolating three data points left and right of each excited frequency, excluding other exciting frequencies.

$$J(\theta) = \sum_{k=1}^{N_f} \frac{|\hat{H}_{g_{H,V}}(\cdot_{H,V}[k]) - H_{g_{H,V}}(\cdot_{H,V}[k], \theta)|^2}{|\hat{H}_{g_{H,V}}(\cdot_{H,V}[k])|^2} \tag{15}$$

$$\mathrm{VAF}(\theta) = \left(1 - \frac{\sum |g_{H,V} - g_{s_{H,V}}(\theta)|^2}{\sum g_{H,V}^2}\right) \times 100\% \tag{16}$$

$$\rho_g^2(\omega_{H,V}) = 1 - \frac{\hat{S}_{g_{H,V}g_{H,V_n}}(\omega_{H,V})}{S_{g_{H,V}g_{H,V}}(\omega_{H,V})} \tag{17}$$

III. Results

A. Performance

Performance was monitored, see Fig. 9. Within subjects, a paired samples t-test shows a significant difference in horizontal performance (μ = 0.0598, σ = 0.0042) and vertical performance (μ = 0.0676, σ = 0.0117) for the 1D conditions; $t(23)$ = -2.816, p = 0.01. For the 2D condition, there was a significant difference in horizontal performance (μ = 0.0619, σ = 0.0043) and vertical performance (μ = 0.0675, σ = 0.0090) as well; $t(23)$ = -3.218, p = 0.004. Thus, in general horizontal performance was superior over vertical performance.

TABLE IV: Parameter estimation models

Model	θ				Weights
	K_g	τ_g	ζ_g	ω_g	
M2-W1	X	X			Unity
M4-W1	X	X	X	X	Unity
M2-WR	X	X			ρ_g^2
M4-WR	X	X	X	X	ρ_g^2
M2-WB	X	X			Ref. [23]
M4-WB	X	X	X	X	Ref. [23]

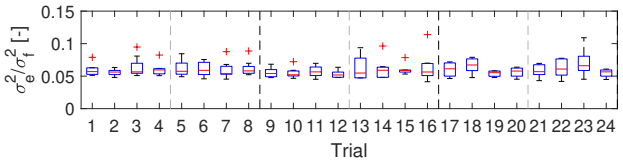

(a) Horizontal performance in 1D-H condition.

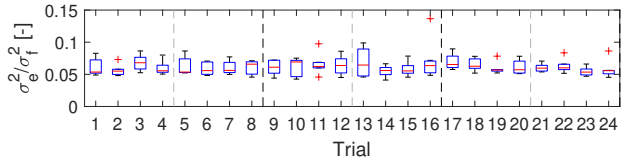

(b) Horizontal performance in 2D condition.

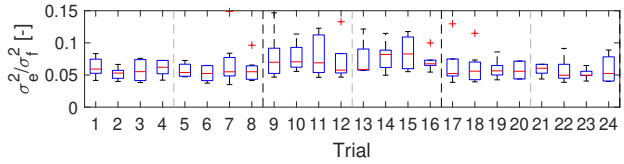

(c) Vertical performance in 1D-V condition.

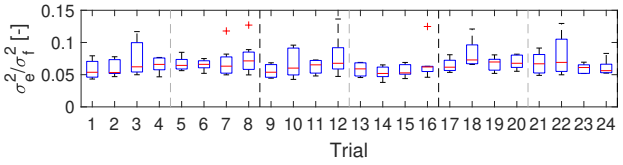

(d) Vertical performance in 2D condition.

Fig. 9: Performance (left gaze) per trial per condition; short breaks are indicated with light gray dashed lines, longer breaks are indicated with black dashed lines.

To identify learning effects, performance was monitored per trial, Fig. 9. The familiarization trial was excluded in this analysis. A learning curve appears absent, performance remains approximately constant, although its variance varies. This was confirmed by performing a Friedman test, both applied to all trials and only the first four trials. For horizontal performance in the horizontal condition ($\chi(23)$ = 15.220, p = 0.887 and $\chi(3)$ = 1.457, p = 0.692) and 2D condition ($\chi(23)$ = 16.610, p = 0.828 and $\chi(3)$ = 5.600, p = 0.133), and vertical performance in the vertical condition ($\chi(23)$ = 30.260, p = 0.142 and $\chi(3)$ = 3.400, p = 0.334) and 2D condition ($\chi(23)$ = 24.360, p = 0.384 and $\chi(3)$ = 2.600, p = 0.457), no significant differences are found.

B. SACCADES

The number of saccades varies from 2 to 4 per second within subjects. This is similar to the results found in earlier research [17]. In Fig. 10, plots are shown for the direction and amplitude of saccades. The saccades for the left and right eye are indicated in blue and red, respectively, including the number of saccades and inclination α. The size of the target stimulus is shown for perspective. Each saccade starts in the center of these plots, and ends in at the marked position, indicating amplitude and direction. The outer edge of the stimulus is indicated with the green circle for perspective. In general, the saccade directions of the 1D-H condition were inclined according to approximately a fixed angle α, varying per subject, for example, shown in Fig. 10a. For the 1D-V condition, this effect was visible as well, see for example Fig. 10b, but was less common than horizontal inclination, and less severe as well. For the 2D condition, for example shown in Fig. 10c, this pattern could not be identified due to the variation of the saccade directions. In general, saccade amplitude was comparable between subjects, while saccade direction variation was not.

The average amount of saccades towards each direction was examined as well. For the 1D-H condition, the amount of saccades towards the left and right differs less than 20%, whereas the amount of saccades up and down differs, in general, more than 20%. Furthermore, 7 of 22 subjects generated more saccades towards the right in this condition. In the 1D-V condition, the variation in differences in upward and downward saccades was larger. Subject 1 (59% more downward saccades) and Subject 3 (47% more upward saccades) had significantly more saccades to a particular side, implying superior smooth pursuit upwards and downwards, respectively. This effect was not observed in the 2D condition for Subject 1 and Subject 3. Subject 20 showed difficulty in tracking the stimulus in the 1D-H condition with the right eye, indicated by the number of saccades per trial for left (136.5 ± 21.0) and right (331.4 ± 70.4) gaze. However, at the 1D-V and 2D conditions, the number of saccades for left (110.5 ± 7.7 and 169.9 ± 5.7, respectively) and right gaze (140.5 ± 18.1 and 220.0 ± 38.5, respectively) were less apart, but still present. This could imply that the right eye had a blurred image of the target.

C. GAZE DYNAMICS

An example of a Bode plot with the frequency response function of $H_{g_H}(j\omega)$ in the 1D-H condition is shown in Fig. 11. As can be seen, a characteristic peak and second-order decay at higher frequencies, which would indicate the presence of neuromuscular system dynamics, is absent. The VAF scores of each model were examined for each subject to investigate the influence of the neuromuscular system, see Fig. 12. The VAF scores of the right eye had similar trends and were therefore omitted for the sake of brevity. For all conditions, the M2-models showed consistently lower VAF scores compared to their M4 equivalent. In general, the highest means and lowest standard deviations were obtained for the WR models.

The estimated parameters are shown in Fig. 13 for all models from Tab. IV. In Fig. 13c, $\zeta_g = 1$ is indicated with a black dashed line, as for $\zeta_g > 1$, the neuromuscular dynamics from (14) has two real poles, indicating two natural frequencies, instead of a complex conjugate pair with one natural frequency. In Fig. 13d, frequency domains are indicated. The white area covers $\omega_{H,V}$. The light gray area represents the parameter estimation frequency range for θ_{ω_g}, which are the examined frequencies to fit ω_g for the cost function value from (15). A penalty was applied if the MATLAB's *fminsearch* algorithm examined values of $\omega_g > 40$ rad/s, such that frequencies beyond this value are not obtained, indicated by the dark gray area in Fig. 13.

To have a significant effect on the VAF, the estimated ω_g values should be in the white area of Fig. 13d. Statistical values of ω_g are shown in Table V. As can be seen, mean values are 20.8 rad/s or higher, which were less than 2.3 rad/s from the highest frequency component of $\omega_{H,V}$. Therefore, the influence of the neuromuscular part was further investigated by analyzing the ω_g, as this defines the bandwidth of the neuromuscular part. The VAF was calculated for varying ω_g, see for typical examples Fig. 14, where the gray areas are identical as those in Fig. 13d. As can be seen, a characteristic peak at high-frequency components of $\omega_{H,V}$ is missing. Furthermore, a more optimal VAF score

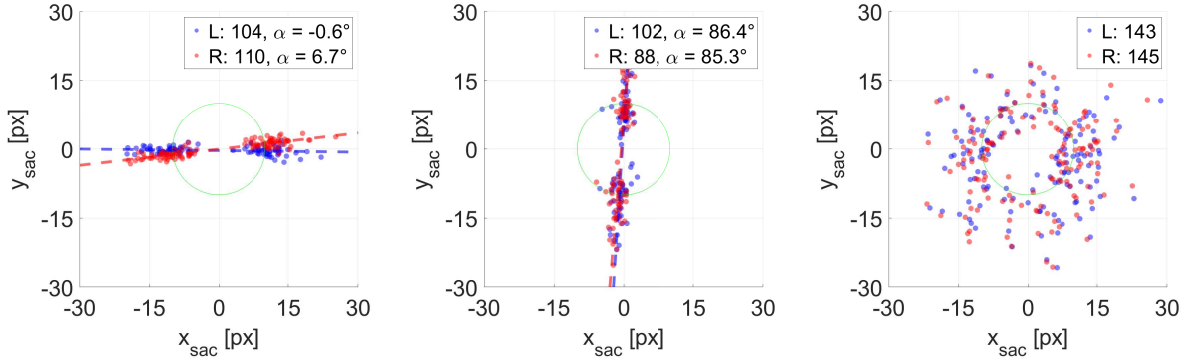

(a) 1D-H condition, S-8.13. (b) 1D-V condition, S-16.18. (c) 2D condition, S-10.12.

Fig. 10: Examples of saccadic amplitude and direction in every condition, including the number of saccades for the left L and right R eye and a least squares fit with angle $\alpha = \text{atan}(\frac{y_{sac}}{x_{sac}})$ in equal colors. Subject and trial are indicated as S-X.Y, with subject ID X and trial number Y. The green circle represents the target stimulus size to serve as a reference.

can be obtained for other ω_g values, which indicates artifacts during fitting. Therefore, one can conclude that including the neuromuscular part does not contribute to explaining gaze dynamics for this gaze pursuit task. Thus, the bandwidth of the neuromuscular part was beyond the forcing function frequency domain, which could be caught using higher bandwidth target forcing functions. Consequently, M4-models were omitted in the parameter estimation procedure.

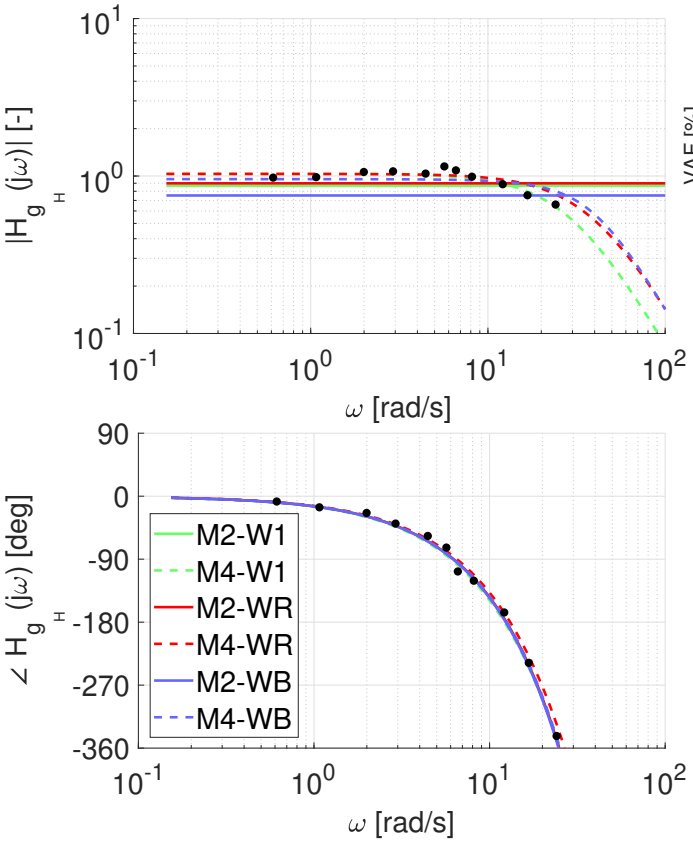

Fig. 11: Example Bode plot of left gaze of Subject 1 in the horizontal condition for different models from Table IV. Bode plots of the 1D-V and 2D condition look similar, for both left and right gaze.

TABLE V: ω_g statistics ($\mu \pm \sigma$ rad/s , N = 21) for the M4-models in every condition, for the left eye. For the 2D condition, the horizontal (2D(-H)) and vertical (2D(-V)) directions are separated. For the right eye, similar results were obtained.

Model	Condition			
	1D-H	1D-V	2D(-H)	2D(-V)
M4-W1	23.5 ± 4.8	27.4 ± 9.3	25.7 ± 6.7	22.6 ± 8.8
M4-WR	25.2 ± 6.8	27.5 ± 9.5	25.1 ± 5.5	20.8 ± 7.4
M4-WB	29.5 ± 6.8	35.2 ± 5.8	32.6 ± 7.9	33.9 ± 6.8

While comparing the VAF scores from models M2-W1, M2-WR and M2-WB, model M2-WR showed the highest means and lowest standard deviations. Therefore, this model was considered as most consistent and chosen for further analysis. An analysis of the relative remnant as defined in Equation (17) is shown in Fig. 15. This is the applied weight in parameter estimation fitting of M2-WR. This figure shows the relative remnant at $f_{H,V}$, where different transparency is used

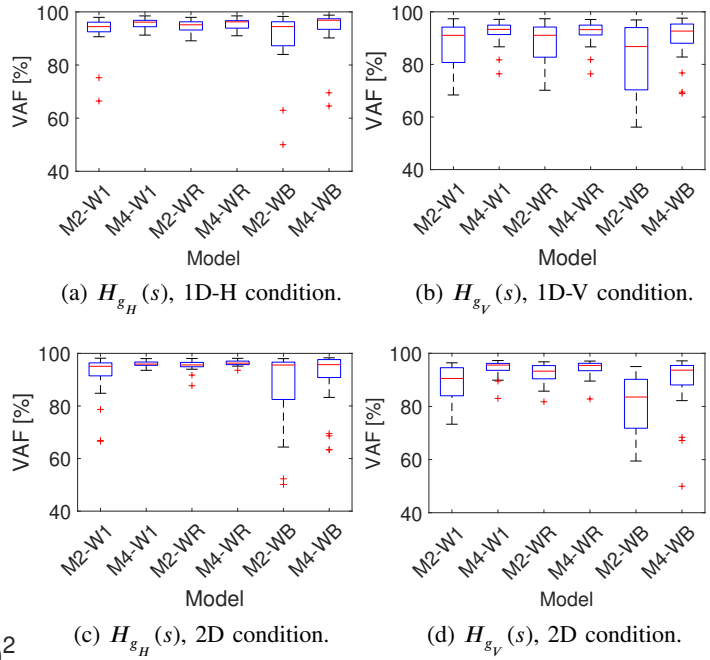

(a) $H_{g_H}(s)$, 1D-H condition. (b) $H_{g_V}(s)$, 1D-V condition.

(c) $H_{g_H}(s)$, 2D condition. (d) $H_{g_V}(s)$, 2D condition.

Fig. 12: VAF scores of different estimated gaze models ($H_{g_{H,V}}(s)$) according to Table IV for each condition for the left eye. Right models show similar results.

to show different percentiles. Variations in behavior appear at high-frequency components. For horizontal gaze at the 1D-H and 2D conditions, the relative remnant is about unity for all frequency components, whereas the relative remnant of vertical gaze in the 1D-V and 2D conditions show degradation at the higher frequencies. Remarkably, some recovery was obtained at the highest frequency component of f_V in the 1D-V condition, which was not observed at vertical gaze in the 2D condition. This effect was not observed for horizontal gaze.

D. GAZE DYNAMICS MODELLING RESULTS

The estimated parameter values for M2-WR are visualized in Fig. 17, where the gain and time delay for both horizontal and vertical gaze models are visualized for both eyes. The Shapiro-Wilk test showed that for K_g, none except the vertical gain in 2D condition (g_V at 2D(-V)) were normally distributed. For τ_g, all except the vertical time delay in the 2D condition (g_V at 2D(-V)) were normally distributed. As these were the only exceptions, it was assumed that K_g was not normally distributed, but τ_g was. For K_g, a Wilcoxon Signed Rank test was used for analysis, while for τ_g, a paired samples t-test was used.

The statistical test results are shown in Table VI, with results for K_g in the upper right half (◹), and τ_g in the bottom left half (◺). Two generic trends were observed. First of all, the left and right gains were comparable, and vertical tracking in the 2D condition had lower gains; comparing horizontal and vertical gains, vertical gains were 7.6% lower in the 1D conditions and 9.5% lower in the 2D condition for the left eye, and 3.6% and 10.9% for the right eye, respectively. Secondly, a clear difference was present for horizontal and vertical time delays, while within both horizontal and vertical time delays, little or no significance was obtained; comparing horizontal

TABLE VI: Statistical difference for K_g (right upper half (◹), Wilcoxon Signed Rank test with Z-scores) and τ_g (bottom left half (◺), paired samples t-test) for M2-WR parameters, where - is not significant ($p \geq 0.05$), * is significant ($p < 0.05$) and ** is highly significant ($p < 0.01$). The rows and column are identical, represented by (a) to (h) for the sake of brevity.

	Left eye				Right eye			
	g_H		g_V		g_H		g_V	
	1D-H (a)	2D (b)	1D-V (c)	2D (d)	1D-H (e)	2D (f)	1D-V (g)	2D (h)
(a)		Z = -3.211*	Z = -2.651*	Z = -3.808**	-	Z = -2.539*	-2.576*	-3.845**
(b)	-		Z = -2.016*	Z = -3.806**	-	-	-	Z = -3.702**
(c)	$t(19)$ = -5.800**	$t(19)$ = -5.793**		Z = -3.024*	Z = -2.763*	Z = -2.427*	-	Z = -2.987*
(d)	$t(19)$ = -6102**	$t(20)$ = -5.985**	-		Z = -3.136*	Z = -3.841**	Z = -3.621**	-
(e)	-	-	$t(19)$ = 5.653**	$t(19)$ = 6.149**		-	-	Z = -3.285*
(f)	-	-	$t(19)$ = 6.187**	$t(20)$ = 6.508**	-		-	Z = -3.910**
(g)	$t(19)$ = -4.820**	$t(19)$ = -5.180**	$t(20)$ = 2.307*	$t(19)$ = 2.664*	$t(19)$ = -4.916**	$t(19)$ = -5.737**		Z = -3.733**
(h)	$t(19)$ = -6.148**	$t(20)$ = -6.092**	-	-	$t(19)$ = -6.436**	$t(20)$ = -6.728**	$t(19)$ = -2.728*	

and vertical time delays, vertical time delays were 7.1% higher in the 1D conditions and 7.7% higher in the 2D condition for the left eye, and 6.1% and 7.5% for the right eye, respectively.

E. CROSS-FEED

Cross-feed was detected by investigating gaze power at cross-frequencies, see Equations (10) and (11) [25]. In general, three cases were observed, which were consistent within subjects. These cases are the absence of cross-feed, little cross-feed, and severe presence of cross-feed, see Fig. 18 and Table VII, where these cases are represented by white, light gray or dark gray cell colors, respectively. In general cross-feed was only present in $H_{g_{cH}}(s)$, thus g_V in presence of f_H, see (2). In general, cross-feed was mostly observed in the right eye, see Table VII. Cross-feed was constant within subjects within conditions, as deviations in cross-feed percentage was never higher than 0.05. Subject 8 showed consistent severe cross-talk in the right eye for both the 1D-H and 2D conditions. Cross-feed was always induced at the low-frequency components of $\omega_{H,V}$, see for example Fig. 18d and 18g.

In Fig. 19, the contribution of each frequency set is shown for the same subjects as shown in Fig. 18. The error at ω_H, ω_V and ω_N (all frequencies except $\omega_{H,V}$) are shown in blue, red and yellow, respectively. Predominantly the error was caused in the direction of stimulus motion. The 2D condition was generally a superposition of the horizontal and vertical condition, which implies that there are no different systems involved when either a 1D or 2D target has to be tracked.

Some uncommon behavior was observed when analyzing the cumulative error plots (Fig. 19). Subjects 11 and 17 showed after the transition from 1D-V to 1D-H severe cross-feed at the first trial of the 1D-H condition. This effect declined to little cross-feed for consecutive trials. For Subjects 5 and 23, who had identical condition orders, see Table II, this effect was not observed. Furthermore, for the transition from 2D to 1D-H, this effect was not observed for any subject. For the transition from neither 1D-H nor 2D to 1D-V, this effect was observed.

IV. DISCUSSION

An experiment was conducted in which 24 young adults (aged 24.6 ± 1.1) performed a gaze pursuit tracking task, where binocular gaze records were measured and analyzed. The research goal was to identify horizontal and vertical gaze behavior in 1D and 2D tasks using a cybernetic approach.

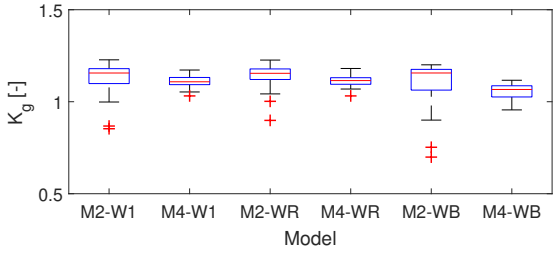

(a) Gain.

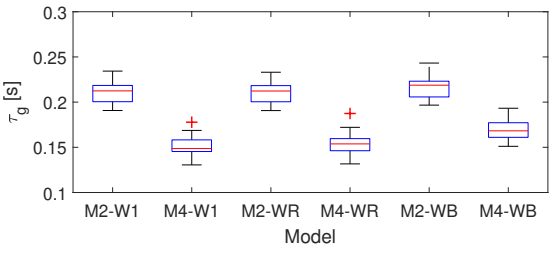

(b) Time delay.

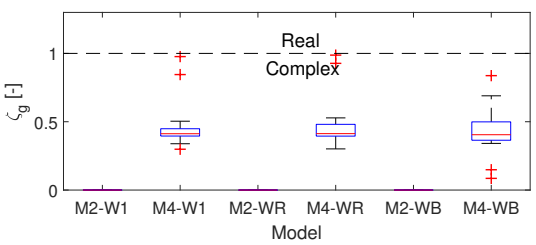

(c) Damping ratio, where $\zeta_g = 1$ is indicated with a dashed line.

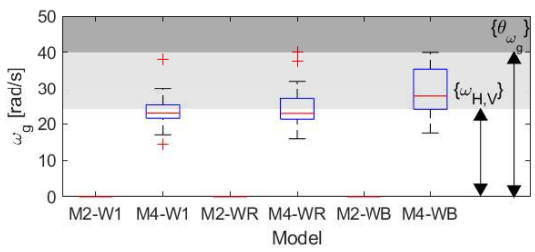

(d) Natural frequency, where frequency domains $\{\theta_{\omega_g}\}$, $\{\omega_{H,V}\}$ correspond with those from Fig. 14.

Fig. 13: Estimated gaze parameters for each model from Tab. IV of the left eye for the horizontal condition.

TABLE VII: Cross-feed percentage of error signal ($\mu \pm \sigma$) for both eyes for all conditions. Cross-feeds larger than 10% and 20% are indicated with light and gray dark cell colors, respectively. Subject and dominant eye (left or right) are abbreviated with 'S' and 'DE' ('L' or 'R'), respectively.

		$e_H(\omega_V)/e$ [%]						$e_V(\omega_H)/e$ [%]					
		left eye			right eye			left eye			right eye		
S	DE	1D-H	1D-V	2D	1D-H	1D-V	2D	1D-H	1D-V	2D	1D-H	1D-V	2D
1	R	0.05 ± 0.00	0.03 ± 0.00	0.04 ± 0.00	0.06 ± 0.00	0.04 ± 0.00	0.04 ± 0.00	0.16 ± 0.01	0.04 ± 0.00	0.09 ± 0.00	0.07 ± 0.00	0.04 ± 0.00	0.11 ± 0.00
2	R	0.05 ± 0.00	0.03 ± 0.00	0.04 ± 0.00	0.05 ± 0.00	0.03 ± 0.00	0.04 ± 0.00	0.05 ± 0.00	0.05 ± 0.00	0.05 ± 0.00	0.04 ± 0.00	0.05 ± 0.00	0.07 ± 0.00
3	L	0.03 ± 0.00	0.02 ± 0.00	0.03 ± 0.00	0.04 ± 0.00	0.02 ± 0.00	0.03 ± 0.00	0.19 ± 0.01	0.04 ± 0.00	0.11 ± 0.00	0.13 ± 0.00	0.03 ± 0.00	0.11 ± 0.00
4	R	0.02 ± 0.00	0.02 ± 0.00	0.03 ± 0.00	0.02 ± 0.00	0.01 ± 0.00	0.02 ± 0.00	0.02 ± 0.00	0.04 ± 0.00	0.06 ± 0.00	0.12 ± 0.01	0.04 ± 0.00	0.17 ± 0.00
5	L	0.02 ± 0.00	0.01 ± 0.00	0.03 ± 0.00	0.02 ± 0.00	0.02 ± 0.00	0.03 ± 0.00	0.10 ± 0.00	0.02 ± 0.00	0.10 ± 0.00	0.03 ± 0.00	0.03 ± 0.00	0.03 ± 0.00
7	R	0.04 ± 0.00	0.01 ± 0.00		0.04 ± 0.00	0.02 ± 0.00		0.05 ± 0.00	0.08 ± 0.00		0.04 ± 0.00	0.10 ± 0.00	
8	L	0.02 ± 0.00	0.01 ± 0.00	0.03 ± 0.00	0.02 ± 0.00	0.01 ± 0.00	0.02 ± 0.00	0.02 ± 0.00	0.03 ± 0.00	0.08 ± 0.00	0.65 ± 0.05	0.04 ± 0.00	0.43 ± 0.02
9	R		0.03 ± 0.00	0.06 ± 0.00		0.02 ± 0.00	0.04 ± 0.00		0.05 ± 0.00	0.10 ± 0.00		0.05 ± 0.00	0.14 ± 0.01
10	R	0.02 ± 0.00	0.01 ± 0.00	0.03 ± 0.00	0.02 ± 0.00	0.01 ± 0.00	0.02 ± 0.00	0.02 ± 0.00	0.02 ± 0.00	0.07 ± 0.00	0.07 ± 0.00	0.02 ± 0.00	0.02 ± 0.00
11	R	0.04 ± 0.00	0.04 ± 0.00	0.04 ± 0.00	0.03 ± 0.00	0.06 ± 0.00	0.03 ± 0.00	0.18 ± 0.03	0.03 ± 0.00	0.05 ± 0.00	0.17 ± 0.02	0.04 ± 0.00	0.05 ± 0.00
12	L	0.02 ± 0.00	0.00 ± 0.00	0.04 ± 0.00	0.02 ± 0.00	0.01 ± 0.00	0.03 ± 0.00	0.04 ± 0.00	0.05 ± 0.00	0.06 ± 0.00	0.34 ± 0.03	0.04 ± 0.00	0.06 ± 0.00
13	L	0.02 ± 0.00	0.02 ± 0.00	0.02 ± 0.00	0.02 ± 0.00	0.01 ± 0.00	0.02 ± 0.00	0.01 ± 0.00	0.05 ± 0.00	0.05 ± 0.00	0.13 ± 0.01	0.05 ± 0.00	0.06 ± 0.00
14	L	0.02 ± 0.00	0.01 ± 0.00	0.02 ± 0.00	0.04 ± 0.00	0.01 ± 0.00	0.03 ± 0.00	0.11 ± 0.00	0.02 ± 0.00	0.10 ± 0.00	0.06 ± 0.00	0.02 ± 0.00	0.06 ± 0.00
16	R	0.02 ± 0.00	0.06 ± 0.00	0.06 ± 0.00	0.03 ± 0.00	0.11 ± 0.00	0.07 ± 0.00	0.11 ± 0.00	0.03 ± 0.00	0.12 ± 0.00	0.07 ± 0.00	0.04 ± 0.00	0.14 ± 0.00
17	R	0.04 ± 0.00	0.01 ± 0.00	0.03 ± 0.00	0.05 ± 0.00	0.02 ± 0.00	0.05 ± 0.00	0.07 ± 0.00	0.03 ± 0.00	0.06 ± 0.00	0.23 ± 0.03	0.04 ± 0.00	0.10 ± 0.00
18	R	0.03 ± 0.00	0.03 ± 0.00	0.02 ± 0.00	0.03 ± 0.00	0.01 ± 0.00	0.03 ± 0.00	0.09 ± 0.00	0.04 ± 0.00	0.06 ± 0.00	0.07 ± 0.00	0.04 ± 0.00	0.04 ± 0.00
19	R	0.02 ± 0.00	0.02 ± 0.00	0.04 ± 0.00	0.02 ± 0.00	0.00 ± 0.00	0.02 ± 0.00	0.11 ± 0.01	0.04 ± 0.00	0.05 ± 0.00	0.14 ± 0.01	0.04 ± 0.00	0.22 ± 0.01
20	R	0.02 ± 0.00		0.04 ± 0.00	0.02 ± 0.00		0.03 ± 0.00	0.06 ± 0.00		0.15 ± 0.00	0.14 ± 0.01		0.13 ± 0.00
21	L	0.01 ± 0.00	0.02 ± 0.00	0.02 ± 0.00	0.01 ± 0.00	0.01 ± 0.00	0.02 ± 0.00	0.07 ± 0.00	0.03 ± 0.00	0.06 ± 0.00	0.11 ± 0.00	0.03 ± 0.00	0.06 ± 0.00
22	L	0.02 ± 0.00	0.02 ± 0.00	0.03 ± 0.00	0.02 ± 0.00	0.02 ± 0.00	0.02 ± 0.00	0.02 ± 0.00	0.04 ± 0.00	0.02 ± 0.00	0.17 ± 0.00	0.04 ± 0.00	0.05 ± 0.00
23	R	0.05 ± 0.00	0.02 ± 0.00	0.04 ± 0.00	0.03 ± 0.00	0.01 ± 0.00	0.05 ± 0.00	0.09 ± 0.01	0.05 ± 0.00	0.06 ± 0.00	0.12 ± 0.01	0.04 ± 0.00	0.05 ± 0.00
24	R	0.01 ± 0.00	0.01 ± 0.00	0.02 ± 0.00	0.01 ± 0.00	0.01 ± 0.00	0.02 ± 0.00	0.05 ± 0.00	0.03 ± 0.00	0.04 ± 0.00	0.03 ± 0.00	0.03 ± 0.00	0.03 ± 0.00

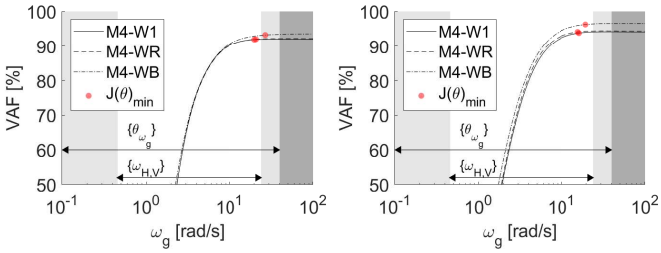

(a) 1D-H condition, S-9.22.

(b) 1D-V condition, S-9.6.

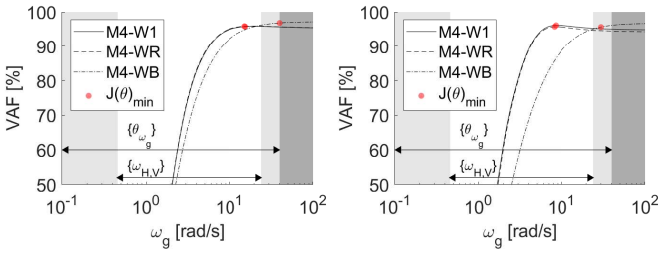

(c) 2D condition, horizontal model, S-9.9.

(d) 2D condition, vertical model, S-9.9.

Fig. 14: Typical example of the influence of ω_g on the VAF, where the light gray area is outside the excited frequency domain, and dark gray area outside the parameter fitting domain. Horizontal (-H) and vertical (-V) models are separated for the 2D condition. The fitted ω_g for which $J(\theta)$ was minimal is indicated as well. The gray areas correspond with those from Fig. 13d. Subject and trial are indicated as S-$X.Y$, with subject ID X and trial number Y.

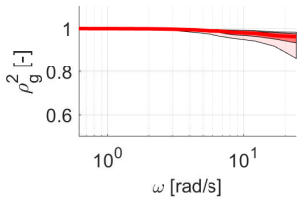

(a) $G_H(\omega_H)$, 1D-H condition.

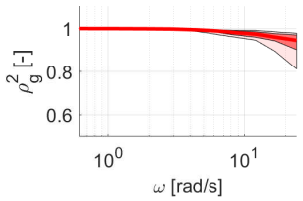

(b) $G_H(\omega_H)$, 2D condition.

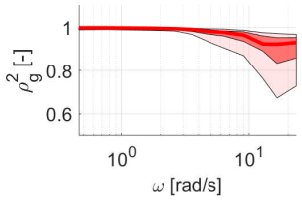

(c) $G_V(\omega_V)$, 1D-V condition.

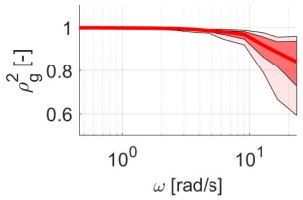

(d) $G_V(\omega_V)$, 2D condition.

Fig. 15: Relative remnant of left gaze with median, 25^{th} to 75^{th} percentile (dark red area) and 10^{th} to 90^{th} percentile (light red area), right gaze showed similar results.

In this way, eye movements could be described by different characteristics compared to classical gaze analysis, which, e.g., focus more on reaction times, precision and velocity profiles (e.g., Rottach et al. [24]).

In this research, it was found that learning effects appeared to be absent, but contrary to hypothesized, fatigue effects were as well. A Friedman test was applied for two cases; to all trials, and to the first four trials. For both cases, no statistical differences were found for performance between trials. This also means that recovery after breaks was found to be absent as well. During the experiment, multiple subjects complained about fatigue after repeated trials, especially near the end of the experiment, but performance did not show any degradation. This can be due to the fact that the extra-ocular muscles differ fundamentally from other muscles [36], which is visible in amyotrophic lateral sclerosis (ALS), where the eyes are usually preserved [34]. The absence of learning effects implies that fewer trials per condition are required for obtaining gaze records in pursuit tasks. Furthermore, training phases can be omitted in pure gaze pursuit tasks, but a familiarization phase is still recommended.

The polar plots of saccadic eye movements, detected using an acceleration threshold, for the 1D-H condition showed a general trend of an inclined relationship between saccade amplitude and direction, constant within subjects, but different between subjects. In the 1D-V condition, a trend was less common. In the 2D condition, no trends could be spotted due

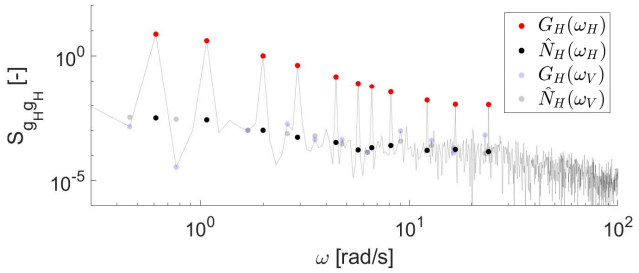

(a) 1D-H condition.

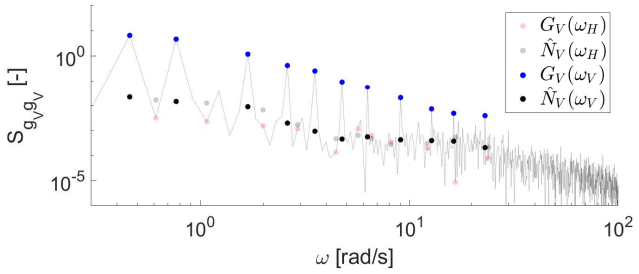

(b) 1D-V condition.

Fig. 16: Example power spectra of left horizontal and vertical gaze. Gaze $G_{H,V}$ and estimated noise $\hat{N}_{H,V}$ are indicated at $\omega_{H,V}$, where the transparent nodes indicate the excited frequencies of the perpendicular axis.

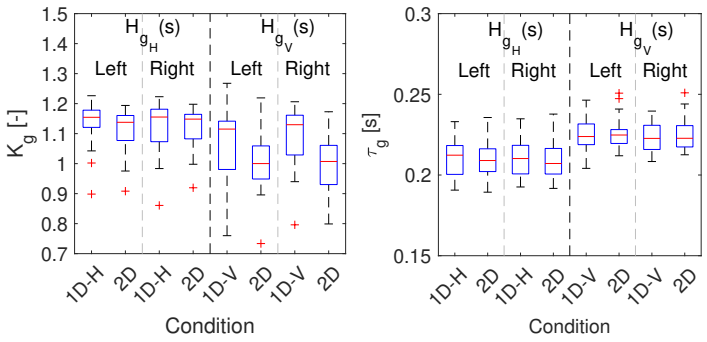

(a) Gain. (b) Time delay.

Fig. 17: Estimated parameters for M2-WR.

to the variability in saccade direction. The angle of inclination α appeared not to relate to cross-feed, but could be explained by other factors, such as blurred vision. The variation in directions in 1D conditions and difference in the number of lower and upper saccades in 1D-V condition indicates an oculomotor signature, discussed by Bargary et al. [37]. In that research, however, no inclinations of saccade patterns were observed nor mentioned, but different paradigms were applied. The number of saccades were consistent with earlier findings [17]. For two subjects, smooth pursuit was clearly superior towards either the upper or lower side, concluded from the differences in amounts of upward and downward saccades. For the saccade analysis, binocular gaze records were essential.

In the frequency-domain, a gaze dynamics model was fitted. This model consisted of a gain and time delay, and was fitted using the relative remnant as frequency-dependent weights. This model was selected as the neuromuscular system dynamics contribution to explaining the measurements was not convincing based on the influence of ω_g on the VAF, see Fig. 14.

It was expected that 1D and 2D gaze dynamics would be identical. However, frequency significantly lower K_g for vertical target stimuli (1D-V, 2D), but in general insignificant τ_g values were found, see Table VI, for the 2D condition, compared to 1D-H and 1D-V. Furthermore, both significantly lower K_g and τ_g were found for $H_{g_V}(s)$ in the 1D-V and 2D condition, compared to K_g and τ_g for $H_{g_H}(s)$. Lastly, for the left and right eye, insignificant differences were found for identical conditions. This indicates a difference in gaze dynamics for 1D-V and 2D conditions, which can be explained using Fig. 15. It can be seen that at high-frequency components of $\omega_{H,V}$ in the 1D-V condition, gaze dynamics were able to cope with high-frequency movements (Fig. 15c). For the 2D condition, where the movements of the target stimuli were more complex for the brain, this was not the case (Fig. 15d). For horizontal movements (Fig. 15a and 15b), this effect was less present, and therefore one can conclude that horizontal tracking has priority over vertical tracking near the bandwidth of the target forcing function. This can be explained as fewer muscles are involved [4], development asymmetry is present between horizontal and vertical smooth pursuit systems [38], [39], and due to the fact that horizontal movements are more common [17].

It was hypothesized that horizontal and vertical eye movements are independent. However, frequency analysis showed that there was cross-feed present in horizontal pursuit, i.e., $H_{g_{c_H}}(s) \neq 0$. For Subject 8, this effect turned out to be significant for the right eye, see Table VII. For vertical pursuit, little cross-feed was detected. Comparing cross-feed and eye dominance does not reveal a clear pattern, indicating these effects are independent. Frequency decomposition showed that the cross-talk was mostly present at the lower frequencies, degrading for higher frequencies. One type of eye movement relating to low-frequency movements is the OKR [40]. Its presence can be investigated by using a structured background [17], instead of a plain black background, although Collewijn and Tamminga [17] concluded that this inhibits both horizontal (∼10%) and vertical (∼20%) smooth pursuit. As the observed cross-feed in this research was mostly present in vertical movements, this could indicate that the brain partly uses the OKR to achieve smooth pursuit tracking at low-frequency target motions, as both types of eye movement have overlapping pathways [41], if a relation with the OKR can be found. The OKR dynamics can be investigated as well by using a pattern of multiple moving stimuli simultaneously according to the forcing function described in this research. Other types of eye movements are not examined in this research. However, the influence of vergence can be investigated by performing this experiment at different distances from the screen, but scaling the target size accordingly. Furthermore, torsional eye movements, which cannot be captured with the current eye-tracking method, might play a role as well. As cross-feed was different for left and right eye, binocular gaze records are necessary.

Different behavior was identified for the 1D and 2D vertical motion. This was clearly visible in Fig. 15. This could be

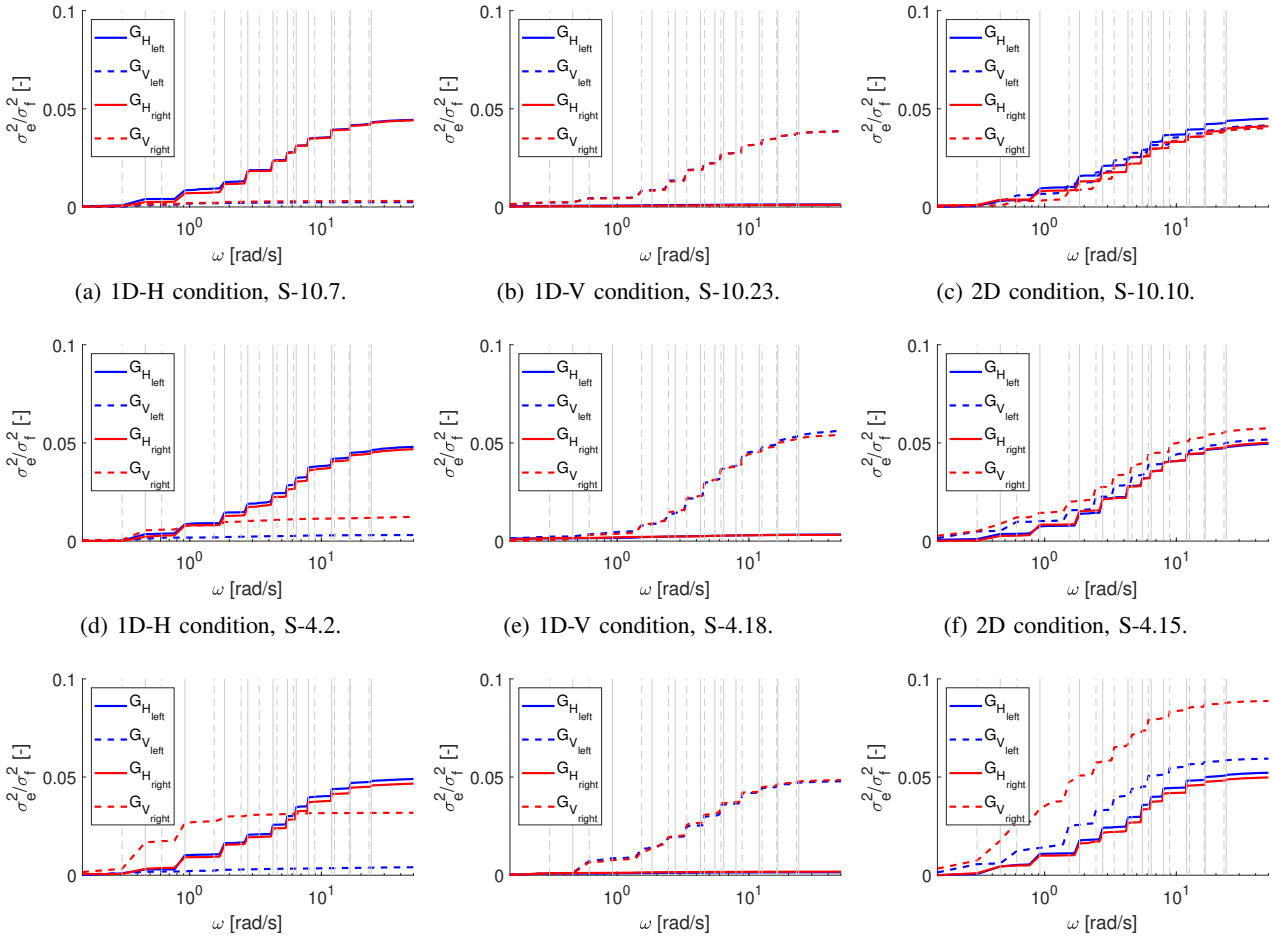

(a) 1D-H condition, S-10.7. (b) 1D-V condition, S-10.23. (c) 2D condition, S-10.10.

(d) 1D-H condition, S-4.2. (e) 1D-V condition, S-4.18. (f) 2D condition, S-4.15.

(g) 1D-H condition, S-8.10. (h) 1D-V condition, S-8.20. (i) 2D condition, S-8.7.

Fig. 18: Cumulative gaze performance over frequency, where ω_H and ω_V are indicated with solid and dashed gray lines, respectively. Variations in cross-feed severity is present. Subject and trial are indicated as S-X.Y, with subject ID X and trial number Y.

explained by the challenging task in horizontal and vertical direction simultaneously; the subject gives up to track high-frequency target motion in vertical direction, while at the 1D task, these frequencies can be tracked. Due to the more complex vertical eye movements, these will fail first. This was also visible in Fig. 14, where a distinct peak was absent for the 1D conditions, but was present, for some models, for the 2D condition. Therefore, one can conclude that the bandwidth of the forcing function should be increased to better identify the bandwidth of the neuromuscular part in 1D conditions. The amplitude could be increased such that a better fit and higher VAF scores can be found for ω_g, as this would increase task difficulty as well. This was applied by Büskens [23], where a clear contribution of the neuromuscular dynamics to the VAF was obtained, as a larger amplitude was applied.

For this gaze tracking task to become a suitable tool for the classification and quantification of neurodegeneration, some next steps can be performed. First of all, the target signal bandwidth should be increased, such that the neuromuscular dynamics are within the bandwidth, which includes parameters relating to neurodegeneration, as concluded by Büskens [23]. Secondly, saccadic events and other artifacts could be separated from smooth pursuit, such that it can be analyzed separately, as was done in earlier research [17], [24]. This could lead to additional parameters quantifying neurodegeneration. Thirdly, a structured background could be used to investigate the possible influence of the OKR. Finally, a longitudinal study should be performed investigating the effect of certain medical treatment doses within subjects on their gaze dynamics. In the meantime, gaze records can be obtained from both patients and controls to create a database.

V. Conclusions

To develop clinical tools to help classify and quantify neurodegeneration, 24 young, healthy adults participated in a pure gaze tracking task experiment. The goal of this experiment was to reveal differences in horizontal and vertical gaze dynamics and 1D and 2D tracking. In a within-subject design, three conditions were considered, where the stimulus was moving in quasi-random fashion in either horizontal, vertical or both screen directions. Binocular gaze records were obtained using video-oculography. Two independent target signals were used to be able to separate horizontal and vertical stimulus response in the frequency domain to detect cross-feed. A model consisting of a gaze gain and time delay, using the relative remnant as weights during parameter estimation, was considered to capture gaze behavior best for this particular tracking task.

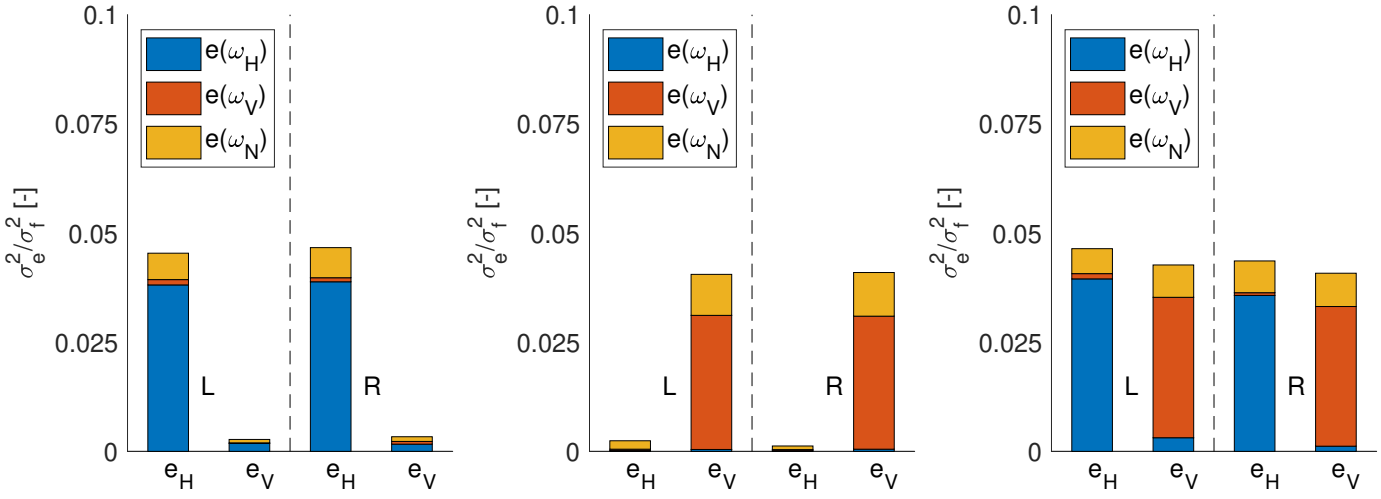

(a) 1D-H condition, S-10.7. (b) 1D-V condition, S-10.23. (c) 2D condition, S-10.10.

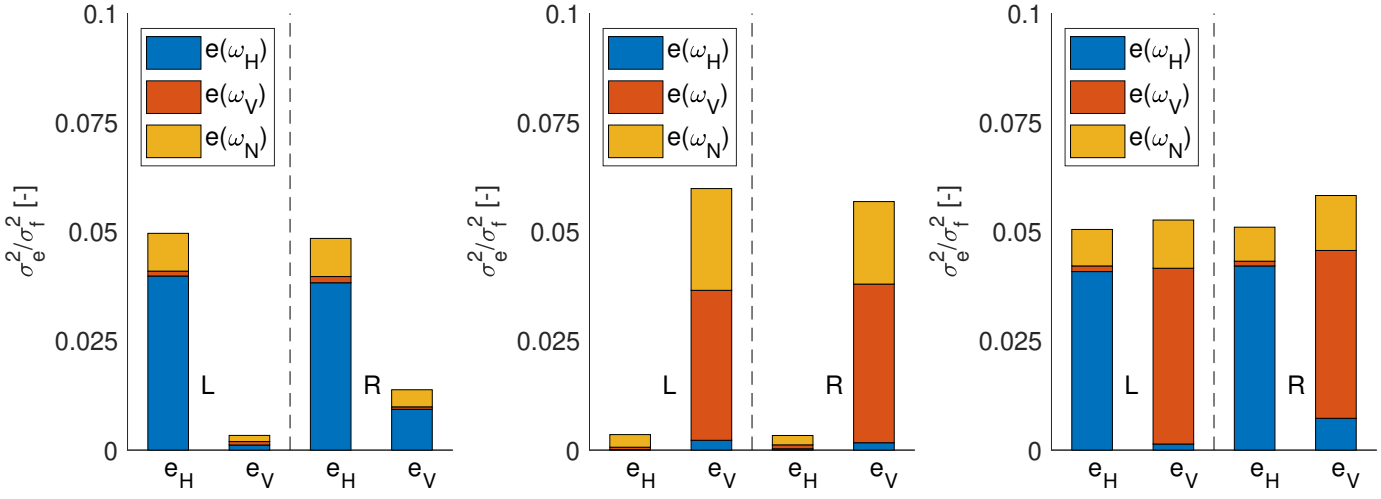

(d) 1D-H condition, S-4.2. (e) 1D-V condition, S-4.18. (f) 2D condition, S-4.15.

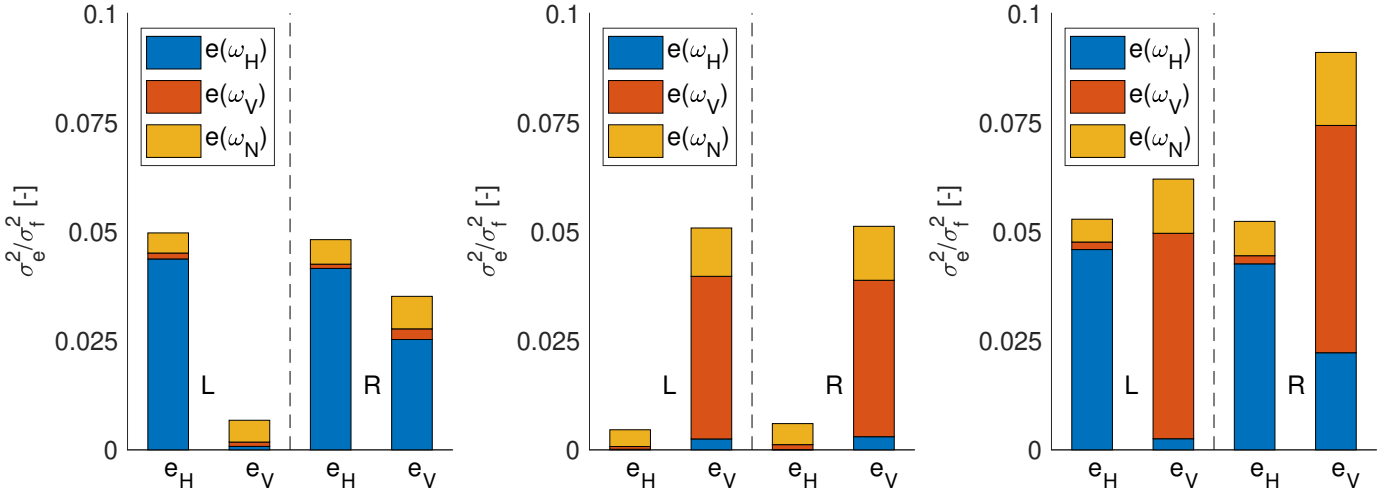

(g) 1D-H condition, S-8.10. (h) 1D-V condition, S-8.20. (i) 2D condition, S-8.7.

Fig. 19: Error signal e decomposition at different frequencies, where ω_N are all frequencies except $\omega_{H,V}$. e_H, e_V are the error in horizontal and vertical direction, respectively, shown for both the left L and right R eye. Subject and trials are matched with Fig. 18. Subject and trial are indicated as S-$X.Y$, with subject ID X and trial number Y.

Both in the 1D and 2D conditions, superior horizontal over vertical performance was found, 13% and 23%, respectively. Learning and fatigue effects were absent, indicated by a constant level of performance over trials. Furthermore, the amount of saccadic eye movements varied from 2 to 4 appearances per second. Different behavior was obtained comparing 1D and 2D conditions, which was attributed to the complexity of the target forcing function in the 2D condition. At high-frequency components of the target forcing functions, vertical gaze dynamics were not able to track the target, whereas it was able to in the 1D-V condition. Different gaze dynamics were obtained for horizontal and vertical gaze. Horizontal gain was in general higher; 4.9% comparing 1D-H and 1D-V, and 10.8% comparing 2D horizontal and vertical dynamics, respectively. Furthermore, vertical time delays were systematically higher than horizontal time delays; 7.3% comparing the 1D-H and 1D-V conditions, and 7.9% comparing the horizontal and vertical performance in the 2D condition. In general, vertical gaze due to cross-feed was detected at low-frequency (up to $\sim$3 rad/s) in the presence of a horizontal moving stimulus, both at the 1D-H and the 2D condition. To optimize this gaze tracking task, the number of trials could be halved, and the 2D condition will suffice to capture gaze dynamics. A target forcing function with a higher bandwidth should be applied to capture the bandwidth of the neuromuscular gaze dynamics. Furthermore, saccadic eye movements and pursuit should be separated, such that pure smooth pursuit dynamics can be obtained and analyzed. If one is not interested in cross-feed, monocular gaze records suffice for healthy controls. Binocular records are strongly recommended in any case if patients are used.

This research contributes to the development of novel paradigms to be used as clinical tools to assess neurodegenerative processes in humans, both healthy and impaired, by proposing a novel gaze pursuit tracking task evoking smooth pursuit and saccadic eye movements. Challenges remain in optimizing this task, and investigate other types of eye movements as well. If the full breadth of gaze dynamics can be modeled with a cybernetic approach, clinicians can use this tool to control and monitor neurodegeneration efficiently, increasing life quality of patients.

REFERENCES

[1] C. J. Erkelens, "Coordination of smooth pursuit and saccades", *Vision Research*, vol. 46, pp. 163–170, 2005.

[2] R. J. Krauzlis, "The Control of Voluntary Eye Movements: New Perspectives", *The Neuroscientist*, vol. 11, no. 2, pp. 124–137, 2005.

[3] R. J. Leigh and D. S. Zee, The Neurology of Eye Movements, 3rd ed., New York, NY, US: Oxford University Press Inc., 1999.

[4] D. Purves, G. J. Augustine, D. Fitzpatrick, W. C. Hall, A.-S. LaMantia, J. O. McNamara and S. M. Williams (Eds.), Neuroscience, 3rd ed., Sunderland, MA, US: Sinauer Associates, 2004, pp. 453–467.

[5] A. G. Shaikh and D. S. Zee, "Eye Movement Research in the Twenty-First Century - a Window to the Brain, Mind, and More", *The Cerebellum*, vol. 17, pp. 252–258, 2018.

[6] C. Kennard and R. J. Leigh (Eds.), Using saccades as a research tool in the clinical neurosciences, *Progress in Brain Research*, vol. 171, pp. 1–613, A Symposium in Honor of Jean Büttner-Ennever, 2008.

[7] K. Morita, K. Miura, M. Fujimoto, H. Yamamori, Y. Yasuda, M. Iwase, K. Kasai and R. Hashimoto, "Eye movement as a biomarker of schizophrenia: Using an integrated eye movement score" *Psychiatry and Clinical Neurosciences*, vol. 71, pp. 104–114, 2017.

[8] D. Tweed and T. Vilis, "Geometric Relations of Eye Position and Velocity Vectors During Saccades", *Vision Research*, vol. 30, no. 1, pp. 111–127, 1990.

[9] H. von Helmholtz, Handbuch der Physiologischen Optik, vol. 3, 1st ed., Hamburg: Voss, 1867. Third edition translated into English by J. P. C. Southall as *Helmholtz's treatise on physiological optics* (1925), Rochester NY: Optical Society of America.

[10] D. Tweed, T. Haslwanter and M. Fetter, "Optimizing Gaze Control in Three Dimensions", *Science*, vol. 281, pp. 1363–1366, 1998.

[11] E. M. Klier, H. Meng and D. E. Angelaki, "Three-Dimensional Kinematics at the Level of the Oculomotor Plant", *The Journal of Neuroscience*, vol. 26, no. 10, pp. 2732–2737, 2006.

[12] D. A. Robinson, "The Use of Control Systems Analysis in the Neurophysiology of Eye Movements", *Annual Review of Neuroscience*, vol. 4, pp. 463–503, 1981.

[13] D. A. Robinson, J. L. Gordon and S. E. Gordon, "A Model of the Smooth Pursuit Eye Movement System", *Biological Cybernetics*, vol. 55, pp. 43–57, 1986.

[14] C. Rashbass, "The Relationship between Saccadic and Smooth Tracking Eye Movements", *Journal of Physiology*, vol. 159, pp. 326–338, 1961.

[15] C. Bonnet, J. Hanuška, J. Rusz, S. Rivaud-Péchoux, T. Sieger, V. Majerová, T. Serranová, B. Gaymard and E. Růžička, "Horizontal and vertical eye movement metrics: What is important?", *Clinical Neurophysiology*, vol. 128, pp. 2216–2229, 2013.

[16] C. de Boer, "Visuomotor integration in neurodegenerative brains", PhD diss., Erasmus University Rotterdam, 2015.

[17] H. Collewijn and E. P. Tamminga, "Human Smooth and Saccadic Eye Movements During Voluntary Pursuit of Different Target Motions on Different Backgrounds", *Journal of Physiology*, vol. 351, pp. 217-250, 1984.

[18] D. C. Niehorster, W. W. F. Siu and L. Li, "Manual tracking enhances smooth pursuit eye movements" *Journal of Vision*, vol. 15, no. 11, pp. 1–14, 2015.

[19] D. T. McRuer and H. R. Jex, "A review of quasi-linear pilot models," *IEEE Transactions on Human Factors in Electronics*, vol. 8, no. 3, pp. 231–249, 1967.

[20] M. Mulder, D. M. Pool, D. A. Abbink, E. R. Boer, P. M. T. Zaal, F. M. Drop, K. van der El and M. M. Van Paassen, "Manual Control Cybernetics: State-of-the-Art and Current Trends", *IEEE Transactions on Human-Machine Systems*, 2017, doi: http://dx.doi.org/10.1109/THMS.2017.2761342.

[21] R. J. De Vries, *A Tracking Task for Quantifying Loss of Motor Skills due to Parkinson's Disease*, Master's thesis, Delft University of Technology, Faculty of Aerospace Engineering, 2016.

[22] Y. Haartsen, *Quantifying loss of motor skills after cerebellar stroke*, Master's thesis, Delft University of Technology, Faculty of Aerospace Engineering, 2017.

[23] J. Büskens, *Quantifying ageing effect on gaze dynamics*, Master's thesis, Delft University of Technology, Faculty of Aerospace Engineering, 2018.

[24] K. G. Rottach, A. Z. Zivotofsky, V. E. Das, L. Averbuch-Heller, A. O. Discenna, A. Poonyathalang and R. J. Leigh, "Comparison of Horizontal, Vertical and Diagonal Smooth Pursuit Eye Movements in Normal Human Subjects," *Vision Research*, vol. 36, no. 14, pp. 2189-2195, 1996.

[25] S. Barendswaard, D. M. Pool, M. M. Van Paassen and M. Mulder, "Dual-Axis Manual Control: Performance Degradation, Axis Asymmetry, Crossfeed, and Intermittency", *IEEE Transactions on Human-Machine Systems*, vol. 49, no. 2, pp. 113–125, 2019.

[26] W. Dai, I. Selesnick, J.-R. Rizzo, J. Rucker and T. Hudson, "A nonlinear generalization of the Savitzky-Golay filter and the quantitative analysis of saccades", *Journal of Vision*, vol. 9, no. 10, pp. 1–15, 2017.

[27] R. Zemblys, D. C. Niehorster, O. Komogortsev and K. Holmqvist, "Using Machine Learning to Detect Events in Eye-tracking Data", *Behavior Research Methods*, vol. 50, pp. 160–181, 2018.

[28] P. M. T. Zaal, D. M. Pool, J. De Bruin, M. Mulder and M. M. Van Paassen, "Use of Pitch and Heave Motion Cues in a Pitch Control Task," *Journal of Guidance, Control, and Dynamics*, vol. 32, no. 2, pp. 366-377, 2009.

[29] H. J. Damveld, G. C. Beerens, M. M. Van Paassen and M. Mulder, "Design of Forcing Functions for the Identification of Human Control Behavior," *Journal of Guidance, Control, and Dynamics*, vol. 33, no. 4, pp. 1064-1081, 2010.

[30] J. Büskens, J. J. M. Pel and D. M. Pool, "Effects of Multisine Signal Bandwidth on Eye Movement Dynamics", *Proceedings of the 14th IFAC/IFIP/IFORS/IEA Symposium on Analysis, Design, and Evaluation of Human-Machine Systems, Tallinn, Estonia*, 2019.

[31] D. B. Liston, A. E. Krukowski and L. S. Stone, "Saccade detection during smooth tracking", *Displays*, vol. 34, pp. 171–176, 2013.

[32] S. Stuart, A. Hickey, R. Vitoria, K. Welman, S. Foo, D. Keen and A. Godfrey, "Eye-tracker Algorithms to Detect Saccades during Static and

Dynamic Tasks: A Structured Review", *Physiological Measurement*, vol. 40, no. 2, 2019.

[33] D. T. McRuer, D. Graham, E. S. Krendel and W. J. Reisener, "Human Pilot Dynamics in Compensatory Systems, Theory Models and Experiments with Controlled Element and Forcing Function Variations," Air Force Flight Dynamics Laboratory, Wright-Patterson Air Force Base (OH), Wright-Patterson AFB (OH), Technical Report AFFDL-TR-65-15, 1965.

[34] M. Ahmadi, J.-X. Liu, T. Brännström, P. M. Andersen, P. Stål and F. Pedrosa-Domellöf, "Human Extraocular Muscles in ALS", *Investigative Ophthalmology & Visual Science*, vol. 51, no. 7, pp. 3494–3501, 2010.

[35] F. M. Nieuwenhuizen, P. M. T. Zaal, M. Mulder, M. M. Van Paassen and J. A. Mulder, "Modelling Human Multichannel Perception and Control Using Linear Time-Invariant Models", *Journal of Guidance, Control and Dynamics*, 2008.

[36] C. L. Shumway, M. Motlagh and M. Wade, Anatomy, Head and Nec, Eye Medial Rectus Muscles, https://www.ncbi.nlm.nih.gov/books/NBK519026/: StatPearls Publihing LCC, 2019.

[37] G. Bargary, J. M. Boston, P. T. Goodbourn, A. J. Lawrance-Owen, R. E. Hogg and J. D. Mollon, "Individual differences in human eye movements: An oculomotor signature?", *Vision Research*, vol. 141, pp. 157–169, 2017.

[38] H. Grönqvist, G. Gredebäck and C. Von Hofsten, "Developmental asymmetries between horizontal and vertical tracking", *Vision Research*, vol. 46, no. 11, pp. 1754 - 1761, 2006

[39] I. Ingster-Moati, L. Vaivre-Douret, E. Bui Quoc, E. Albuisson, J.-L. Dufier and B. Golse, "Vertical and horizontal smooth pursuit eye movements in children: A neuro-developmental study", *European Journal of Paediatric Neurology*, vol. 13, pp. 362–366, 2009.

[40] G. Schweigart, T. Mergner, I. Evdokimidis, S. Morano and W. Becker, "Gaze Stabilization by Optokinetic Reflex (OKR) and Vestibulo-ocular Reflex (VOR) During Active Head Rotation in Man", *Vision Research*, vol. 37, no. 12, pp. 1643–1652, 1997.

[41] C. K. Schraa-Tam, A. Van Der Lugt, M. Smits, M. A. Frens, P. C. Van Broekhoven and J. N. Van Der Geest, "Differences between smooth pursuit and optokinetic eye movements using limited lifetime dot stimulation: a functional magnetic resonance imaging study", *Clinical Physiology and Functional Imaging*, vol. 29, no. 4, pp. 245–254, 2009.

Part II:

Preliminary report

2

Introduction

For humans to perform daily tasks, such as riding a bike or grabbing some cutlery, the central nervous system (CNS, fig. 2.1) of the human body plays a major role as the center of decision and communication for muscle activation, and hence performing the action. These muscles should be activated at the correct time, with the correct amplitude, to generate the intended movement. However, due impairment of the CNS, these simple daily tasks can become daily challenges.

The CNS impairment can have several causes. One could think of a lesion due to an impact or collision, or simply due to aging. The damage can result in neurodegeneration, which is the dead of neurons or their pathways. Unfortunately, these neurons cannot be repaired, hence this is an irreversible process. Moreover, this can result in well known diseases, such as Alzheimer's disease or Parkinson's disease. Though, precise knowledge on the exact origin of these disease is still lacking.

Current medical knowledge about these disease allow diagnosis, yet not at an early stage. Moreover, quantitative measures of disease specific effects are lacking (De Boer 2015). At the moment, clinicians mostly rely on (subjective) feedback from patients and a trial-and-error based approach to define the medication dose, instead of using a data driven approach. Therefore, new tools should be evaluated to provide additional grips for clinicians in diagnosing patients, and for better understanding neurodegenerative processes.

As functional magnetic resonance imaging allows to pinpoint certain locations in the brain relating to certain actions, knowledge on the interconnection of neural brain networks is expanding rapidly. Apparently, a significant part of the human brain is involved in visual information processing, merely overlapping with neural networks related to neurodegenerative diseases (De Boer 2015). As many abnormalities in eye movements are distinctive and point to certain locations or disturbances in the CNS (Leigh & Zee 2006), the impairment of vision and oculomotor performance could reveal valuable clues to identify and quantify neurodegeneration in various stages of neurodegenerative processes.

In a joint effort to improve diagnostic methods by investigating novel clinical tools, the department of Neuroscience of the Erasmus Medical Center in Rotterdam and the faculty of aerospace engineering of the Technical University of Delft collaborated to investigate certain neurodegenerative diseases. This hybrid approach has thus far contributed to research involving quantification of loss of motor skills due to Parkinson's disease (De Vries 2016) and Cerebellar stroke (Haartsen 2017). This is done by evaluating a manual tracking task. From this, the human control dynamics can be caught in a mathematical model. This so-called 'cybernetic approach' is introduced by McRuer & Jex (1967). This model induces quantification, and by comparing the model parameters of patients and controls more insight in neurodegenerative processes is obtained.

These tools merely focus on eye-hand coordination and on manual control identification, rather than oculomotor control. Yet, Büskens (2018) has provided a first step in oculomotor analysis by investigating gaze performance due to aging of healthy adults. However, the

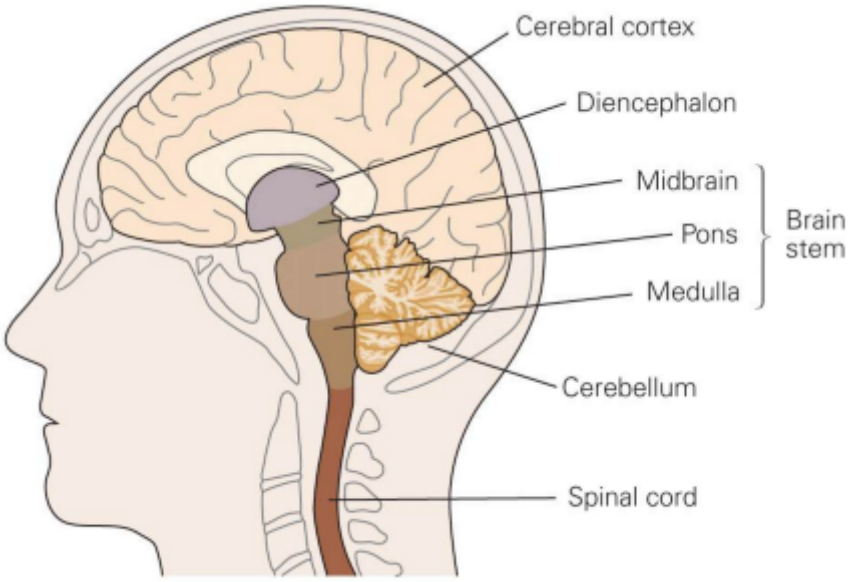

Figure 2.1: The CNS consists of the brain and the spinal chord (Kandel et al. 2000).

research from Büskens (2018) lacks information on the differences and interaction of horizontal and vertical eye movements. This gap of knowledge is the main focus of this research, and accordingly an objective is established:

Investigate the interaction and performance of horizontal and vertical smooth pursuit eye movements using a tracking task and system identification methods.

This study serves as a preliminary study, containing background information and state-of-the-art research of relevant material for aforementioned objective. First, a brief introduction of the eye and its movements is presented in section 3.3. Then, two generic methods for analyzing oculomotor performance are stated. The first one (chapter 4) is a frequency-domain method, and the second one (chapter 5) is a time-domain method, which includes a pilot study of gaze learning effects in a gaze tracking task based on gaze records from Büskens (2018). Lastly, in chapter 6 a research experiment is proposed based on the frequency method, to investigate the interaction of horizontal and vertical eye movements, and a verification experiment is proposed, to close the gap with Büskens (2018).

3

Eye movements

In this chapter are eye movements, or gaze, examined in detail. The purpose of this chapter is to identify certain types of eye movements. It should provide answers to questions on what eye movements are relevant to be analyzed, and how they can be analyzed. Furthermore, by identifying the neuronal pathways of eye movements, deficits in eye movements can be related to certain impaired brain areas. This information can be valuable when performing research to neurodegenerative diseases, or serve in diagnostic processes.

But why is investigating eye movements critical for this type of research? Section 3.1 elaborates on this question. Then, in section 3.2 the muscles responsible for moving the eye are briefly discussed. Hereafter, eye movements are classified in section 3.3 based on their functionality, and their relevance regarding tracking tasks is evaluated. A more detailed description is provided by investigating the neuronal pathways in section 3.4. Lastly, some additional remarks on the eyes are made, which can influence gaze tracking. Note that this chapter is mostly based on work from Kandel et al. (2000) and Leigh & Zee (2006), besides stated otherwise.

3.1. Why study eye movements?

Before diving into theory regarding the eye and its movements, first the benefits of investigating eye movements are clarified. Three main reasons are distinguished.

The first reason to study eye movements, is that eye movements reveal clues for understanding and localizing diseases, which can help in a clinical setting. As simple as it may seem, eye movements are the motor system of our visual world. We cannot see and understand our world around us without making eye movements. And although, moving two equally shaped eye balls with constant masses is quite straightforward, the neurological pathways involved are quit complex and vulnerable for all kinds of impairments. Thus, one of the first tests that patients often undergo are the pencil test and the pupil test.

At the pencil test, a pencil or similar object is moved 30 cm from the eye. The patient has to follow the pencil, such that the clinician can examine the functioning of the extra-ocular muscles. If a patient shows abnormal behaviour, the clinician can define possible causes of the problem, based on the muscle which is abolished. In this way, valuable information can be obtained with limited resources.

The pupil test involves the investigation of the pupillary reflex. By checking each eye independently while shining a light in the eye, the pupil should contract, and dilate again when removing the light. The other eye should exhibit the same contraction and dilution as the lighted eye.

Impaired brain regions or, more specifically, certain nuclei, have specific consequences on eye movement behaviour. Investigating these helps clinicians diagnosing accurately with limited resources, as the impairment or abolishing of eye movements are distinctive and often

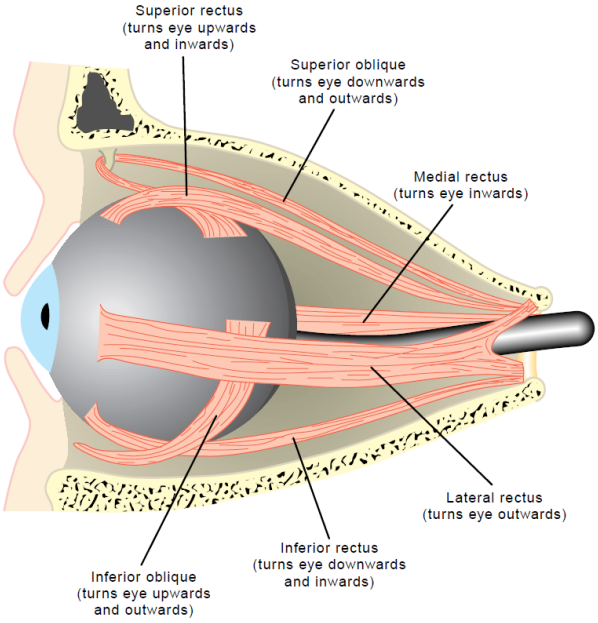

Figure 3.1: Six extra-ocular eye muscles are divided in three antagonistic pairs, shown here in a cutaway view of the (left) eye in its socket, or orbit (Squire et al. 2008).

point to specific regions in the brain.

Secondly, eye movements are fairly easy to be analyzed in a quantitative manner compared to other movements, for example body-limb movements. The first of three main reasons for this, is that eye movements are restricted to rotations only, as translations are negligibly small, and they move in a linear fashion.

Secondly, different eye classifications can be distinguished, as is explained in section 3.3. In this way, certain characteristic features for every class can be distinguished.

Lastly, eye movements are very accessible and readily available in all kinds of environments or test setups for observation. Furthermore, the current standards of eye tracking devices include portable solutions, which provides more freedom in gathering gaze data.

The last benefit of investigating eye movements is that activities related to eye movements can be found in a large variety of neural brain networks, which are spread all over the brain. This means that numerous brain related problems can be identified by the impairment of eye movements.

In section 3.4 these regions are discussed, and some of them are described in more detail. However, first one must understand the muscles involved for generating eye movements. This is explained in next section.

3.2. Extra-ocular eye muscles

The eye can be moved by rotations around three axis, made possible by three antagonistic pairs of extra-ocular muscles. These pairs are the superior and inferior rectus, superior and inferior oblique, and medial and lateral rectus. A schematic view is shown in fig. 3.1. These muscle pairs should overcome two major force components to move the eye to its new position, which are the viscous drag and elastic restoring forces imposed by the orbital supporting tissues.

Besides antagonistic pairs, one can define yoked muscle pairs. These are pairs of muscles, one member for each eye, that invoke eye movements in the same direction, according to Hering's law of equal innervation. This means that the lateral rectus of one eye, and medial rectus of the other eye, are a yoked muscle pair. Similarly, the superior rectus is yoked with the superior oblique of the other eye, and the inferior rectus is yoked with the inferior oblique

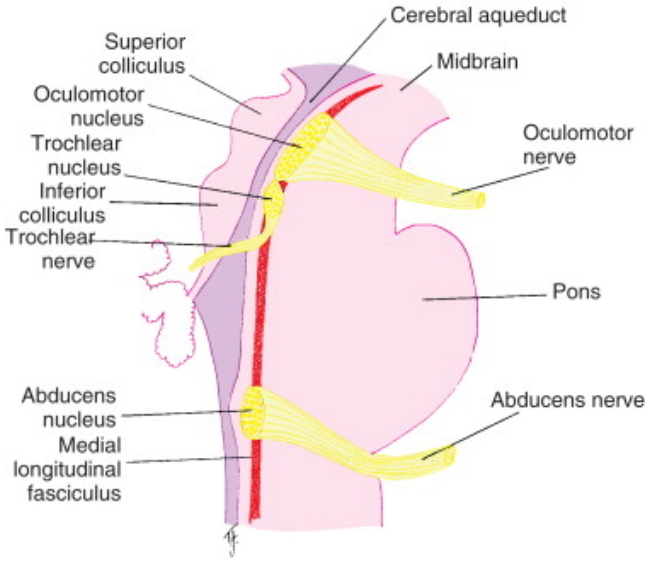

Figure 3.2: Schematic view of the locations of the oculomotor, trochlear and abducens nuclei (Remington 2012).

of the other eye.

The lateral and medial rectus are responsible for the horizontal eye movements, i.e. abduction (temporal) and adduction (nasal). For vertical (elevation and depression) and torsional (intorsion is the rotation of the top of the eye towards the nose, extorsion vice versa) eye movements, the other four muscles are mainly involved.

Vertical eye movements are induced by the vertical recti and oblique muscles. Their contribution for elevation and depression depends on the angular state of the eye. If the eye is more adducted, elevation is dominated by the inferior oblique, while depression is dominated by the superior oblique. Contrary, when the eye is more abducted, the inferior and superior rectus are more dominant.

The sixth extra-ocular muscle is responsible for moving up the upper eyelid. However, this muscle is not included in the scope of this research, as it has no influence on eye position.

The muscles are controlled by motor neurons from three different nuclei, which are the oculomotor, abducens and trochlear nucleus. The abducens and trochlear nuclei control the lateral rectus (for abductive movements, hence its name) and superior oblique respectively, while the oculomotor nerve controls the other ocular muscles. Note that this is not according to the horizontal and vertical partitioning, meaning that an impairment of the oculomotor nucleus can have influence on both horizontal and vertical eye movements. When performing the eye-muscle test as mentioned earlier, a patient with this abolished oculomotor nucleus will have trouble to move the eyes nasally.

Two of each aforementioned nuclei are present, one for each eye. The oculomotor and troclear nuclei are situated in the midbrain, while the abducens nuclei are situated in the pons, see fig. 3.2. The trochlear nuclei have contralateral connections, while the others have ipsilateral connections. This means that the right trochlear nuclei projects to the left eye, while the right abducens and oculomotor nuclei project to the right eye. Various connections in the human body are contralateral, for example the left visual field of both eyes is processed in the right part of the visual cortex.

Before taking a more detailed look at the generation of these oculomotor signals, eye movements are classified based on their functionality to filter relevant eye movements for this research.

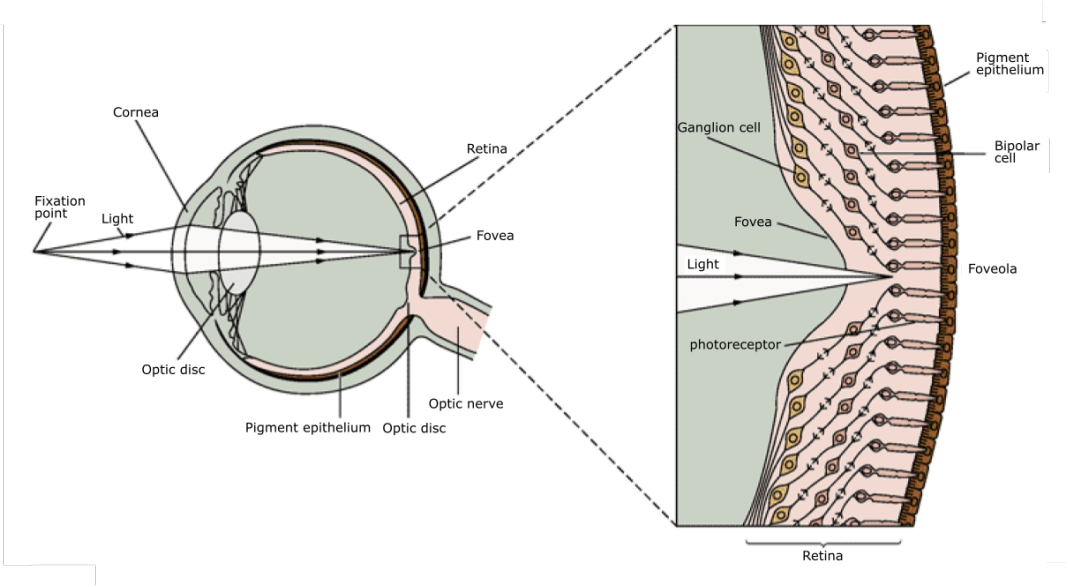

Figure 3.3: The eye with a detailed view of the region around the fovea. Light passes trough the cornea and optic disc to reach the fovea, where it proceeds through different nerve cells, after which is its processed by photoreceptor cells (Kandel et al. 2000).

3.3. Classification of eye movements

As mentioned in the introduction of this chapter, a critical advantage of studying eye movements is their ability to be quantified. To support quantification, different classes of eye movements are distinguished. Quantification is critical for objective diagnoses in a clinical setting.

In this chapter, a commonly used classification is introduced, which is a function-based classification. It is divided in gaze stabilizing and gaze shifting functions. An introduction of several type of eye movements based on this classification is provided. For the ones relevant for this research, a more thorough one is delivered in section 3.4.

3.3.1. Gaze stabilizing eye movements

From a biologic historical point of view, the most important function of the eye is to keep an image still on the retina, as the fovea had not yet developed (see fig. 3.3). The retina is the part of the eye where light is captured by photo-receptor cells. These can be either rods (sensible to light) or cones (sensible to color). The light and color information from the retina is sent to the brain to create an image.

Cones are critical for a high acuity image, but their density at the retina is generally low, hence the eye should be fixed or stabilized with respect to the environment to create a (low acuity) image. To achieve this stability, the vestibulo-ocular reflex (VOR) and optokinetic reflex (OKR) filter out self-motion and environmental motion respectively.

The OKR and VOR cover the whole range of motion frequencies to achieve this. The OKR uses visual input, which has a relatively slow feedback loop, to generate a compensating movement, usually a nystagmus. A nystagmus can be considered as a repeated process of a slow drift of the eyes, followed by a fast recovering eye movement to the (new) target. The OKR is very efficient in repeated patterns in environmental scenes. It can be triggered by self motion and/or environmental motion. It usually covers the low frequency movements.

The VOR covers movements from self motion. It uses the vestibular system, a fast feedback loop, as its input source to generate smooth eye movements opposing head motion. This reflex allows to maintain sharp vision on a stationary target while undergoing self motion. A simple test to demonstrate the speed of the VOR system is by swinging the tip of a finger quickly at an arm length with fixated head, and compare this to the same swing of head while

fixating the finger. One would see that the visual feedback loop (tracking the moving finger) is not able to follow the finger accurately, while the vestibular feedback loop (counteracting head movements) is.

3.3.2. Gaze shifting eye movements

However, with the development of the fovea, a second function of eye movements arose. The fovea, an area with a high density of photo-receptors (see fig. 3.8) on the retina in humans and certain animals, enables high acuity images. Though, this requires the fovea to be directed at specific targets, which is not efficient using gaze stabilizing eye movements only. Therefore, gaze shifting properties are necessary. These gaze shifting type of eye movements are smooth pursuit (SP) and saccadic eye movements.

SP eye movements are induced by a continuously moving target on the retina. The purpose of SP is to follow this moving target along its path. Using a visual feedback loop, the eye velocity is matched with the target velocity, which is determined at different regions of the visual cortex in the brain. Targets with velocities up to 100 deg/s can be tracked, with a latency of approximately 130 ms.

Fixation was long considered as a special case of SP, where the target velocity equals zero. However, it appears to be a dynamic process (Krauzlis et al. 2016). The visual fixation system is different than the SP system, and it actively suppresses eye movements to enhance fixation. However, the eyes are not completely fixed. Instead, very small eye movements are generated to avoid saturation of the photo-receptors.

Saccades are very rapid eye movements, generated to bring an objects of interest from the retina into the fovea. Saccades are mainly used to quickly scan an environment, or for example while reading. Humans generate approximately three saccades every second while awake (Bargary et al. 2017).

These type of eye movements are extremely fast, they can reach velocities up to 900 deg/s. Therefore, their duration is usually short. The saccade has a ballistic nature, meaning it is not possible to adjusts its trajectory once started. As a result, follow-up saccades might be necessary to converge to the target.

The latency of saccades is about 200 ms. However, this latency is valid for the initial saccade. The follow up saccades, or express saccades, have shorter latency, down to 20 ms. These corrective saccades are automatically made if SP fails.

Another revolutionary aspect is involved in gaze shifting eye function. The development from monocular vision to binocular vision enabled the perception of a three dimensional environment, and required vergence eye movements, such that the target falls on both retinas for high acuity vision.

Convergence is the movement of the pupils to each other, while divergence is the movement of the pupils away from each other. Convergence is applied when fixating on a nearer target, while divergence is applied when fixing on a target farther away. Convergence is highly linked with changing the ocular lens shape, or accommodation, and pupil size. This type of eye movement is different from other eye movements in the fact that the eyes do not rotate in the same direction (conjugate), but in opposite direction (disconjugate).

3.3.3. Voluntary eye movements

Six types of eye movements are discussed based on a function-based classification. These are the SP, fixation, saccades, vergence, OKR and VOR. Other classifications are voluntary and involuntary, or reflexive, eye movements. The voluntary eye movements are the SP, saccadic and vergence eye movements. The reflexive eye movements are the OKR and VOR. Fixation could be parted in both classes, as one voluntarily fixates at a target, but involuntarily microsaccades are created to compensate for saturation effects. In this research, only voluntary eye movements are considered to limit the scope.

3.3.4. Relevant eye movements

Tracking tasks as described by De Vries (2016), Haartsen (2017) and Büskens (2018) use multisine input signals. For these type of input signals, SP (and catch-up saccades) are the most relevant type of eye movements. SP eye movements are mostly used while following a continuously moving target. And if SP fails, a catch-up saccade should be made towards the target.

The VOR requires self-motion or environmental motion, which induces several implications for experiment design. One could think of a moving platform, which induces complexity and costs.

To trigger the OKR, an environmental motion system could be developed. This is easily achieved when a repeated pattern moves across a computer screen. However, the tracking task used by De Vries (2016), Haartsen (2017), Büskens (2018) have quasi-random target signals. For this, the OKR is not suitable, as constant patterns should be used.

Vergence eye movements can be interesting as well for this type of research, for example by using a haploscope. This is a device which manipulates the distance between the eyes. In this way, depth perception and relative vergence changes. This means that the eyes should be converted more compared to the normal condition if an object is brought nearer. This type of research could be relevant for using depth perception on a 2D computer, or using virtual reality. However, it is decided to SP eye movements in this research.

Concluding, the focus in this research put on voluntary SP and corrective saccadic eye movements. The next section describes the pathways of the signals to create SP and saccadic eye movements.

3.4. From stimulus to eye movement

Previous section concluded that SP and saccadic eye movements are most suitable to be analyzed. As their definition is clear, a closer look is taken to the path of their (motor) signals, the neuromachinery, which control the extra-ocular eye muscles to generate these type of eye movements.

In this section, both movements are described in detail, starting at the appearance of a (moving) stimulus, all the way to a voluntarily generated eye movement. The stimulus can be anything to catch the attention of the participant. This does not have to be a visual target, but can for example also be a sound. To keep the amount of variables limited in this research, a visual stimulus is used, being a simple shape on a solid background with a different color.

As the generation of eye movements is the focus of this research, some visual processes are described less thoroughly. Furthermore, the cognitive aspect is omitted entirely.

3.4.1. Visual pathways

As light passes through the eyes to reach the retina, photo-receptor cells convert the information of light into action potentials while passing several different cell layers. Then, this information, of each eye independently, reaches the lateral geniculate nucleus (LGN) of the thalamus via the optic nerve and optic chiasm, see fig. 3.5. The thalamus projects to the primary visual cortex, the first stage of visual information processing. The visual information is projected in this cortex such that a map of sight is created using neuronal signals.

The primary visual cortex (V1) is a subarea of the visual cortex, a spatial map of human's sight in the back of the brain, which consists of a striate and extrastriate cortex. The primary visual cortex is part of the striate cortex, while the other visual areas (V2, V3, V4 and V5) are part of the extrastriate cortex. These areas are interconnected in various ways to process visual information.

However, the retina also projects to the frontal eye field (FEF), the supplemental eye field (SEF) and the superior colliculus (SC), another spatial map of sight, where the two colliculi represent each half of the visual field. The colliculi consist of several layers, of which the deeper layers contain neurons related to the activation of eye movements.

From here, the SP and saccadic eye movements take different neuronal paths. First, saccades are discussed, followed by SP. Before continuing on their pathways, first the motor signals for extra-ocular muscles to create these eye movements are shortly explained.

3.4.2. Neuronal activity

Three different neurons play a crucial role to regulate the contraction of the eye muscles. These are the tonic neurons, omnipause neurons and burst neurons.

The eye muscles from section 3.2 are constantly innervated by tonic neurons. The tonic neurons have two important functions, which is moving the eye smoothly by changing their fire rate, and keeping position in the new state by fixating their fire rate. The latter is needed to maintain the muscular strength to withstand elastic restoring forces. If the eye rotates towards the origin of the muscle, viscous drag and additional elastic forces are counteracting, hence a higher tonic pulse is needed.

For the antagonistic pairs, this means that if in the agonist muscle the fire rate decreases, the antagonist fire rate increases, and vice versa. For example, if the left eye should be moved to the left, the tonic fire rate in the abducens nucleus of the left eye should increase, and in the medial rectus of the left eye should decrease.

On the other hand, for yoked muscle pairs the opposite is true. Considering previous example, the tonic fire rate in the abducens of the left eye and the medial rectus of the right eye increase. And according to previous paragraph, in the antagnostic yoked musle pair, the fire rates of the abducens muscle of the right eye and medial rectus of the left eye decreases.

However, if using just this change in fire rate to move the eye, eye movements would be very slow due to the sluggish behaviour of the eyeball. Therefore, the fire rate should be very high for a short period of time. Here, the burst neurons come into play. This type of neuron is responsible for the fast movement of the eye, having a very high firing rate, to move the eye quickly to its new position: The saccade.

3.4.3. Saccades

Two types of burst neurons are present, which are long lead burst neurons (LLBN) and (medium lead) burst neurons (BN). The first type of burst neurons announce a saccade by building up neuronal activity, reducing saccade latency, as explained by Munoz & Fecteau (2002). This type of neuron is highly present if a saccade is expected, for example in the gap paradigm. In this paradigm, subjects focus on a steady dot in the center of the screen. At some point, the dot disappears, and after a short interval a new dot appears at a random location in the peripheral field, towards a saccade should be made.

The latter type of burst neurons are the actual burst neurons defining the saccade. These burst neurons are generated in the paramedian pontine reticular formations (PPRF) and rostral interstitial nucleus of the medial longitudinal fasciculus (miMLF) for horizontal and vertical/torsional saccades respectively. The PPRF is located in the pons, while the riMLF is located in the brainstem.

Burst neurons are constantly available for saccades in all directions. However, if the eye should handle all these saccades, vision would become very chaotic. To prevent this, omnipause neurons play a crucial role. Like the tonic neurons, omnipause neurons fire at a constant rate, which serves to block all burst neurons. Only if a saccade should be made, the omnipause neurons stop firing just before and during a saccade, letting the burst neurons pass to generate the saccade. Hence, omnipause neurons tonically inhibit all burst neurons.

A neural integrator, the interstitial nucleus of Cajal, integrates the outcome of all the neurons, the motor signal, to determine the new eye position. This information is fed back to the tonic neurons. They adjust the fire rate accordingly to maintain the new position.

A sketch of neuronal firing activity is shown in fig. 3.4 for a extra-ocular muscle which should be more contracted. The omnipause neurons stop firing to evoke a saccade. The actual saccade signal is present in the BN, during which the eye velocity peak is reached. The fire rate is increased of the tonic neurons after the saccade from the integration of the BN signal, hence the muscle is more contracted at the new eye position. The complete motor signal for the extra-ocular muscle is represented with the OMN in fig. 3.4. Note that omnipause neurons have a constant fire rate.

A simplified model of the horizontal and vertical (pre)motor saccadic pathways are shown in fig. 3.5. A short loop is present to create conjugate eye movements for the agonist and

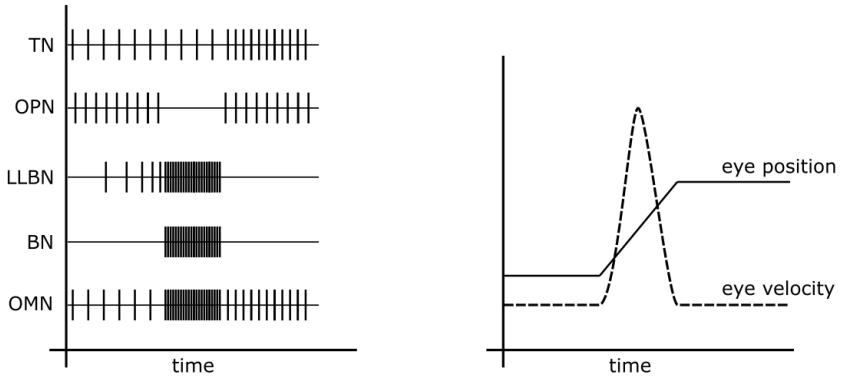

Figure 3.4: Schematic overview of neuronal activity for saccadic eye movements. On the left, the fire rates of the tonic neurons (TN), burst neurons (BN) and omnipause neurons (OPN) together form an oculomotor neuronal (OMN) command. The long-lead burst neurons (LLBN) 'announce' a saccadic burst. On the right, the resulting eye position and velocity profiles are shown as a result from the OMN activity.

antagonist muscle, which need excitatory and inhibitory signals to increase and decrease their fire rates respectively. The SC inhibits LLBN to inhibit ON, which is the gap in ON from fig. 3.4. This causes excitatory burst neurons (EBN) of the PPRF and riMLF to start firing. The LLBN and fastigial nucleus of the cerebellum excite inhibitory burst neurons (IBN) of the antagonist muscle. The IBN inhibits contralateral EBN, which inhibits the contralateral IBN of the antagonist muscle at this side. Hence, a conjugate eye movement is created.

The role of the cerebellum is more or less understood in this process, as it manages the termination of saccades via the fastigial nucleus. Furthermore, copies of oculomotor commands reach the cerebellum via the SC, which are integrated here as well to determine eye position. In this way, the cerebellum plays an important role for the accuracy of saccades. However, precise knowledge on neuronal pathways and processing of oculomotor commands in the cerebellum is lacking (Voogd & Barmack 2006).

The SC and FEF seem complementary to each other, but the generation of saccades is still possible if either one is abolished (Munoz & Fecteau 2002). Furthermore, the centers seem to generate different types of saccades (Purves et al. 2004). Types of saccades are the regular saccade, express saccade and anti-saccade. Express saccades are follow-up/catch-up saccades to converge to a target. They have a shorter latency than regular saccades. Regular and express saccades are pro-saccades, or a saccade towards the target. Anti-saccades, however, are saccades made in opposite direction of a target. In this paradigm, the subject has to both suppress and mirror a saccade to the visual target (Munoz & Fecteau 2002). In this research, catch-up saccades are expected to be mostly present.

The SC does not only generate saccade commands based on visual inputs, but also on other inputs, for example auditory inputs (Zambarbieri 2002). This is shown via the connections of the SC with the basal ganglia in fig. 3.5, and connections with the thalamus. However, this is out of the scope of this research.

3.4.4. Smooth pursuit

Historically, the SP and saccadic systems were treated as separate systems (Krauzlis 2005). However, as can be seen while comparing fig. 3.5 and fig. 3.7, overlap exists, as indicated by Krauzlis (2005). Many cortical and cerebellar regions play a role in both voluntary SP and saccadic eye movements, as can be seen in fig. 3.6.

SP eye movements are voluntary and, therefore, mostly initiated in the cerebral cortex. Retinal information proceeds from the visual cortex to the middle temporal area (MT) and medial superior temporal area (MST). These areas determine the speed and direction of the target (Missal & Heinen 2017). From here, two different streams descent to the vestibular nuclei, as can be seen in fig. 3.7 (Fukushima et al. 2013).

One path leads via the dorsolateral pontine nuclei (DLPN) and the floccular complex in the cerebellum. The other pathway leads via the nucleus reticularis tegmenti pontis (NRTP)

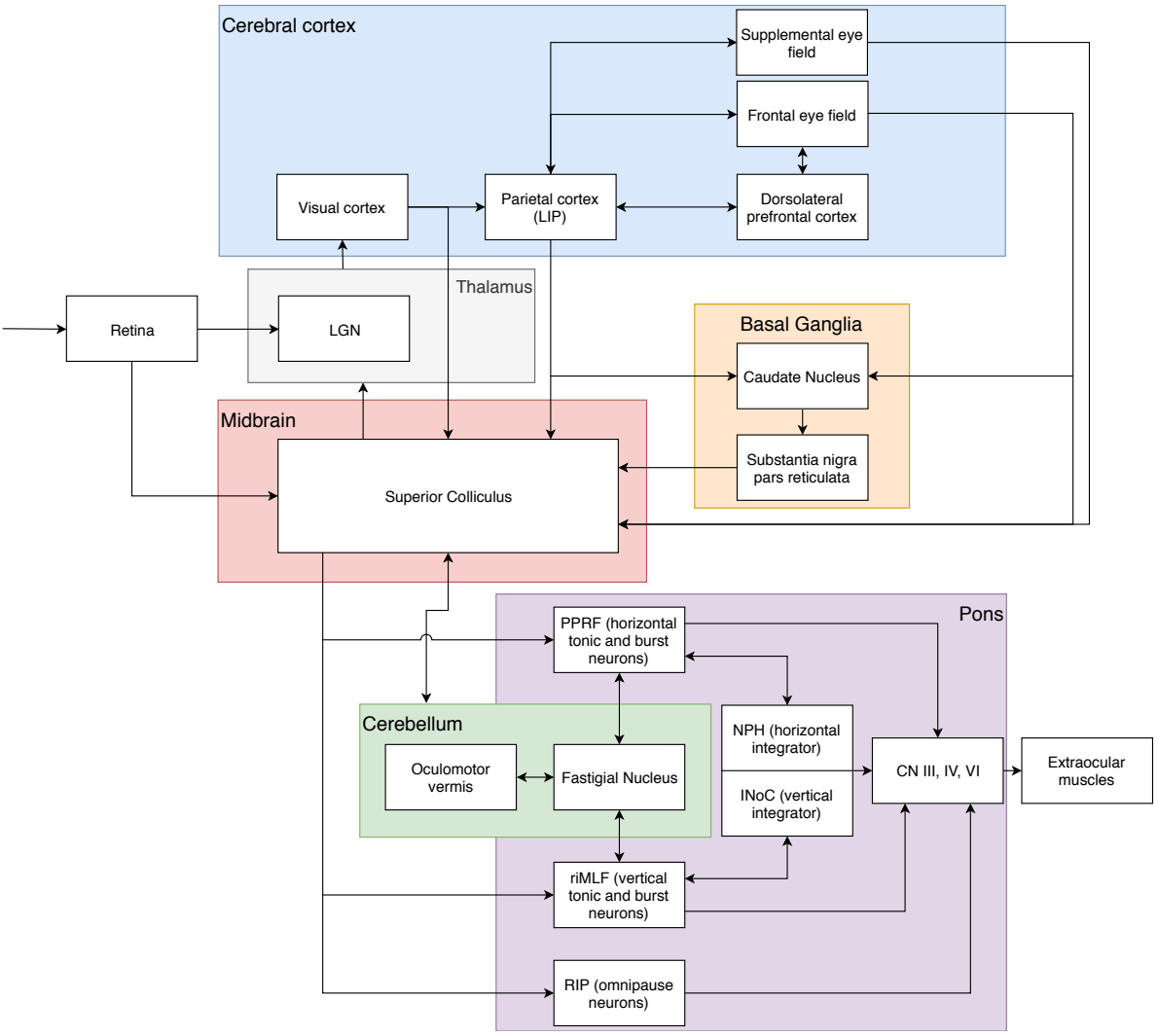

Figure 3.5: Schematic overview of important structures for generating saccadic eye movements after a local stimulus on the retina. Neuronal commands from the PPRF (paramedian pontine reticular formation), riMLF (rostral insterstitial nucleus of the medial longitudinal fasciculus) and RIP (nucleus raphe interpositus) form a oculomotor command for the CN (cranial nerves) to stimulate eye muscles. Constructed by combining work from Munoz & Fecteau (2002), Munoz (2002), Enderle (2002) and Harting & Updyke (2006).

via the oculomotor vermis and fastigial nucleus of the cerebellum, to the vestibular nuclei.

In the vestibular nuclei, several signals are integrated to form premotor commands for the oculomotor, trochlear and abducens nuclei. Besides the SP signals, information of head movements from the semicircular canals reach the vestibular nuclei. The premotor commands are send to the oculomotor nuclei, both directly and via the horizontal and vertical neural integrator.

The SC appears to play a role in SP eye movements as well, as neurons from the SC fire different for saccades made to stationary versus moving targets. Furthermore, the firing rate of omnipause neurons drops during SP eye movements with about a third, compared to fixation (Krauzlis 2005).

Contrary to saccades, SP eye movements are very difficult be generated in absence of a visual stimulus. Only when a human is subjected to repetitive visual stimuli, SP can be evoked, probably due to velocity information storage in premotor neurons (Barnes et al. 1997).

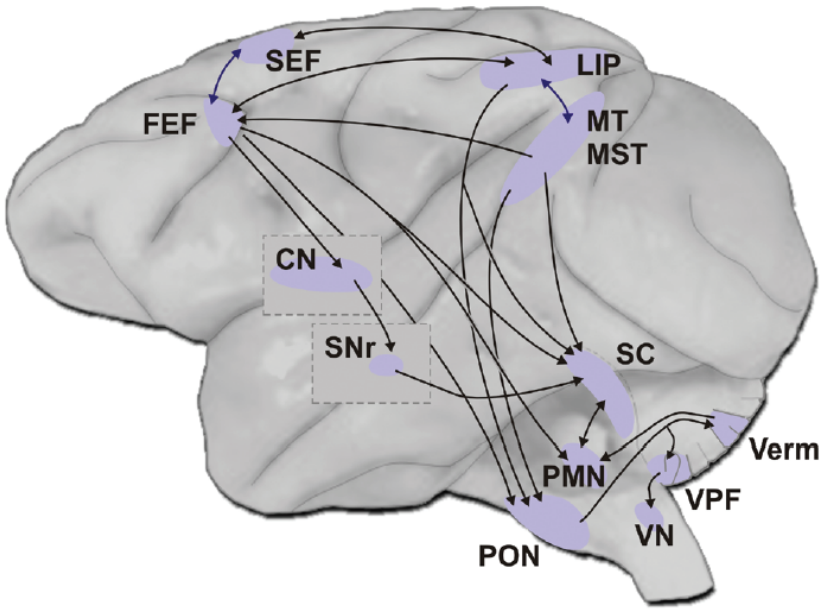

Figure 3.6: Schematic and simplified outline of smooth pursuit and saccadic pathways in the monkey brain. Indicated are the CN (caudate nucleus), FEF (frontal eye field), LIP (lateral intraparietal area) MT (middle temporal area), MST (medial superior temporal area), PMN (brain stem premotor nuclei), PON, (precerebellar pontine nuclei), SC (superior colliculus), SEF (supplementary eye field), SNr (substantia nigra pars reticulate), Verm (oculomotor vermis), VN (verstibular nuclei) and VPF (ventral paraflocculus) (Krauzlis 2005).

3.5. Eye movement analysis

The neural substrates of the two most important eye movements for this research are clear. In this section, some final attention is given to details which could have a great influence on the research. First of all, the influence of stimuli characteristics is shortly discussed. Hereafter, some common eye features are examined, for example the influence of dominance of a particular eye, and lastly some remarks concerning eye tracking devices are stated.

3.5.1. Stimulus

A stimulus is something which triggers a sensory response. This can be for example noise, touch or light. This research focuses on a visual stimuli, in this case a moving target on the screen which should be tracked by a subject. This stimulus can have several characteristics, like shape, size and color. This paragraph gives insight in the possible influences on oculomotor performance of these characteristics.

First, the shape of the stimulus is discussed. Thaler et al. (2013) investigated the effect of target shape on the stability of fixational eye movements. They found that a stimulus being a combination of bulls eye and cross hair resulted in the most stable fixation. During fixation, small, involuntary eye movements are made. However, their amplitude is probably negligible to the eye tracking measurement noise.

Furthermore, fixation is not the type of eye movement most relevant for this research, and Thaler et al. (2013) only used limited stimuli arrangements/tasks in their research. Therefore, a more basic shape is considered as well. A dot is recommended, as it has equal properties in all directions of the 2D plane.

Research on stimulus size has been conducted by, among others, Steinman (1965) and McCamy et al. (2013). The latter found that micro-saccades are influenced by the fixation target size. Apparently, micro-saccade rate decreases linearly and micro-saccade magnitude increases linearly with fixation target size. Moreover, a directional pattern is spotted, as the preference for horizontal direction saccades decreases with target size. Therefore, a target which is not too small should be chosen, to minimize the appearances of micro-saccades.

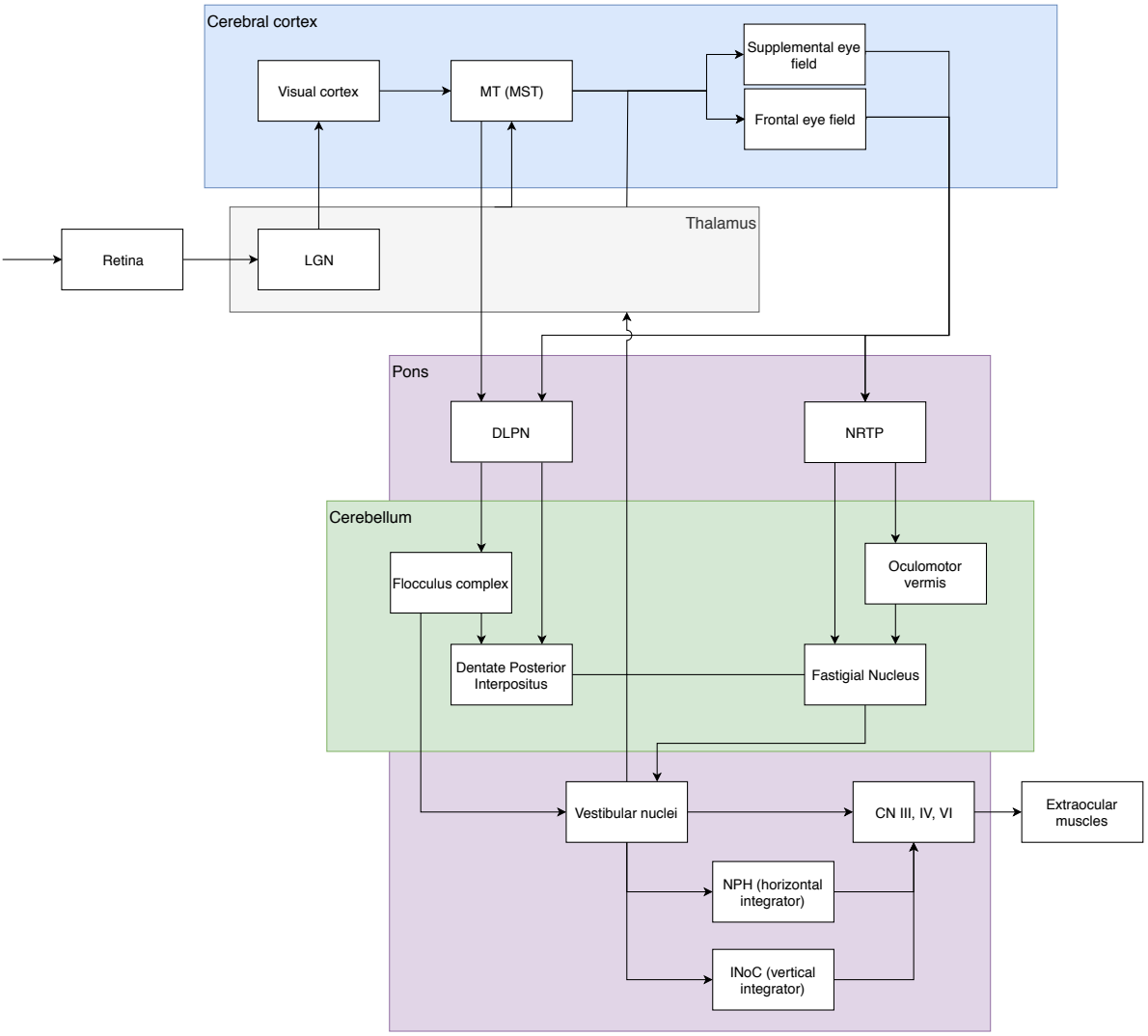

Figure 3.7: Schematic overview of important structures for generating smooth pursuit eye movements. Constructed from work from Fukushima et al. (2013)

With the observer to screen distance of 50 cm such as in Büskens (2018), a dot with 2 cm diameter would approximately cover 2 to 2.5 degrees of the field of view, which is approximately equal to the area covered by the fovea. As cones have a higher signal processing speed compared to rods, and more cones are present in the fovea (see fig. 3.8), sufficient performance should be reachable with this stimulus size (Kandel et al. 2000).

For determining the color of the stimulus, the cones in particular play a critical role. Three types of cones are present, denoted as the short, medium and long cones. These names do not refer to their actual size, but to the wavelength they are sensitive to. Their peak wavelength values vary near 440 nm, 535 nm and 565 nm respectively, but exact values vary among people, and research (Hunt 2004).

The three types of cones work together to create a color map of sight. The peak values of the cones correspond with blue, green and red light, and by varying the intensity of these, different colors are created. This principle is used as well in computer science, where the RGB-scale varies the amount of red, green and blue to create a color (Hunt 2004).

Research is performed to the luminosity function (Vos 1979, Sharpe et al. 2005), which is the average spectral sensitivity of human visual perception of brightness. Apparently, humans perceive different brightness levels for different colors, and light at wavelengths near 560 nm, which corresponds with green and red light, is perceived as the most bright. In

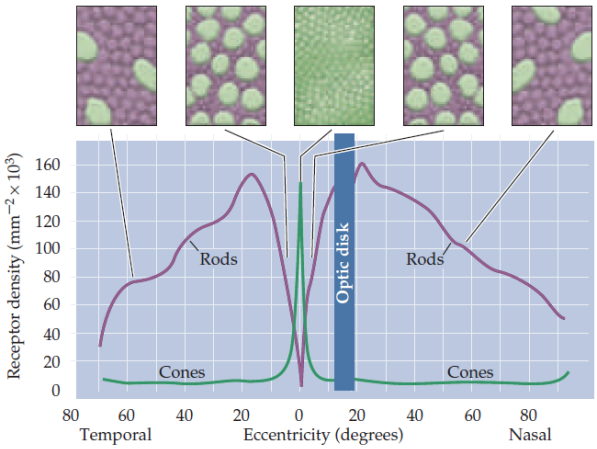

Figure 3.8: Distribution of rods and cones on the retina (Purves et al. 2004).

low-light environments, this number drops to about 500 nm, which corresponds with blue and green light (Goodman et al. 2016). Therefore, green light is most suitable for stimulus color, as both in normal and low light conditions, significant brightness levels are reached.

To minimize tracking errors due to visual stimuli other than the target stimuli and a relative large pupil size, a low-light environment is preferred. To create a low-light environment, a black display background color can be used, and windows and doors can be blinded.

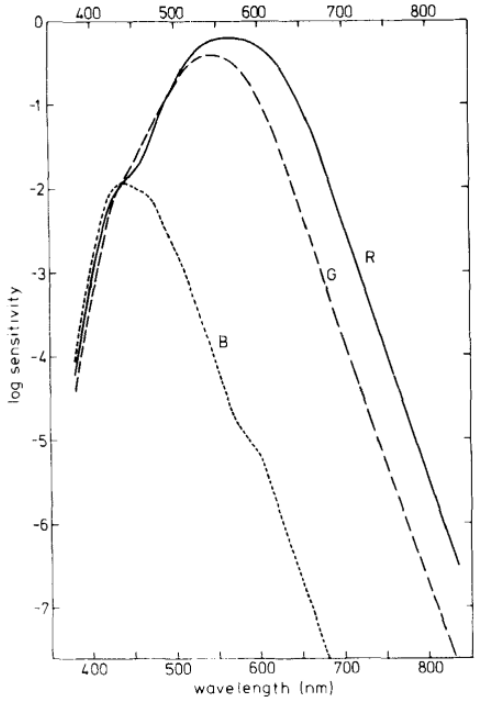

Figure 3.9: Spectral sensitivity of the three receptor primary systems: blue (B), green (G) and red (R) (Vos 1979).

3.5.2. The visual field

In monocular vision, the visual field is created by one eye. For binocular vision, some overlap exists (for humans) in this visual field, such that a three dimensional image can be created. As a results, the visual information of one eye should have priority because of the parallax effect. This section shortly addresses these features.

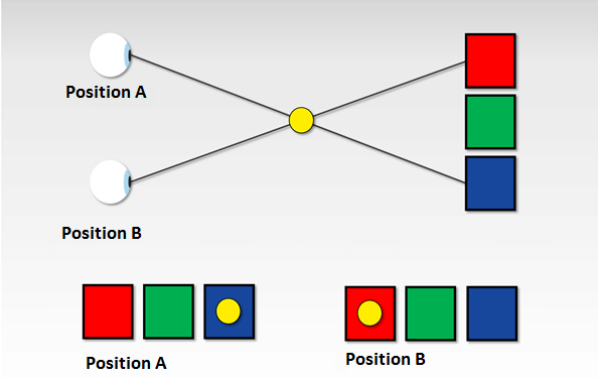

Figure 3.10: The parallax effect (1&1 IONOS Products 2017).

In monocular vision, no depth perception is possible, as objects are examined with one eye only. Some creatures with two eyes still have monocular vision, as the visual field of the eyes are not overlapping. In binocular vision, the visual field of both eyes are (partly) overlapping, such that depth perception is possible (Kandel et al. 2000). As the stimulus is displayed on a computer screen, no depth perception is necessary. Hence, both monocular and binocular tracking should result in similar results.

As humans have a certain preference for handiness, for example for writing or throwing, also there is dominance of the visual input of a certain side. Binocular vision requires a dominant eye because of the parallax effect. This effect is visualized in fig. 3.10. One position is preferred over the other by the brain.

Note that this dominance does not have to be on the same side, cross-dominance is possible as well. For over a century, research has been performed to discover whether there are any benefits or functions of this eye dominance (e.g., by Schneor & Hochstein (2005)). However, other research does not lead to vast conclusions on other benefits or functions of eye dominance (Barrett 2016).

3.5.3. Visual processing issues

Some humans need glasses or contact lenses to achieve an acceptable visual acuity. However, more visual processing issues are present. Some abnormalities may have very limited influence on eye visual performance, but some may have. This section highlights the most common issues and their possible consequences on eye tracking performance. If significant consequences are present, subjects suffering this abnormality should be excluded.

The most common visual processing problem is caused by refractive errors, as mentioned in previous paragraph. Here, light does not fall properly on the retina, such that blurry images are generated. One can use glasses or contact lenses, or one can undergo laser eye surgery, or LASIK, to correct for refractive errors.

Once someone is talking about this ‘green’ shirt, while its real color is red, you might be dealing with a person suffering from a form of color blindness. Approximately 8% and 0.5% of men and women respectively with northern European ancestors have the common form of red-green color blindness (The National Eye Institute 2015*b*). Mostly, color blindness is inherited, caused by abolished genes responsible for generating the proper photo-pigments of the cones.

Problems with green or red cones are most common. Deuteranomaly (approx. 5% of males) yields an abnormal green photo-pigment, where yellow and green appear more red. Other red-green anomalies (protanomaly: abnormal red cones; protanopia: no working red cones; deuteranopia, no working green cones) occur at 1% of men. Blue-yellow color blindness is rare, and affect men and women equally (The National Eye Institute 2015*b*). As the

stimulus color is determined to be green, subjects with red-green anomalies should be excluded, as the center of the stimulus is less distinguishable.

Cataract is another form of vision impairment. Cataract occurs when proteins clump together on the lens. If these clumps grow bigger and bigger, light gets distorted on its way to the retina, resulting in blurred vision.

For elderly, cataract is a common problem. More than 50% of the Americans reaching 80 years old have or have had cataract. Age-related cataract can start from 40 years old, but other causes are likely to exist as well, for example diabetes or smoking. To diminish the possible influence of cataract, young healthy adults are suitable for being subjects (The National Eye Institute 2015*a*).

The Computer Vision Syndrome (CVS) is a disorder which is very common among humans working with digital screens at a daily basis (Blehm et al. 2005). Symptoms include both ocular and extra-ocular issues. Ocular problems include eyestrain, tired eyes, surface-related problems and visual problems, such as blurred vision. As the stimulus is displayed on a computer screen, intensively tracked by the participant, CVS should be monitored frequently. Sufficient breaks between a number of consecutive trials should be considered.

3.5.4. Eye trackers

To gather gaze data for analyzing eye movements, eye trackers are used. This section describes the state-of-the art of eye-tracker technology. An important remark is made by Duchowski (2017) considering this technology, who stated that "in all eye tracking work, a tacit but very important assumption is usually accepted: we assume that attention is linked to foveal gaze direction, but we acknowledge that it may not always be so." (Duchowski 2017, p.13). Or in other words, we might track a spot which is different than the actual spot focused on. Furthermore, in this section, available resources at the department of Neuroscience of the Erasmus Medical Center in Rotterdam, where the experiments are to be conducted, are shortly discussed.

Two main categories in eye tracker devices can be distinguished. One that captures the eye's orientation with respect to the head, and one that captures the eye's orientation in space (Duchowski 2017).

Furthermore, four main categories of eye tracking techniques can be distinguished. These are Elektro-OculoGraphy (EOG), scleral contact lens, Video- or Photo-OculoGraphy (V/POG), and video-based combined pupil and corneal reflection (Duchowski 2017).

- EOG tracks eye movements relative to the head, using electric potential differences in the skin near the eyes, see fig. 3.11. As the eye rotates, the corneoretinal potential changes, which serves as a measure of eye rotation (Young & Sheena 1975).
- A very precise eye tracking technique is the scleral contact lens, or search coil technique. However, it is also an intrusive method, and therefore not always desired. This method involves wearing a contact lens, wired with a coil (or even linkages), such that eye movements disturb a magnetic field, see fig. 3.12. Analyzing these disturbances results in very precise eye movement (Duchowski 2017).
- POG and VOG techniques are based on distinguishable features of the eyes during eye movements using cameras, see fig. 3.13. For example, the boundary of the iris-sclera can be tracked to determine gaze. Visual processing of recordings should be performed to gather gaze data. Usually the head position should be fixed, hence a bite bar or chin rest could be useful (Young & Sheena 1975).
- Most aforementioned techniques have trouble to determine the eye's position with respect to space. To tackle this, either the head should be perfectly fixed, or head movement and eye rotation should be separated by tracking multiple features using a remote system. This can be done by tracking the pupil and corneal reflections. This technique is probably the most widely used method at the moment (Duchowski 2017). It uses a

light source to create these reflections, and based on its position and direction a gaze vector can be constructed, see fig. 3.14.

Figure 3.11: EOG for vertical eye movements (Mind Media 2019).

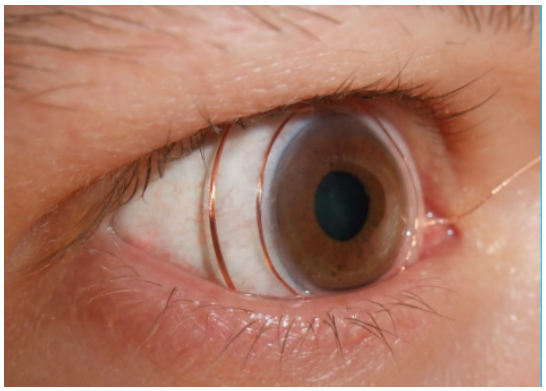

Figure 3.12: Scleral search coil (Chronos Vision 2017).

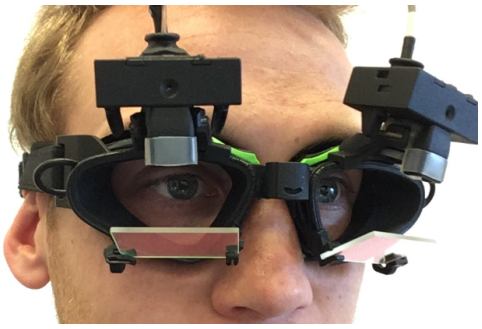

Figure 3.13: VOG: EyeSeeCam Sci eye tracker device.

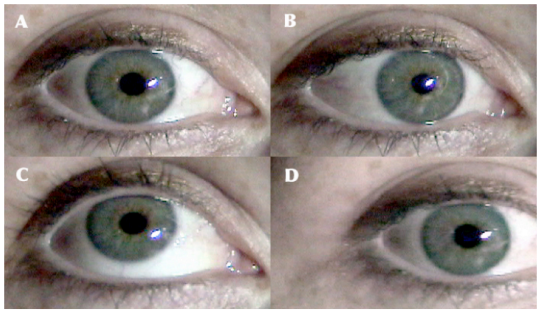

Figure 3.14: The corneal reflections produced by different eye-head positions. The corneal reflection appears as a bright white dot, just to the right of the pupil (A). The relative positions of the pupil and the corneal reflection change when the eye rotates around its vertical (B) and horizontal (C) axes. This relationship does not change, however, when the head moves and the eye is stable (D) (Richardson & Spivey 2008).

3.5.5. Eye tracking devices

At the Erasmus Medical Center, research involving eye tracking is performed at the department of Neuroscience. Several types of eye trackers are available, which are the EyeSeeCam Sci, Tobii Pro X2-60 (former T60) and Pro X3-120 (former T120) and Tobii glasses 2. This section should clarify which eye tracker device is most suitable to be used in this research.

The EyeSeeCam Sci is a VOG-based head-mounted eye tracker, see fig. 3.13. The device records images of the eye with one infrared camera for each eye using wavelengths starting from 850 nm (Colagiogio et al. 2013). Additionally, head movements are monitored using a six degree of freedom inertial measurement unit (IMU) (EyeSeeTec GmbH 2017). Though, the IMU output data quality is very noise, hence this data is not used.

A software package can be used to monitor and gather eye and head movement data. Furthermore, the sampling rate can be set to either 50, 60, 84, 120, 220, 256, 304 and 496 Hz. A recent project at the Erasmus Medical Center included the design of a 220 Hz pulse-train using an Arduino device, to be able to synchronize data acquisition of a remote computer

Figure 3.15: The Tobii Pro X3 (left) in use (right), Tobii AB (2019).

with the eye tracking data. This is useful for matching stimulus and gaze data, especially when timing is of critical importance.

The Tobii Pro X2 and X3 are screen-mounted VOG-based eye trackers. Their sampling rates are 30 Hz (X2), 60 Hz (X2) and 120 Hz (X3). As can be seen in fig. 3.15, these type of eye trackers are almost unnoticeable if the user is not notified in advance.

3.6. Conclusion

In this chapter the importance of studying eye movements is discussed. In tracking tasks with multisine input signals, SP, saccadic and vergence eye movements can be investigated. Though, to limit the scope of this research, vergence eye movements are omitted.

SP and saccades share features in their neuronal pathways, but have different characteristics. The same yields for horizontal and vertical eye movements. Although the muscles to generate movements in these directions are exclusive, this research tries to investigate the interaction of horizontal and vertical eye movements.

4

Frequency domain analysis: The cybernetic approach

McRuer & Jex (1967) introduced the foundation for describing human control dynamics with mathematical models, i.e. as quasi-linear, time-invariant feedback systems (Mulder et al. 2017). The main benefit of this approach within the scope of this research, is the resulting ability to quantify the behaviour of this human controller (HC) when performing certain control tasks, such as driving a car, or similar, more simplistic tasks on a single display. However, the model of the HC can also be analyzed to identify certain deficits, by comparing a healthy HC with an impaired HC when performing these simplistic tasks.

This cybernetic approach (Mulder et al. 2017) includes several main steps to be taken, as mentioned by Van der El (2018). First, offline predictions (if available) of human control behavior and adaption are made. Then, human control data is gathered using a tracking task experiment.

From the experiment output data, the frequency response function (FRF) estimates of the human's control dynamics can be obtained by applying system identification techniques. Hereafter, theoretic models can be constructed from estimated FRFs and parameter estimation can be applied to fit these models to the data. Lastly, the obtained mathematical models and parameters can be compared for different design variables.

In this chapter, first the steps of the cybernetic approach are discussed. They include the description of the human controller and its control strategy, system identification and parameter estimation. Hereafter, this application to gaze dynamics is discussed.

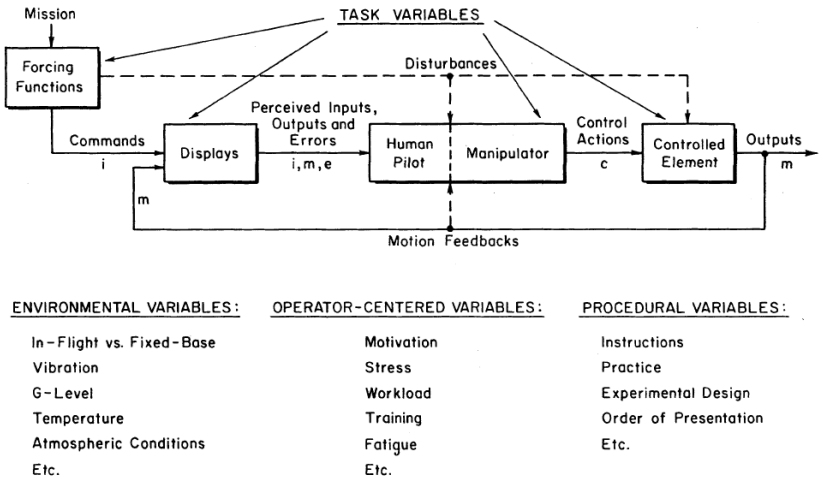

Figure 4.1: Design variables affecting the tracking task (McRuer & Jex 1967).

4.1. The human controller

When analyzing a control system, often a block diagram is made to schematically represent the system, such as in fig. 4.1 or fig. 4.2, using the Laplace variable s. In such a system, each block represents a subsystem, having certain inputs and outputs. Using control theory, one can determine whether the complete system has certain properties, for example stability. In this way, subsystems can be adjusted such that the complete system meets certain desired characteristics.

However, when humans are taken into the loop, for example a pilot in an aircraft, a mathematical model of the human dynamics is required to be able to apply control theory. Obtaining this model is not a straightforward task as, according to McRuer & Jex (1967), "The human pilot is a multimode, adaptive, learning controller capable of exhibiting an enormous variety of behavior." Instead, several variables should be dealt with, as shown in fig. 4.1. These variables are task, environmental, operator-centered or procedural dependent.

The models from McRuer & Jex are based on the frequency domain, which uses a special case of the Laplace variable s. This is the Fourier transform, which converts the signal from the time domain to the frequency domain, where $s = j\omega$.

4.1.1. Successive Organization of Perception

The strategy of humans to perform well in control tasks depends highly on the nature and resources of the control task, based on a hierarchy, for developing skill-based behaviour. This hierarchy, the Successive Organization of Perception (SOP), has three stages, being compensatory, pursuit and precognitive control (Mulder et al. 2017). Each is shortly discussed.

The compensatory stage

So far, compensatory tracking is thoroughly examined, mostly using unpredictable target signals in the form of multisine signals. Compensatory tracking is characterized by the HC acting only on the error of the target signal and system output, e in fig. 4.1. In fig. 4.2 a schematic representation of a compensatory tracking task is shown.

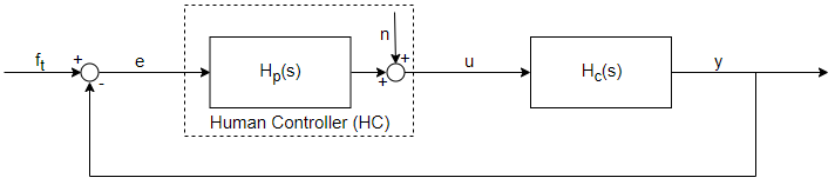

Figure 4.2: Systematic representation of the human controller in a compensatory control task.

The controlled element dynamics, $H_c(s)$, is the element which the human controls. The output of this element, y, is the state of the element, which is fed back to the human. For example, a Human Controller (HC) is driving a car with constant speed on a winding road (f_t). Depending on the position of the car (y) with respect to the center or edges (e), the HC controls the car (u) using the steering wheel. Therefore, the car's direction changes according to its dynamics ($H_c(s)$), and its position (y) is updated.

The HC is represented by a linear, time-invariant (LTI) part ($H_p(s)$) and remnant (n). The latter represents a myriad of non-linear factors influencing the HC's control behaviour. Attempts to model the remnant (Levison et al. 1969, Metz 1982) have not lead to satisfying insights.

A number of LTI models are introduced to catch HC compensatory dynamics, of which the crossover model from eq. (4.1) and the simplified precision model from eq. (4.2) is most widely used (Mulder et al. 2017).

In the latter, the H_p tries to adapt to H_c, to achieve similar dynamics as eq. (4.1). Thus, the composition of the pilot equalization (in this case the gain) may differ depending on the

H_c dynamics. For example, single or double differentiator or integrator dynamics can be present. The fraction part of eq. (4.2) accounts for neuromuscular limitations of the HC. The neuromuscular part is modeled as a mass-damper system.

$$H_p(j\omega)H_c(j\omega) = \frac{\omega_c}{j\omega}e^{-j\omega\tau_c} \tag{4.1}$$

$$H_p(j\omega) = K_p e^{-j\omega\tau}\frac{\omega_{nm}^2}{j\omega^2 + 2\zeta_{nm}\omega_{nm}j\omega + \omega_{nm}^2} \tag{4.2}$$

The pursuit stage

In the next stage, pursuit tracking is considered, and research has been performed for this stage (e.g., by Hess (1981)). The classic pursuit tracking task is represented as in fig. 4.3. Modelling the HC pursuit dynamics is difficult due to the fact that pursuit tracking often enables various control strategies. The HC can use the feed forward response of f_t, the compensatory feedback e, similar as in fig. 4.2 (not shown in fig. 4.3), and the feedback response of the system output y (Mulder et al. 2017).

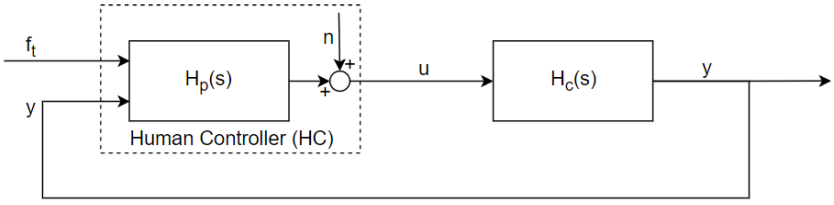

Figure 4.3: Systematic representation of the human controller in a pursuit tracking task.

The precognitive stage

The last stage of the SOP is the precognitive stage, where perfect tracking is achieved, as if the pilot can fully predict and follow the target. In this stage, the HC does not rely on any feedback for some time, and creates an open-loop system. For predictable target signals, this stage can be achieved. However, when using quasi-random target functions, this is not the case, hence this stage is out of the scope of this research.

4.2. Tracking task: display design

The human control dynamics data is obtained by means of a tracking task experiment. For pilot tracking tasks, this is mostly manual control data, but in this research gaze control data is considered.

As real-life experiments are often expensive, difficult to modify, and hard to reproduce, computer-based experiments are performed. In this way simplified displays can be used to focus on task-related information.

The compensatory task shows only the error $e(t)$ of the input signal and the output of the controlled element. This error should be brought to a reference, usually the center position, by the HC. If no input is provided by the HC, the output of the system would be equal to zero, so the error signal will be identical to the input signal.

As the HC is controlling the error signal, the signal characteristics of the target signal are biased. Hence, using input signals with different characteristics to avoid predictability is not necessary. It is unlikely that the HC shows the exact same movements each trial, which would result in a repeating error signal for each trial. Instead, the error signal will be different each trial.

The preview task shows both the input state as the controlled element state. In this way, the HC is pursuing the target signal, either with additional information on future state (preview), or not. As mentioned earlier, the HC can use three different states in this task: the controlled element state, the target state, and the error between these two states.

As the input signal is a direct input to the HC, predictability for identical input signals can be an issue here. Therefore, the input signal should be altered in consecutive trials, such that unwanted learning effects are omitted.

Aforementioned types of displays require feedback from a control device, for example a joystick, steering wheel or touchscreen. Time delays in these devices can be of critical influence on the system dynamics, and can have negative consequences for human control behaviour.

4.3. System identification

To analyze these control systems, a black box identification technique is used by analyzing the Fourier coefficients at the excited frequencies from the input signal. Black box identification means that the model is purely based on the input-output relation of the system. These are the opposite of white-box identification, where the system is described based on first principles.

Contrary to white-box identified systems, black-box identified systems are only to be used within the examined domain. To be able to compare the system over time, this analysis is performed in the frequency domain. This is done by using a special case of the Laplace transform, the Fourier transform, where the Laplace variable $s = j\omega$ instead of $s = \sigma + j\omega$. In the frequency domain, for the system from fig. 4.4, one can construct equation eq. (4.3). This can be rewritten in the form of eq. (4.4), such that the FRF of the human can be determined.

However, this would require the dynamics of the remnant component as well, which is unknown and varies continuously. Therefore, an input signal f_t is chosen with significant power at certain frequencies ξ, such that the signal-to-noise ratio of the remnant signal is small compared to the signal-to-noise ratio of the output of the HC (u). Then, the second term on the right hand side is negligibly small, as shown in eq. (4.5). This allows for an estimate of the FRF at these frequencies ξ of the linear part of the HC, $H_p(s)$.

Hereafter, a gaze model can be constructed by selecting a suitable model and performing parameter estimation to fit a model through the obtained data points, hence quantifying the human. First, the input signal (target signal) is discussed. Then, this gaze model is constructed.

$$U(j\omega) = F_t(j\omega)H_p(j\omega) + N(j\omega) \tag{4.3}$$

$$H_p(j\omega) = \frac{U(j\omega)}{F_t(j\omega)} - \frac{N(j\omega)}{F_t(j\omega)} \tag{4.4}$$

$$\hat{H}_p(j\omega;\xi) = \frac{U(j\omega;\xi)}{F_t(j\omega;\xi)} - \frac{N(j\omega,\xi)}{F_t(j\omega;\xi)} \approx 0 \tag{4.5}$$

4.4. Input signal: the forcing function

As can be seen in eq. (4.5), the human dynamics is dependent on the input signal f_t, which should therefore be chosen carefully. Sinusoidal forcing functions are very suitable, as they have a homogeneous response, such that probabilistic properties do not change over time (Mulder et al. 2017). As the FRF should be identified at several frequencies to cover an interesting spectrum, a multisine signal is used, in the form of eq. (4.6).

$$f_t(t) = \sum_{k=1}^{N_t} A_t[k]\sin(\omega_t[k]t + \phi_t[k]) \tag{4.6}$$

This signal consists of three parameters which can be altered, which are the amplitude A_t, frequency ω_t and phase ϕ_t. Each of the N_t number of sinusoids has its own combination of

these parameters. These are chosen in a fixed order, starting with the amplitude. Hereafter, the frequencies are chosen. Lastly, the phases are generated.

So first the amplitude are shaped. The amplitude spectrum A_t can have a myriad of combinations, varying from constant amplitudes or constant power (McRuer et al. 1965), or with shaping filters, e.g., as used by Zaal et al. (2009).

Next, the frequency components ω_t are chosen. The frequency components are a multiple of the base frequency ω_0, which is dependent on the measurement length T_m, as shown in eq. (4.7). Because of the nature of the Fourier transform, no sinusoids with a smaller frequency than this base frequency can be extracted, as the Fourier transform fits the signal an integer amount of times in the measurement window. If this would not be the case, leakage could occur, which causes biased identification results.

Moreover, to avoid repeating patterns because of harmonics, prime integers (n) are chosen to be multiplied with the base frequency to determine the frequency components of the sine waves, as shown in eq. (4.8). These primes are chosen such that the frequency components cover a wide range of frequencies, to reveal interesting features of the HC.

$$\omega_0 = \frac{2\pi}{T_m} \tag{4.7}$$

$$\omega_t = \omega_0 n \tag{4.8}$$

The last component of the multisines to be constructed are the phases ϕ_t. This is done by evaluating a myriad of combinations of phases, randomly generated, and comparing the crest factor (CF) of the signal accordingly. The CF is determined by the ratio of the maximum absolute value of the signal and the root mean square of the signal, as can be seen in eq. (4.9). One should aim for an average CF when choosing suitable phase combinations.

$$CF = \frac{max(|f_t(t)|)}{rms(f_t(t))} \tag{4.9}$$

4.5. Parameter estimation

Parameter estimation is performed to construct a model of H_p, using features from eq. (4.2). These features are based on theory and the shape of the FRF in a Bode plot. In general, a gain K_p and time delay τ are present, and in when muscles are involved, which are modeled as a spring-damper system, the neuromuscular part is involved as well. Furthermore, the dynamics of the controlled element can be of influence. Then, the shape of the FRF function in a Bode plot usually reveals whether a (second order) low-pass and/or high-pass filter could be applied as well.

A cost function is established to fit the model from eq. (4.2) with the FRF. A myriad different cost functions can be used. The normalized least squares cost function is usually applied. An example of this function is shown in eq. (4.10). Here, $\hat{H}_p(j\omega[k])$ is the estimated FRF from eq. (4.5). $H_p(j\omega[k],\theta)$ is the model to be fitted, where different parameters values ($\theta = [K_p, \tau, \zeta_{nm}, \omega_{nm}]$) of the selected features from eq. (4.2) are examined to find a minimum cost function value. In MATLAB this is possible using the $fminsearch$ routine. As these parameters cannot be smaller than zero, an additional penalty can be applied for the cost function value if one of these parameters is less than zero.

To improve the model fitting, one could consider to apply certain weight to some of the frequency components. For example, the lowest frequency components are slow movements, and are therefore rather likely to be tracked well by the HC. Thus, these low-frequency FRF data points could be given a higher weight. On the other hand, at the highest frequency components, the opposite is true, and additionally a low signal-to-noise ratio is present. The lower the signal-to-noise ratio, the higher the contribution of the remnant, such that the assumption from eq. (4.5) is not valid anymore. Hence, this can have a significant effect on the actual contribution of the H_p-block from the HC (see fig. 4.4). Therefore, the weight at the highest frequencies could be considered to be close to zero.

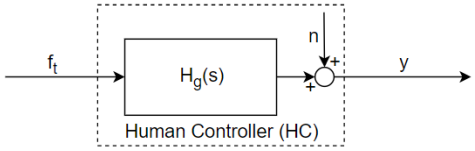

Figure 4.4: Systematic representation of the human controller in a gaze pursuit task.

$$J(\theta) = \arg\min_{\theta} \sum_{k=1}^{N_t} \frac{|\hat{H}_p(j\omega[k]) - H_p(j\omega[k],\theta)|^2}{|\hat{H}_p(j\omega[k])|^2} \tag{4.10}$$

4.6. Gaze analysis

Research is performed trying to catch neurodegeneration using the 'cybernetic' approach. First by analyzing manual control dynamics (De Vries 2016, Haartsen 2017), later by including oculomotor control dynamics as well (Büskens 2018). Büskens (2018) established a gaze model using aforementioned system identification and parameter estimation methods. These results are shortly discussed. Hereafter, a method to analyze a bi-axial task is investigated to be able do investigate both horizontal and vertical gaze in one task.

4.6.1. Oculomotor models

In this research, the focus is put on gaze dynamics, in which the feedback loop is performed inside the human, as visual information is processed to determine whether the target is placed in the fovea. As this all happens inside the gaze control block of the human ($H_g(s)$), the 'external' control loop is shown in fig. 4.4. However, inside the $H_g(s)$-block, a closed loop is present, as the retinal error is used as input source.

Three FRF models are considered to approximate the obtained gaze data. These are shortly discussed, and this research aims to investigate which model is most practical to be used for quantification in a clinical setting.

- Büskens (2018) used a similar pilot model as described in eq. (4.5) to model oculomotor dynamics, i.e., pilot equalization consisting of a gain and time delay, combined with neuromuscular system dynamics similar to a mass-damper system. This model is commonly used for manual tracking tasks, and can be extended with a low or high pass filter in pilot equalization.

- Though, Enderle & Zhou (2010) introduced a third order model to capture the oculomotor plant. Furthermore, because of the nature of the eye, omitting the neuromuscular contribution could be representative as well. This research will investigate which representation of neuromuscular system dynamics is the most accurate representation of oculomotor control dynamics.

- Lastly, one could also consider to capture the oculomotor dynamics with just a gain and time delay, as the eye makes very fast, direct movements over a relatively small rotation. Therefore, post-processing should give insight in which of these three oculomotor model has most practical relevance for usage in a clinical setting.

Results of the parameter estimation of the gaze tracking task from Büskens (2018) are shown in fig. 4.5 and 4.6. In the latter, the results of the gaze model for the eye-hand tracking tasks are shown as well, where the subject had to track the target with the index finger of the dominant hand as well, using a touchscreen. The FRF is estimated at the excited frequencies from the input signal. Using a cost function and weighted data points, a pilot model is constructed to approximate the FRF.

These results represent the horizontal gaze dynamics. Knowledge on such a model for vertical gaze is lacking, including possible interaction effects. Therefore, a gaze tracking task is proposed in chapter 6 to identify whether interaction effects are present, and to identify differences and similarities in the horizontal and vertical gaze model.

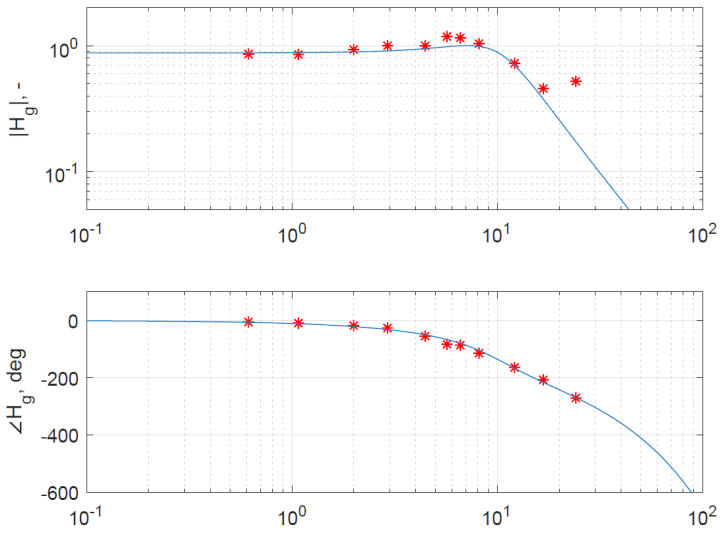

Figure 4.5: Example Bode plot of FRF (red asterisks) and fitted pilot model (blue line), obtained from Büskens (2018).

4.6.2. Dual-axis analysis

To distinguish horizontal and vertical gaze, one could simply separate these movements and analyze their behaviour independently. However, interaction effect would be unobserved, hence a different approach should be considered. Therefore, a similar method as used by Barendswaard et al. (2016) should be applied.

Barendswaard et al. (2016) investigated human control dynamics in a pitch-roll task, where pilots were asked to reduce the error for both pitch and roll simultaneously. To be able to identify interaction effects, two different sets of frequencies are used, one for each axis. In this way, one could observe the contribution of roll in the pitch-frequencies and vice versa, the crossfeed.

As can be seen in fig. 4.7, the single axis task ('S') does not contain any contribution of crossfeed control dynamics, whereas the dual axis task ('D') does. This is shown in fig. 4.8 as well, as significant power is present at the off-axis target frequencies (crossfeed).

Earlier conducted research from Haartsen (2017) involved a disturbance rejection task, for which two sets of frequencies are available, one for the target signal and one for the disturbance signal. These frequencies could be used for the horizontal and vertical axis respectively.

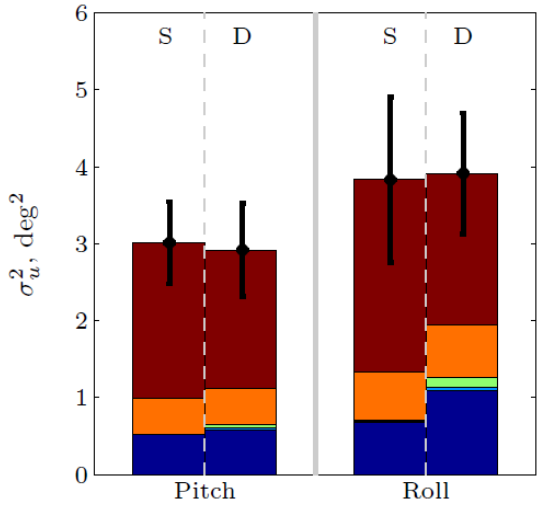

Figure 4.7: Control signal variance composition Barendswaard et al. (2016).

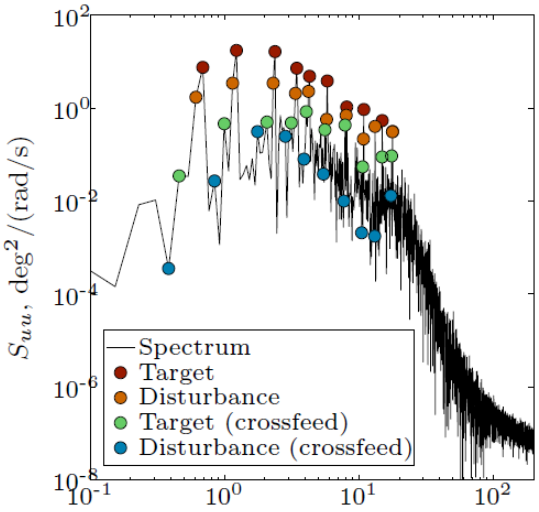

Figure 4.8: Example PSD for dual-axis task Barendswaard et al. (2016).

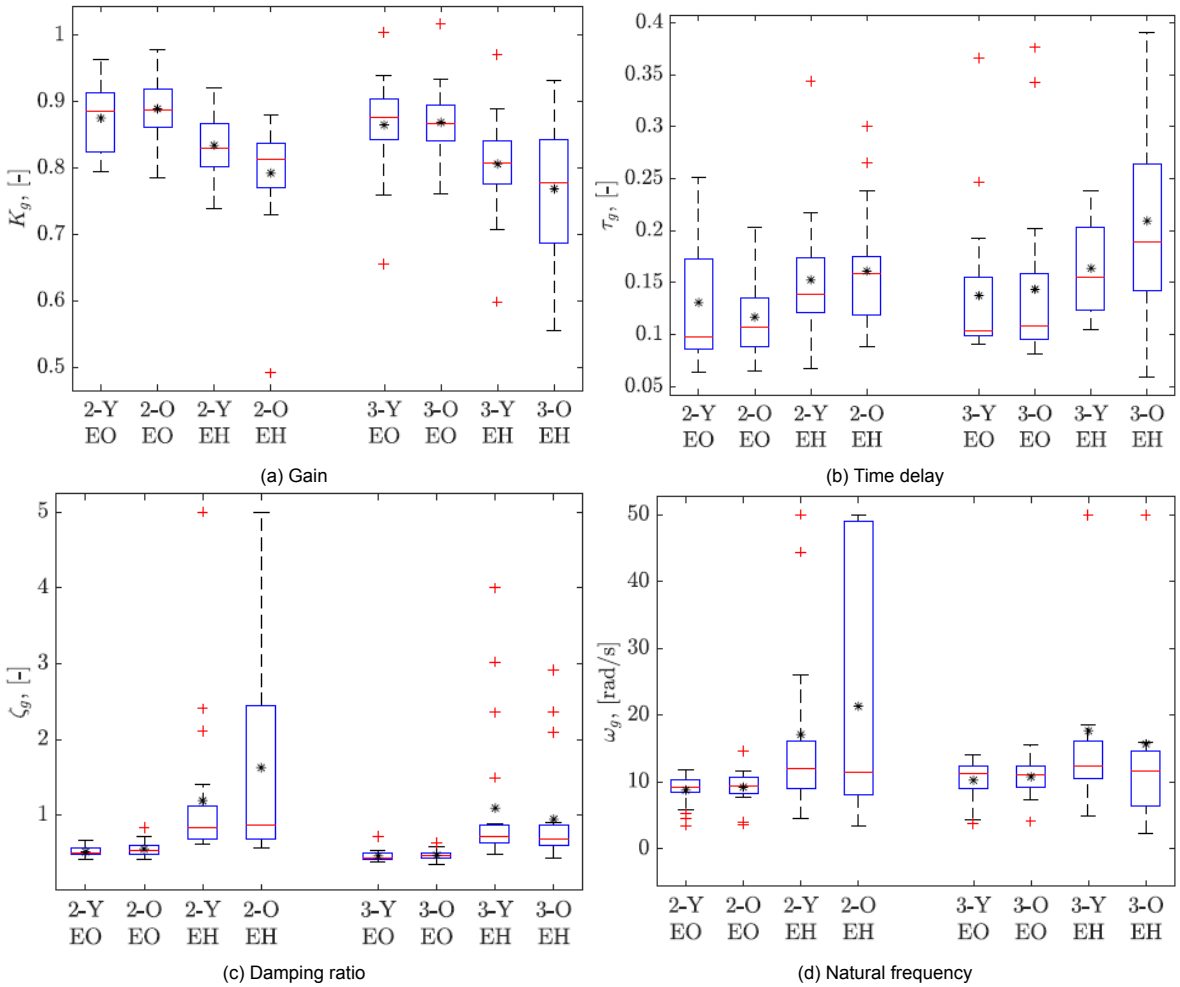

(a) Gain

(b) Time delay

(c) Damping ratio

(d) Natural frequency

Figure 4.6: Gaze parameters as obtained by Büskens (2018) for an eye-hand (EH) and eye-only (EO) tracking task for different input signal bandwidths ('2' or '3'), for old (O) and young (Y) adults.

In oculomotor tracking tasks, feedback is generally not possible, as eye trackers usually have significant delay before their signal is fed back in real-time. For some eye tracking systems, this is not even possible. Additionally, gaze should be perfectly calibrated in order to serve as feedback signal. Therefore, a classic compensatory or pursuit display is not possible, but only the stimulus is shown on the display.

4.7. Conclusion

In this chapter the cybernetic approach is discussed, which is a frequency-domain analysis method. To separate horizontal and vertical gaze, two different sets of frequencies are required, such that interaction effects can be observed.

A research objective arising from this chapter deals with the selection of the proper gaze model features, as different features can be selected to model human gaze dynamics.

5

Time domain analysis: Pattern recognition

Besides the frequency-domain analysis of recorded gaze data, a time domain-analysis is planned as well, which has some advantages. First of all, in the frequency-domain, the assumption is made that the remnant is negligible. Though, for the time-domain, this 'remnant' can be investigated. Secondly, time-dependent features can be captured, for example switching from smooth pursuit to saccades or vice versa. Lastly, directional information is lacking in the frequency-domain method, i.e., one cannot determine whether movements to the left or right is worse.

In this chapter, pattern recognition is introduced to serve as the time-domain analysis method. This is used to identify saccadic eye movements. Furthermore, learning effects based on gaze performance can be determined in the time-domain, based on recorded gaze data from Büskens (2018), which is included as well.

5.1. Principles

Bishop (2006) described the field of pattern recognition to be involved with "the automatic discovery of regularities in data through the use of computer algorithms and with the use of these regularities to take actions such as classifying the data into different categories."(Bishop 2006, p.1). Pattern recognition can be applied on many different types of data, for example on pictures, sounds, and text documents. In this research, pattern recognition concerning time series of eye position, hence gaze, is considered. In this research, off-the-shelve algorithms are applied.

As explained by (Theodoridis & Koutroumbas 2006), features and classifications form the basis of pattern recognition. A certain image, song, or character in a text document can possess different, prescribed, feature characteristics. For example for a character, one could think of the amount of curvatures and straight lines, and their orientation. Combining these feature characteristics puts the inspected element in a certain class, for example 'Number', 'Letter', or 'Punctuation', or even more specific, in '1', 'i' or '!'. Based on this, dependent on the application, further actions can be taken. For example, at a bank, an image of a written transaction can automatically be converted to a digital transaction.

As pointed out by Theodoridis & Koutroumbas (2006), this is not as straightforward as it may sound. Questions arise on what features to use and how many features to use. Furthermore, what are the 'bounds' of a class, i.e. what classifier should be used? And how is the system's performance to be determined? An overview of the stages to be performed for a pattern recognition system is shown in fig. 5.1, each is shortly discussed.

To put an inspected element in a certain class, this class must first exist. Therefore, training data can be present, where the system is told to divide certain labeled elements of this training data in a certain class. This is called supervised pattern recognition.

However, this training data does not have to be present. In these type of problems, the system has to find similarities in features of certain data points, and cluster them together.

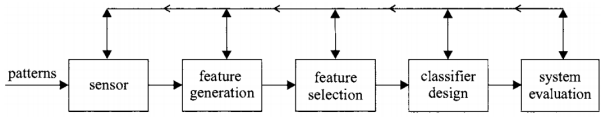

Figure 5.1: The basic stages of a pattern recognition classification system (Theodoridis & Koutroumbas 2006).

This is called unsupervised pattern recognition (Theodoridis & Koutroumbas 2006).

The main focus of this research is the frequency domain method, which is explained in previous chapter. Therefore, the time domain method is not elaborated in depth, and a certain pattern recognition algorithm is chosen based on work from a parallel master thesis project by Versteeg (2019).

5.2. Pattern recognition in gaze data

As stated before, the time-domain analysis has not the highest priority in this research, hence first a pattern recognition algorithm is used to separate smooth-pursuit and saccades.

Separating fixation, smooth pursuit and saccades, or ternary eye movement classification, is not a new practise. The velocity (Erkelens 2006, Komogortsev & Karpov 2013) or acceleration (Büskens et al. 2019) profiles can be used to identify saccades, which can be a challenging process. This is caused by three factors (Komogortsev & Karpov 2013), which are eye tracker inaccuracies, small involuntary eye movements (e.g. microsaccades) and variability of eye movement behavior among humans and tasks.

This section includes recommendations for the stages from fig. 5.1 regarding time samples of gaze data. Each stage is discussed separately in this section.

5.2.1. Sensor

The first stage is the sensor. For gaze tracking, this would cover the eye tracking device. The raw gaze data can be pre-processed before being exposed to the pattern recognition system. One could think of smoothing methods like running averaging, but this can mask the appearances of interesting features, like saccades. However, one could consider Kalman filtering (Welch & Bishop 2004), or a nonlinear realization of the Savitzky-Golay filter (Dai et al. 2017). Furthermore, blinks are filtered out in advance as well.

The covariance matrices of the pupil size are used to identify blinks. The pupil diameter d_{pup} can be determined based on these covariances, as shown in eq. (5.1) to eq. (5.3) (EyeSeeTec GmbH 2016).

$$a = \frac{\sigma_{XX}^2 + \sigma_{YY}^2}{2} \tag{5.1}$$

$$b = \sqrt{a^2 + \sigma_{XY}^2 \sigma_{XY}^2 - \sigma_{XX}^2 \sigma_{YY}^2} \tag{5.2}$$

$$d_{pup} = \begin{cases} \sqrt{a-b} & \text{if } a-b > a+b \\ \sqrt{a+b} & \text{if } a-b \leq a+b \end{cases} \tag{5.3}$$

5.2.2. Feature generation & selection

Several features could be considered to be generated. These features can be extracted from the available output variables. In table 5.1, all output variables from the EyeSeeCam Sci (EyeSeeTec GmbH 2017) eye tracker are listed. Additionally, the units and availability are shown, the latter indicating whether the parameter values are meaningful values.

Regarding features, the most interesting output variables are the eye rotations (LeftEyeVer, LeftEyeHor), whether or not in comparison with target signal properties. These are the features which will be used predominantly. From the rotations and its derivatives, smooth

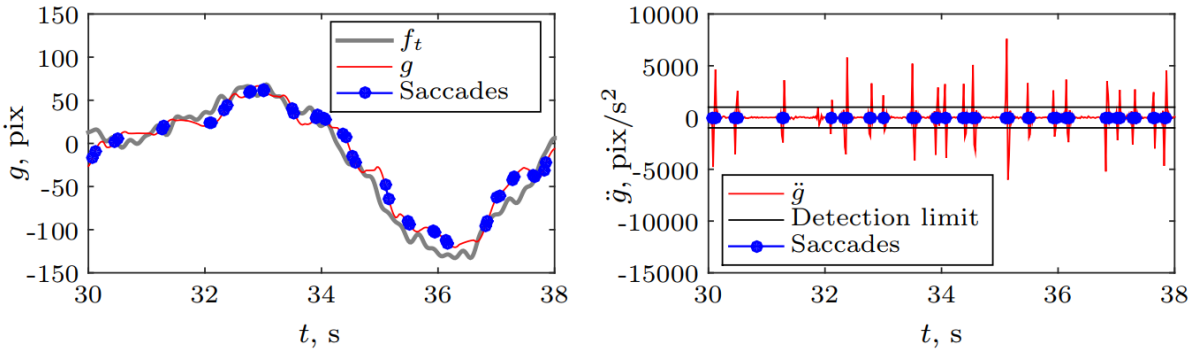

Figure 5.2: Saccade detection based on gaze acceleration (Büskens et al. 2019).

pursuit and saccadic eye movements can be distinguished by investigating sudden jumps in gaze position. In recent work from Büskens et al. (2019), a saccade detection algorithm is applied based on gaze acceleration, as can be seen in fig. 5.2.

The precision of saccades are a relevant feature, and the amount of follow-up saccades, although the latter might be hard to determine due to eye tracker inaccuracies. However, these features can be used in future research, as the classification process give promising results.

Once a saccade is made, certain follow-up saccades may be present due to the inaccuracy of the initiated saccade. Furthermore, the exact precision can become difficult to estimate, as the head is not fixed, such that small inaccuracies can be present despite calibration. These can be variables to help classifying neurodegeneration in the time-domain.

Additionally, features could be created by using the input signal characteristics. For instance the error between gaze position and derivative of the input signal might be an interesting feature. Other combinations can be investigated as well, but the main focus of this research is the frequency domain method, hence no extensive research will be performed for all the possible features in this time domain method.

It is likely that the features to be selected are the horizontal and vertical gaze signals and the input signal characteristics. Usually, first a large set of features is selected, after which the most relevant ones are selected for final use.

5.2.3. Classifier design

The classes of the pattern recognition algorithm are straightforward. One could choose for a simple division, by having a SP class and a saccade class. However, the saccade class could be extended by having a subdivision in a catch-up saccade, follow-up saccade or regular saccade, the latter being a saccade which is not part of the first type of saccades.

Furthermore, the directional information of smooth pursuit and saccades can be of value as well, because this can provide the clinician with information on what side an impairment is present. Hence this division is recommended as well.

5.2.4. System evaluation

The last stage is the system evaluation stage. Here it is decided how performance is determined. Furthermore, training data is used to decide whether aforementioned design choices should be altered, or parameters should be adjusted, for example one could consider to increase or decrease the time window.

As an off-the-shelve method is used, no extended research on system evaluation will be performed. This research serves as an indication whether time domain analysis is suitable for gaze date from a tracking task experiment.

This aforementiond method is a long short-term memory (LSTM) algorithm, from the *keras* module in Python. The LSTM model basically consists of a memory cell, input gate, output gate and forget gate. It is a supervised machine learning technique, suitable for classification

Name	Unit	Available		Name	Unit	Available
Time	s	Yes		LeftSlippageX	imagewidth	No (0)
LeftTime	s	Yes		LeftSlippageY	imageheight	No (0)
LeftSystemTime	s	Yes		LeftShiftX	imagewidth	No (0)
LeftFrameIndex	frames	Yes		LeftShiftY	imagewidth	No (0)
LeftSyncFlag	bool	Yes		HeadInertialTime	s	No (0)
LeftEyeTor	rot	Yes		HeadInertialVelX	deg/s	Yes
LeftEyeVer	rot	Yes		HeadInertialVelY	deg/s	Yes
LeftEyeHor	rot	Yes		HeadInertialVelZ	deg/s	Yes
LeftEyeVelX	deg/s	Yes		HeadInertialAccelX	g	Yes
LeftEyeVelY	deg/s	Yes		HeadInertialAccelY	g	Yes
LeftEyeVelZ	deg/s	Yes		HeadInertialAccelZ	g	Yes
LeftPupilCol	pixels	Yes		HeadInertialFrame	Count	
LeftPupilRow	pixels	Yes		TargetHor	Units	Yes
LeftPupilCovXX	pixels²	Yes		TargetVer	Units	No (0)
LeftPupilCovXY	pixels²	Yes		visual_pos3	Units	No (0)
LeftPupilCovYY	pixels²	Yes		visual_pos4	Units	No (0)
LeftPupilMethod	enum	Yes		visual_Sync_Time	s	Yes
LeftEyeMarkerTorsion	deg	No (NaN)		visual_Sync_Frame	Units	Yes
LeftEyeLeftMarkerCol	pixels	No (NaN)		SyncboxDigIn0	bool	Yes
LeftEyeLeftMarkerRow	pixels	No (NaN)				
LeftEyeRightMarkerCol	pixels	No (NaN)				
LeftEyeRightMarkerRow	pixels	No (NaN)				
LeftReflexCenterX	mm	Partly (NaN)				
LeftReflexCenterY	mm	Partly (NaN)				
LeftReflexRimX	mm	No (NaN)				
LeftReflexRimY	mm	No (NaN)				

Table 5.1: Monocular EyeSeeCam output variables of left eye, and their availability.

problems. The LSTM model is used as well by Versteeg (2019), a concurrent master thesis research project at the Delft University of Technology.

5.3. Learning

Some time-domain analysis can already be performed, which is the effect of learning in a gaze tracking task. In a manual tracking task experiment, usually a training phase is included to introduce the task to participants, until a stable level of performance is achieved. Hereafter, the measurement phase takes place.

In the setup as used by Büskens (2018), gaze performance is determined during post-processing the gaze recordings, hence it is unknown whether a stable gaze performance is reached once the measurement phase starts. In this research, it was assumed that gaze performance is stable as soon as manual control performance is stable, which value is observed after each trial.

For pure gaze tracking tasks, this manual control performance is not available. Therefore, the learning for gaze tracking tasks should be investigated. This is done by using the available gaze records from the training phase from Büskens (2018).

First, the performance for each trial of each condition is determined, as shown in fig. 5.3. In this boxplot, gaze performance clearly fluctuates in the practice phase. In the measurement phases, the first trial usually has worse gaze performance compared to the other trials from the same condition. The remaining of the trials show stable performance.

However, it is unknown which bandwidth signal was used. In this analysis, the lower bandwidth signal was used to calculate the performance score. Furthermore, the order in which the conditions were presented altered, such that horizontal axis from fig. 5.3 is not representative for the learning curve. This is only valid for the practice phase, which was always performed first. However, in the measurement phase, trials 2 to 8 show consistent performance, hence less trials could be considered here.

Therefore, the learning effect is investigated more thoroughly, as is shown in fig. 5.4. Here, a running average performance (RAP) is shown, i.e., the variance of the error over the variance of the target signal for a certain time window. At each index from fig. 5.4, two seconds (100 indices) before and after are taken as this time window. For the first and last two seconds, a constant value is applied.

One would expect that the variance of the error decreases steadily as the participant get used to the task. However, the RAP shows significant peaks at more or less constant indices, which can be the result of a sudden drop in input signal variance, or increase in error. Furthermore, it can be seen that the initial values are significantly different, which could be the result of a poor calibration procedure. Therefore, it gaze learning will be further investigated for pure gaze tracking tasks.

5.4. Conclusion

In this chapter the time domain method is discussed. The main reason to include this type of analysis is to capture directional issues related to oculomotor performance. Furthermore, other features compared to the frequency domain analysis can be analyzed, such as saccade frequency. For this method, an off-the-shelve algorithm will be applied.

Some questions arise from this chapter. First of all, what features are critical to be able to separate smooth-pursuit and saccades? And, is this time domain analysis suitable for this type of experiments, and should this research be investigated in further research? Lastly, the learning effects in gaze tracking tasks should be further investigated to determine the magnitude of this effect, as no solid conclusions can be drawn yet.

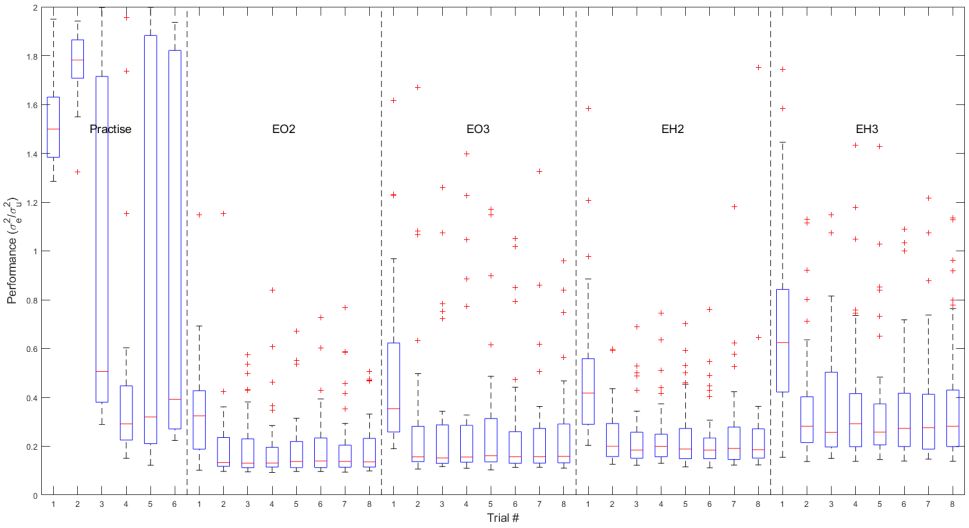

Figure 5.3: Boxplot with gaze performance scores for each trial of each condition from gaze records by Büskens (2018). EO is an eye only tracking task, EH is a eye-hand tracking task, 2 denotes the lower bandwidth, 3 denotes the higher bandwidth.

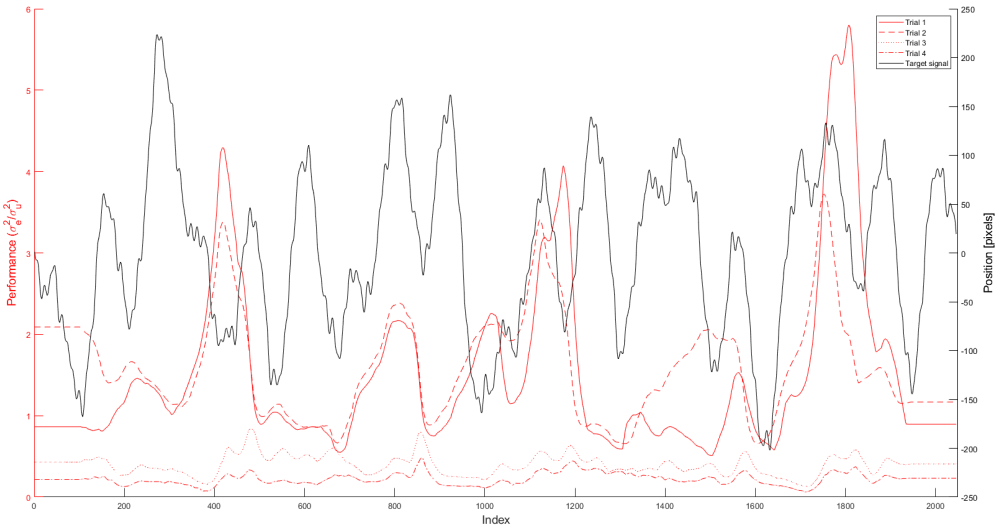

Figure 5.4: Running average performance (red plots, left vertical axis) for the first four trials of the practise phase with the target signal value (black plot, right vertical axis).

6

Research experiments

In this chapter, two gaze tracking tasks are proposed, being the main experiment and a verification experiment. The main experiment involves a gaze tracking task to investigate the oculomotor dynamics of vertical eye movements and the ability to quantify the oculomotor dynamics using a two dimensional gaze tracking task, using a binocular eye tracking system. The verification study is used to identify possible differences with a similar conducted experiment from Büskens (2018) compared to the proposed main experiment.

6.1. Main experiment

A gaze tracking task is proposed in order to investigate oculomotor control dynamics to classify neurodegeneration in various brain areas. Therefore, the task to be performed will challenge participants to continuously follow a target stimulus on a display, to evoke smooth pursuit eye movements and, if smooth pursuit fails, catch-up saccadic eye movements.

6.1.1. Task description

The primary task in the experiment is to follow a moving stimulus by using the eyes. The stimulus moves in a smooth fashion, yet challenging enough for subjects to fixate their gaze upon. Three conditions are considered: A horizontal, vertical and two-dimensional condition, relating to the motion axis of the stimulus. During the entire experiment, no secondary tasks have to be performed.

This research can be considered as a follow-up study of Büskens (2018), hence the setup is almost identical in terms of apparatus. However, compared to the eye-only condition from Büskens (2018), several differences are present. These are shortly discussed.

- The target stimulus will be the only stimulus displayed, colored green with a red center for proper visual attention, and the background of the screen will be black to create a dark environment for sufficient pupil size, which results in more accurate eye tracking compared to a smaller pupil size. Furthermore, a dark background decreases Computer Vision Syndrome complications.
- The experiment procedure includes a pre- and post-calibration phase of twenty seconds. Before and after each trial, this short calibration phase is performed. Consecutive trials share a post- and pre-calibration procedure to save time. A 5-point calibration is applied, where the maximal values of the target signal of that particular trial are used for each corner. The center of the screen where the target signal equals zero is the last calibration point.
- A binocular eye tracker is proposed for the main experiment. However, Büskens (2018) used a monocular eye tracking system. The verification study should reveal possible differences using this setup.
- The target signal is slightly different compared to Büskens (2018). This is more elaborated in section 6.1.5.

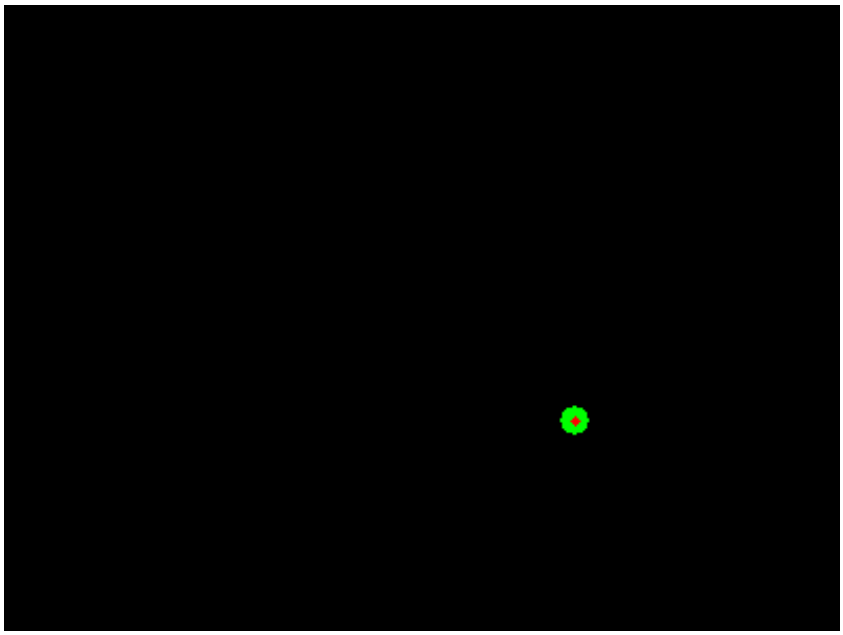

Figure 6.1: Snapshot of experiment display during a trial.

6.1.2. Apparatus

Two computers are used to run the experiment. One Windows computer is used to display the stimulus on a 32 inch touchscreen, using the Cogent graphics toolbox in MATLAB. An impression of the task is shown in fig. 6.1. A MacBook is used for obtaining the gaze data with the eye tracker system. Both computers are connected to an Arduino, which generates a 220 Hz pulse-train, to synchronize the data acquisition.

For gathering the gaze data, the EyeSeeCam Sci eye tracker is used for its relatively high frequency, compared to the Tobii eye trackers. The sample rate of 220 Hz is used. The EyeSeeCam software package automatically converts the gaze data to a *.mat* file, which can be used in a MATLAB environment for further analysis. The GUI of this software package is shown in fig. 6.2.

The experiment room will be blinded to create a dim environment to minimize the appearance of other visual stimuli due to reflections, which might distract the subject. This dark environment should also increase the pupil size, which increases the data quality of the eye tracker device.

As the current eye-tracker setup needs some space for wiring, the experiment room is not completely dark. Instead, a low-light environment is created. As mentioned earlier, a dark environment is desired, as the pupil detection of the eye tracking device is most accurate in these conditions. Head movements are undesired during the data acquisition, hence a chin-rest is used for head stabilization.

Common for pursuit displays is the current state information of the controlled element. As gaze is controlled in this task, its state could be displayed on the screen. However, due to significant delay of the gaze signal from the eye tracker, including gaze feedback is likely to distract the subject, which may deteriorate gaze data quality. It is therefore omitted.

6.1.3. Subjects

Adults are expected to be suitable subjects, as the oculomotor system has developed entirely (Katsanis et al. 1998). Additionally, the youngest and oldest subjects cannot have significant age differences, as of neurodegeneration due to aging (Büskens 2018). Hence, a similar subject group is chosen as the younger group from Büskens (2018), which are 20-30 years old. Preferably, an equal distribution of male and female is used, but this is not a strict requirement.

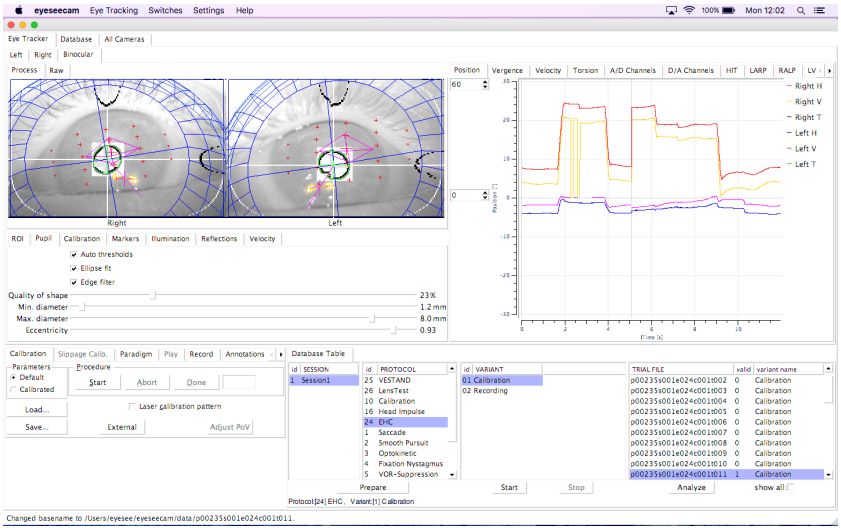

Figure 6.2: Snapshot of EyeSeeCam software of binocular tracking.

Subjects should have no brain impairments or neurodegenerative deficits. Furthermore, the subjects should have normal or corrected-to-normal visual acuity to be able to sharply see the stimulus, and a form of color blindness is not accepted due to the characteristics of the stimulus. Visual acuity problems can be covered by wearing contact lenses, but wearing glasses is not desired from a practical point of view, as the eye tracker is a head-mounted system as well.

6.1.4. Experiment procedures

A familiarization phase and general calibration procedure are applied before the measurement runs start for the monocular and binocular conditions, as shown in fig. 6.3. The familiarization should introduce the task to the participant, such that the task is entirely clear when the measurement phase starts and no measurement data is lost while the subject shows unexpected behaviour.

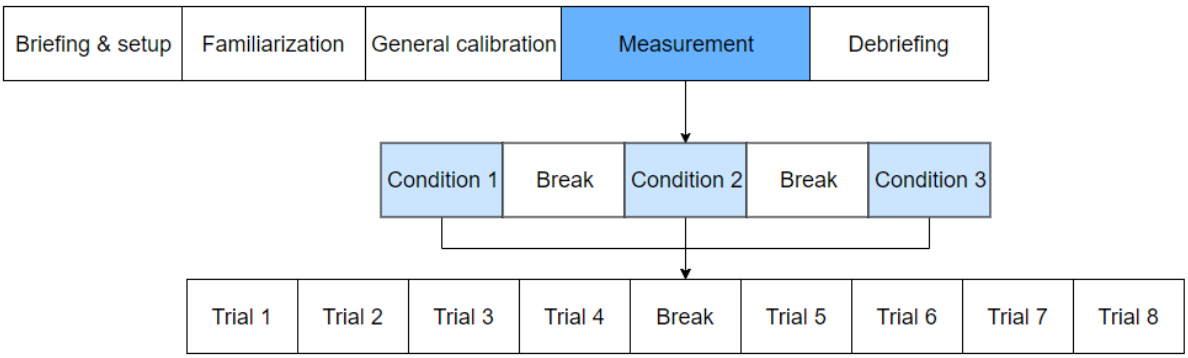

Figure 6.3: Experiment procedure, blocks highlighted in blue contain sub procedures.

The general calibration experiment is a standardized experiment, and creates a more accurate model of the eye, in terms of curvature, which should enhance the quality of the gaze data. This is shown in fig. 6.2, where the blue grid around the eyes resembles the curvature of the eye ball.

After the briefing (appendix A), of which a copy is provided in advance to the participant, participants are asked to give informed consent (appendix B).

Each condition has eight trials. Halfway, a break of 1 to 3 minutes is performed such that the eyes can recover from the task. In between conditions, a longer break is applied. If all conditions and trials were to be executed without breaks, it is expected that the subjects

Table 6.1: Latin square diagram. H = horizontal condition, V = vertical condition

Subject #	Condition		
01, 07, 13, 19	H	V	2D
02, 08, 14, 20	2D	H	V
03, 09, 15, 21	V	2D	H
04, 10, 16, 22	H	2D	V
05, 11, 17, 23	V	H	2D
06, 12, 18, 24	2D	V	H

would barely be able to keep their eyes open at the last couple of trials, and data quality would deteriorate rigorously. Therefore, sufficient breaks are taken into account, which can be extended upon request.

Regarding subject size, a set of 24 subjects is used, which is approximately equal to the subject size as used by Haartsen (2017) and Büskens (2018). A Latin square diagram can be constructed, which is shown in table 6.1. In this diagram, all different combinations of condition orders are used to mitigate biased results of certain conditions due to fatigue. To have sufficient redundancy, combinations of conditions are performed four times, hence the block of subjects 1 to 6 from table 6.1 is identical to the block of subjects 7 to 12.

6.1.5. Input signal

A quasi-random target signal will be used such that participants cannot predict the future states of the target signal. This is achieved by using a sum of eleven sinusoids as input signal (eq. (4.6)). To be able to investigate crossfeed, two different sets of frequencies are used, which are matching the frequencies as used by Haartsen (2017).

A power of 2 is chosen as measurement window, $T_m = 40.96s$, which is common for tracking tasks, as the Fourier transform was only able to deal with data sets having a power of two size. However, this is not the case anymore, such that different measurement windows can be applied as well. Short trials with sufficient breaks guarantee that subjects are able to maintain their focus throughout the experiment, and prevent CVS problems.

The CFs are used for generating the phases of the multisine signal. A myriad combinations of phases are generated, and eventually a set of phases is used which result in an average CF. However, different sets of phases could be used as well which result in the same CF, but this was not desired to limit the amount of variables in the setup.

One significant change compared to the input signal of Büskens (2018) is the use of a second-order low-pass filter, as shown in eq. (6.1), as used by De Vries (2016), where $T_{A_1} = 0.1$ and $T_{A_2} = 0.8$. Using this filter, the high frequency components have significant less power, resulting in an easier signal to be tracked. This was desired as the input signal from Büskens (2018) was deemed too difficult to be tracked in a pure gaze tracking task, especially at the highest frequency components.

$$H_A(j\omega) = \frac{(1 + T_{A_1} j\omega)^2}{(1 + T_{A_2} j\omega)^2} \tag{6.1}$$

The amplitude of the vertical signal is chosen such that the amplitude variance of both signals are equal. The amplitudes are scaled such that the signal covers a significant part of the display, but does not require the participant to move its head.

Furthermore, a new set of phases is obtained by using an average CF. A MATLAB script is constructed to generate the forcing functions. The frequencies are identical to the ones used by Büskens (2018). The target signal values for both the horizontal and vertical signal are shown in table 6.2. The horizontal and vertical axes are referred to as the x-axis and $y-$axis respectively.

A time series of the input signal for the horizontal condition is shown in fig. 6.4. The signal starts with a 5 point calibration of 20 seconds. This yields a range from index 1 to 1000, as the signal is sampled with 50 Hz. Hereafter, a 4 second (index 1001 to 1200) run-in

Table 6.2: Input signal parameters.

k [-]	n_x [-]	n_y [-]	ω_x [rad/s]	ω_y [rad/s]	A_x [pixels]	A_y [pixels]	ϕ_x [rad]	ϕ_y [rad]
1	4	3	0.6136	0.4602	43.1532	40.5878	5.6627	2.0544
2	7	5	1.0738	0.7670	31.0516	33.6087	4.7021	3.1758
3	13	11	1.9942	1.6874	15.6475	16.7602	5.1108	5.1314
4	19	17	2.9146	2.6078	8.9927	9.1773	1.8137	2.7613
5	29	23	4.4485	3.5282	4.6767	5.7677	1.1288	4.3078
6	37	31	5.6757	4.7553	3.2630	3.6447	3.0070	4.4454
7	43	41	6.5961	6.2893	2.6542	2.4390	0.5584	3.6304
8	53	59	8.1301	9.0505	2.0464	1.5661	4.5919	1.5693
9	79	83	12.1184	12.7320	1.3865	1.1508	4.8193	4.9037
10	109	107	16.7204	16.4136	1.1255	0.9797	1.5588	1.3798
11	157	151	24.0835	23.1631	0.9747	0.8501	0.5004	5.4368

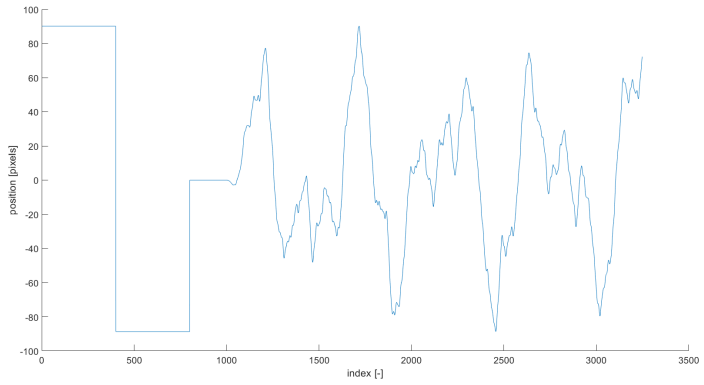

Figure 6.4: Time series of the horizontal component of one trial.

is applied, where the multisine signal is multiplied with a quarter period of a sine squared, as shown in eq. (6.2). After the run in, the 40.96 s (2048 data points, index 1201 to 3248) measurement phase starts. This concludes one trial. To avoid learning effects, every second trial uses a flipped input signal.

$$f_t(t) = f_t(t) \cdot sin^2\left(\frac{2\pi}{16}t\right) \quad \text{for } 20 < t \leq 24 \tag{6.2}$$

Since the horizontal and vertical frequency components are fixed, four combinations are possible to change the target signal for the 2D condition by flipping the signals. To account for loss of data, each trial will be performed twice. Therefore, each condition will have 8 trials, which are two blocks of these combinations. An overview of the target signal with respect to trial is shown in table 6.3.

6.1.6. Hypotheses

The main purpose of this experiment is to investigate horizontal and vertical eye movements and their interaction. Furthermore, the performance of each direction is examined to classify neurodegeneration.

M.1 A perfect performance (variance of the error normalized by the variance of the target signal) would indicate a value of zero. It is expected that the vertical gaze performs slightly less than horizontal gaze, because more muscles are involved, which is more error prone. Therefore, corrective eye movements should be made. Vertical gaze is induced by a combination of the vertical recti and oblique oculomotor muscles, while horizontal eye movements are induced only by using the horizontal recti (section 3.4).

Table 6.3: Forcing function sign conventions for different trials per condition.

	H		V		2D	
Trial	f_x	f_y	f_x	f_y	f_x	f_y
1	+	0	0	+	+	+
2	-	0	0	-	+	-
3	+	0	0	+	-	+
4	-	0	0	-	-	-
5	+	0	0	+	+	+
6	-	0	0	-	+	-
7	+	0	0	+	-	+
8	-	0	0	-	-	-

Concerning the 2D condition, the eyes can move in a more natural manner, where horizontal and vertical eye movements are well adjusted to each other. This could be beneficial for performance. On the other hand, the signal moves both in horizontal as vertical in a random fashion, which is more demanding for the subject. This can decrease performance. The latter is expected to dominate.

To separate aforementioned elements, the variance of the output gaze can be investigated, again normalized by the variance of the input signal. This control activity can give insight whether horizontal or vertical eye movements only require more effort compared to the 'natural' 2D condition, as is expected.

With a decrease in performance, it is expected that more saccadic eye movements are generated in the vertical condition compared to the horizontal condition, and most saccadic eye movements are present in the 2D condition, due to the challenging target signal.

M.2 Considering the mathematical model of the oculomotor dynamics, no significant differences are expected between the horizontal and vertical plant, i.e., the gain, time delay, and neuromuscular damping and natural frequency are comparable. This is because the anatomic substrates of both systems are comparable. However, due to the complexity of the generation of vertical eye movements, the performance of vertical eye movements is expected to be worse, hence the model parameters can show some differences. It is expected that the gain is mostly affected, and will be lower than the gain for the horizontal condition.

For the 2D case, it is expected that the participant shows different behavior than for the other two conditions, because in the 2D case the participant will be able to cut corners to minimize the effort to converge to the target stimulus. This can result in significantly lower gains, than compared to the horizontal and vertical condition, but in lower time delays as well.

M.3 The stimulus is displayed at approximately 50 cm in front of the participant. As the stimulus is relatively small, the participant should accommodate to see the stimulus sharply. As the task duration and number of trials are significant, fatigue is expected to be present at the last couple of trials, espcially at the last condition. Although sufficient breaks are taken into account, this can have a significant effect on both performance and control parameter values. It is expected that with fatigue, the number of both saccades and blinks increase as well.

M.4 Gender differences are present in saccadic scanning paths (Sammaknejad et al. 2017), and in dynamic overshoot of pro-saccades and frequency of catch-up saccades in SP (Bargary et al. 2017). The latter is very relevant for this research, and it is expected that this observation can be made as well in this experiment. This means that more catch-up saccades should be present in trials from males.

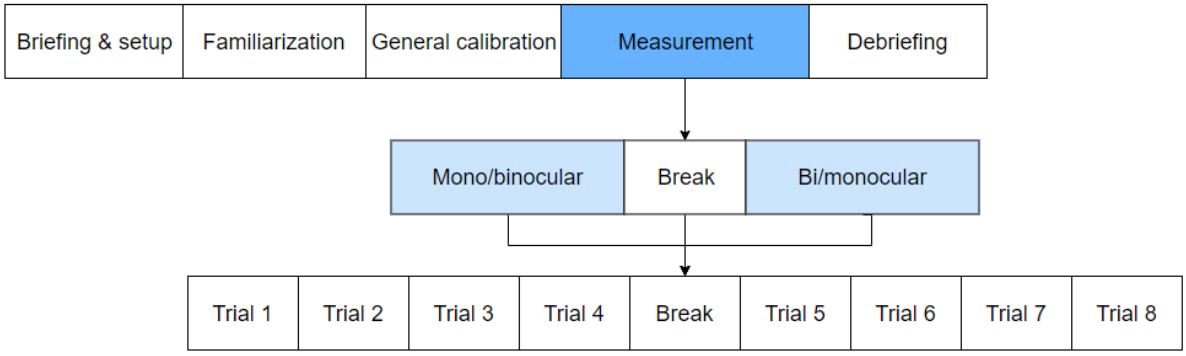

Figure 6.5: Verification experiment procedure, blocks highlighted in blue contain sub procedures.

6.2. Verification experiment

The verification experiment is a subset of the main study, as only the horizontal condition is applied. The main purpose of the experiment is to be able to explain differences which might occur due to a slightly different setup compared to the experiment performed by Büskens (2018).

6.2.1. Task description & apparatus

The task description is identical to the main experiment. Participants have to follow a smoothly moving stimulus on the display with their gaze, without having to perform any secondary tasks.

The experiment procedure is comparable to the main study, but instead of the three directional conditions, only the horizontal condition is applied. This condition will be performed with both a monocular and binocular eye tracker setup. An overview is shown in fig. 6.5.

Four participants are required, such that the small Latin square diagram can be performed twice. This Latin square diagram consists of two rows, one with the monocular setup first, and one with the binocular setup first.

6.2.2. Input signal

The input signal of the horizontal signal is identical to the horizontal input signal of the main experiment. However, as only the horizontal condition is applied, the vertical target signal equals zero for all trials.

6.2.3. Hypotheses

This verification study should close the gap of the proposed experiment in next section, and the eye-only condition from the experiment conducted by Büskens (2018). Compared to this experiment, only minor differences are expected to be present.

V.1 First of all, as a second-order low-pass filter is used for defining the stimulus amplitudes, the high frequency components of the target signal have less power. Therefore, the signal should be easier to track, and therefore it is expected that the error is less, and performance is increased. This should mean that less saccades are present as well.

Additionally, the signal-to-noise ratio is decreased at these high frequency components. This means that the estimated pilot model values at these frequencies (see eq. (4.5)) are more sensitive to errors. This can result in different values for these high frequency components, which will have mainly influence on the neuromuscular system parameters from eq. (4.2). However, Büskens (2018) used a zero weight for the highest FRF data, hence this difference is probably negligible.

V.2 The change in stimulus size and color are expected to increase the performance slightly, as slippage on the retina is less likely to occur due to the small, red dot in the center of the stimulus.

It is expected that the black background image does not directly result in an improved oculomotor performance, but can help for gathering more accurate gaze data due to an increased pupil size.

V.3 As the monocular and binocular eye tracking setups use cameras with identical specifications, it is expected that no significant differences are present.

V.4 The pre- and post-calibration phases are expected to increase the absolute performance of the oculomotor system, as it is more extensive than the calibration process performed by Haartsen (2017) and Büskens (2018). For the pilot model, this is expected to have mainly influence on the gain parameter.

V.5 An increase in performance due to learning is not expected, as eye movements are very natural movement for humans to perform, and no control device is needed. However, it will be interesting to see whether learning effects might be present for some subjects.

6.3. Conclusion

In this chapter two experiments are proposed. The the main experiment includes a vertical and two-dimensional tracking task. The purpose of this experiment is to investigate the performance and interaction of horizontal and vertical SP and saccadic eye movements. In this way, this type of experiment can be used to classify neurodegeneration, such that it can be used as a tool in a clinical setting. The verification experiment should close the gap between an earlier used setup from Büskens (2018) and the main experiment.

7

Conclusions

In this literature survey, an experiment is proposed which should serve as a novel tool to classify neurodegeneration, to be used in a clinical setting. The experiment is a gaze tracking task, where participants are challenged to follow a continuously moving target with their eyes only.

The foundation of this study is the analysis of eye movements, as they are easily quantified, and processes regarding eye movements are spread across the entire brain area. Hence, a certain impairment could provide useful information on brain damage and severity.

A head mounted eye tracking device will be used to capture gaze data. The experiment is constructed such that both a frequency domain method and a time domain method can be used to analyze the gaze dynamics. Both methods have different describing parameters, such that one can serve as validation tool for the other.

Two experiments are proposed. A pilot study should serve as the connection between the main experiment, which examines horizontal, vertical and two-dimensional gaze, and the experiments from earlier, similar research. Accordingly, several established research questions could be solved, which are:

1. *How are smooth pursuit and saccadic eye movements related to each other?*
2. *How are vertical and horizontal eye movements related to each other?*
3. *Which frequency model features should be used to describe the oculomotor model most accurate?*
4. *Is pattern recognition a suitable time domain analysis method for gaze data?*
   (a) *Which features should be used?*
   (b) *Which classes should be used?*
5. *How are the parameters from the time-domain analysis method and frequency-domain analysis method related?*
6. *What learning effects arise in pure gaze tracking tasks?*

Part III:

Paper appendices

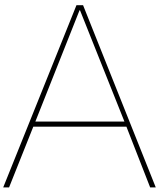

Briefing

Experiment briefing: Two-dimensional gaze tracking task

This document is intended for participants of a two-dimensional gaze tracking experiment performed at the Erasmus Medical Center in Rotterdam, at the department of Neuroscience. The purpose of this document is to provide some general information to the participants, regarding the task to be executed and their rights during the experiment.

1. Experiment goal

The goal of the experiment is to investigate the two-dimensional gaze (eye movements) by analyzing the oculomotor control dynamics during a target-following task. This experiment contributes to the on-going development of tools for classifying neurodegeneration, i.e., to help clinicians with better functional diagnosis based on quantitative measurements.

2. Experiment task

The participant will be seated behind a computer screen wearing a monocular or binocular eye tracker system. A picture of a participant wearing such an eye tracker is shown in Fig. 1. Here, the binocular eye tracker is shown. Both eye trackers use infrared cameras to create an image of the eye via an infrared mirror, from which eye movements are detected.

Fig. 1: Binocular eye tracker

During each trial, participants have to follow a moving stimulus on the computer screen with their eyes only, while keeping their head still. As a fixed head position and orientation is critical for collecting good eye data, a chinrest is used to minimize head movements.

Three different conditions will be tested. One conditions has a stimulus moving only in horizontal direction, one condition has a stimulus moving only in vertical direction, and one condition has a stimulus moving both in horizontal and vertical direction at the same time. A screenshot of the visual stimulus is shown in Fig. 2.

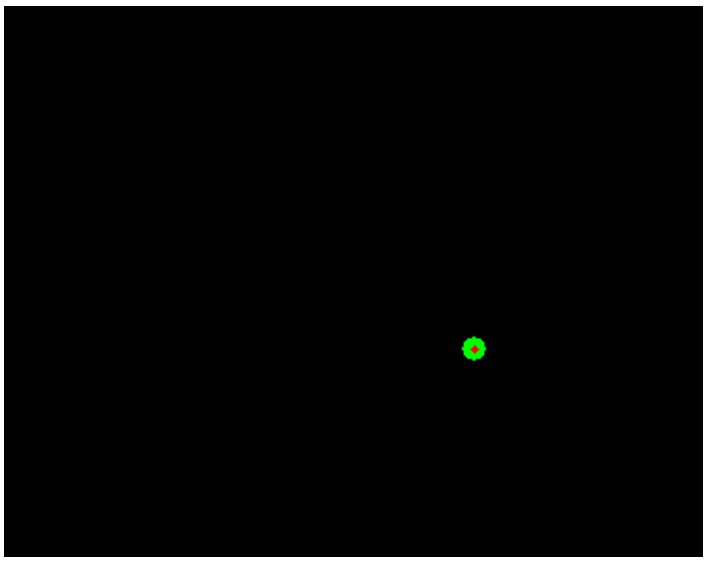

Fig. 2: Screen snapshot of trial phase

3. Experiment procedures

First, a short briefing will introduce the experiment to the participant and highlight some important aspects. Then, the visual acuity of the participant will be tested, before the actual experiment can start. Finally, all participants will be asked to provide written informed consent prior to the start of the experiment.

To introduce the participant with the task, a familiarization phase is included. Then, a general calibration procedure is performed. Hereafter, the participant will run twice through the three conditions. The conditions will be randomized, but each condition consists of 2 blocks of 4 repeated consecutive trials of the same condition. The duration of a single trial is approximately one minute.

Before the start of measurement phases, a general eye-tracker calibration procedure will be performed, where the participant is asked to fixate on the blue dots appearing on the screen. Before each trial, a second calibration procedure is applied, where the participant has to fixate on the small red dots in the larger green dots. After each calibration, the trial will start automatically. At the end of the trial, a new calibration procedure is started immediately. An overview of the experiment procedure can be found in Fig. 4.

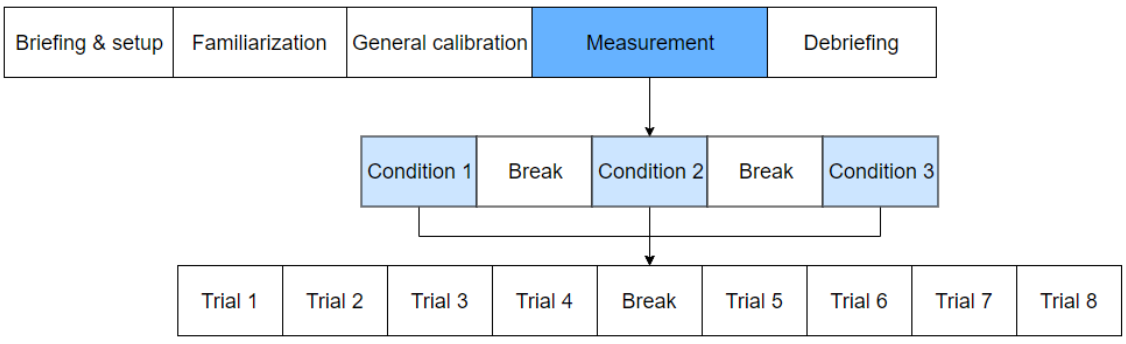

Fig. 4: Schematic overview of experiment procedure, blue cells have sub-procedures

Between each fourth and fifth trial, a short break (ca. 1-3 mins) is scheduled. In between different test conditions, we will take a longer break if desired.

The total duration of the experiment, including briefing and setup, is approximately 60 minutes. The experiment will take place in one session.

4. Participant rights

Participation to the experiment is voluntary. This includes that the participant can decide to stop with the experiment at any moment in time.

Participation to the experiment will be confidential and anonymous. This means that the information of the participant and data collected during the experiment will only be available for the researcher. The collected data will be anonymized in further documentation or publications. Participating on the experiment means that you agree that your anonymized data may be published.

5. Inclusion criteria

For this experiment, the participant has to meet certain inclusion criteria. These are listed below. The participant:

- Should be not younger than 20 years old, nor older than 30 years old.
- Does not have any serious health issues related to neurodegeneration.
- Did not take any sedatives or medication affecting the central nervous system, at least 48 hours before the start of the experiment.
- Cannot wear glasses during the experiment.
- Has good visual acuity (wearing contact lenses is allowed).
- Has no color vision deficiency.

To make sure you have understood all of the above, you are asked to sign an informed consent form (see next page) at the end of the experiment briefing.

Date: 05-04-2019

B

Informed consent form

Experiment Consent Form

Aging effect in quantifying gaze dynamics

I hereby confirm that:

1. I volunteer to participate in the experiment conducted by the researcher (**Viktor de Jonckheere**) under Supervision of **dr.ir. Daan Pool** from the Faculty of Aerospace Engineering of TU Delft and **dr.ir. Johan Pel** from the Erasmus Medical Center. I understand that my participation in this experiment is voluntary and that I may withdraw and discontinue participation at any time, for any reason.
2. I have read the experiment briefing (dated 05-04-2019). Also, I affirm that I understand the experiment instructions and have had all remaining questions answered to my satisfaction.
3. I understand that my participation involves performing a gaze tracking task where eye movements are recorded with an eye tracker devices.
4. I confirm that the researcher has provided me with detailed safety and operational instructions for the hardware (eye tracker) used in the experiment.
5. I understand that the researcher will not identify me by name in any reports or publications that will result from this experiment, and that my confidentiality as a participant in this study will remain secure.
6. I understand that this research study has been reviewed and approved by the TU Delft Human Research Ethics Committee (HREC) and the Erasmus University. To report any problems regarding my participation in the experiment, I know I can contact the researchers using the contact information below or, if necessary, the TU Delft HREC (hrec@tudelft.nl).
7. I have been given a copy of this consent form.

My Signature	Date
My Printed Name	Signature of researcher

Contact information researcher:	Contact information research supervisor
Viktor de Jonckheere	dr. ir. Daan Pool
v.p.a.dejonckheere@student.tudelft.nl	d.m.pool@tudelft.nl
+31 6 48620530	+31 15 2789611

C

Binocular EyeSeeCam validation

C.1. Introduction

For the experiment as described in part I, referred to as the main experiment, a binocular EyeSeeCam model was used. However, earlier research (Büskens (2018), Büskens et al. (2019)) used a monocular version of the same type of eye tracker. To mitigate false conclusions with respect to earlier mentioned research due to differences in eye tracking methods, a validation experiment was performed to find differences in the monocular and binocular records of the EyeSeeCam.

C.2. Methods

4 participants, 3 males and one female, performed two sets of 8 trials of the horizontal condition (1D-H) from the main experiment; one set with the monocular and one set with binocular EyeSeeCam. A small break was applied after each 4 trials. Identical target forcing function and experiment setup was used as described in the main experiment. Alternating, either a subject started with the monocular or binocular method. Three outcome variables are used to identify differences; the percentage of data points discarded in each trial, measurement noise and time delays are expected to be constant within both methods, as the camera models were assumed to be identical.

C.3. Results

A representative example of gaze time trace can be found in Fig. C.1, which does not indicate a clear difference between monocular and binocular records. The amount of discarded data points due to tracking errors, such as blinking, is measured as a percentage of total data points per trial. A repeated measures ANOVA reveals that percentage means do not show significant differences ($F(2,\ 1.195) = 0.839$, $p = 0.477$). Measurement noise is part of the remnant, which signal power is determined in the frequency domain. A repeated measures ANOVA indicates that differences in mean scores of the remnant power were statistically insignificant ($F(5,\ 0.01) = 1.010$, $p = 0.446$). Furthermore, the gaze dynamics model selected in the main experiment, M2-WR, is used to fit τ_g. A repeated measures ANOVA of the mean time delays does not show significant differences ($F(2,\ 2.474\text{E}06) = 0.487$, $p = 0.637$).

C.4. Conclusions

Both the time traces and dependent variables do not reveal differences between monocular and binocular obtained gaze records. Therefore, it can be concluded that the two recording methods are identical.

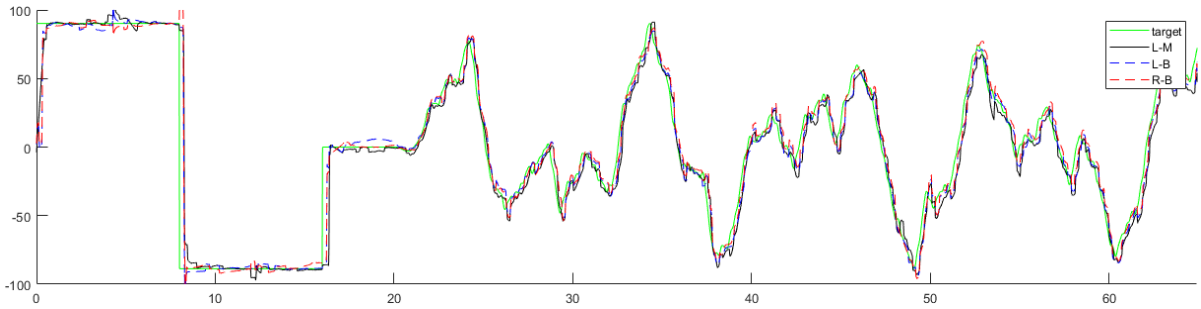

Figure C.1: Example time delay including both monocular and binocular recorded gaze. L-M, L-B and R-B correspond to left monocular, left binocular and right binocular gaze, respectively.

D

Torsional eye movements

D.1. Introduction

One possible cause of cross-feed can be torsional components of eye movements. In the experiment setup of the main experiment, the EyeSeeCam uses the pupil position to determine gaze. However, as this is a black circle, torsional eye movements, rotating the pupil (counter)clockwise, cannot be captured using the EyeSeeCam, as it tracks the pupil's position. However, there is a feature which allows the EyeSeeCam to track torsion as well, which requires the selection of markers in the video records. However, these markers are usually of poor quality, resulting in improper torsion signals. To solve this problem, a contact lens was developed with additional markers, which should increase the torsion signal quality.

D.2. Methods

A pilot experiment was conducted to examine torsion in the 2D condition. Using the experiment setup from the main experiment, four trials of the 1D-H and 2D condition were performed while wearing the lens. Subject 1 had the lens in the left eye, while Subject 2 had the lens in the right eye. It was expected that torsional eye movements are mostly present at vertical excited frequencies, as these muscle pairs are less aligned with the vertical screen direction compared to the medial and lateral recti muscles with the horizontal screen direction. Furthermore, cross-feed is examined as well by inspecting the perpendicular excited frequencies.

D.3. Results

An example time trace of torsion, g_T is shown in Fig. D.1, which is the raw signal. The power spectra show differences in the 1D-H condition between subjects. Subject 1 has smaller signal to noise ratios at ω_H than Subject 2. In the 2D condition, a remarkable difference is present in the power spectra; Subject 1 shows torsion at the vertically excited frequencies, whereas Subject 2 shows torsion at the horizontally excited frequencies. However, the high peaks at Fig. D.2b and D.2d can be induced by improper calibration. The absence of torsion at ω_V in Fig. D.2d can imply a perfect synchronization of oblique and superior and inferior rectus muscles. Inspecting cumulative torsional variance, which were not normalized with the target signal variance as these have different units, it can be noticed that torsion is mostly present at one or two low-frequency components of the gaze torsion signal.

D.4. Conclusion

In this pilot study, torsional eye movements were briefly investigated using video-oculography gaze records. Due to improper calibration and small subject size (N = 2), solid conclusions cannot be drawn, but frequency analysis shows interesting results, as torsional eye movements are mainly induced at low-frequency components of the used target signal. As this is the region where cross-feed was detected as well, these could be correlated.

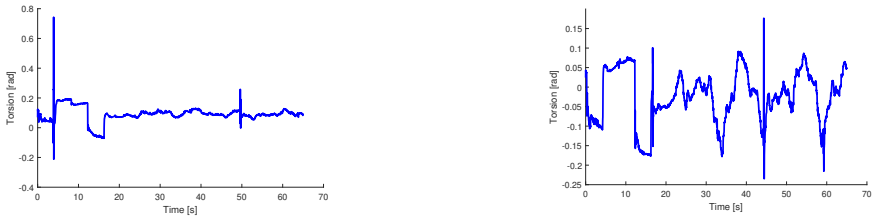

(a) 1D-H condition

(b) 2D condition

Figure D.1: Example of torsional eye movements of Subject 1, raw signal.

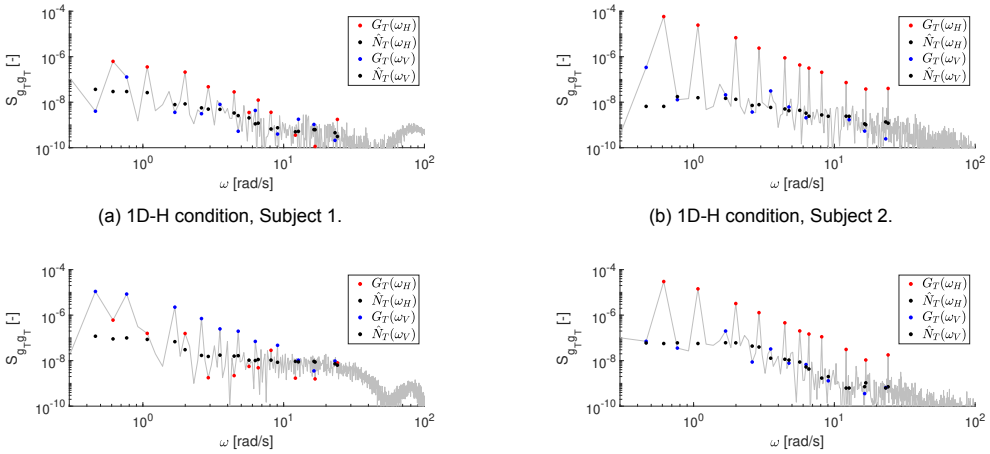

(a) 1D-H condition, Subject 1.

(b) 1D-H condition, Subject 2.

(c) 2D condition, Subject 1.

(d) 2D condition, Subject 2.

Figure D.2: Example power spectra for both subjects in both conditions.

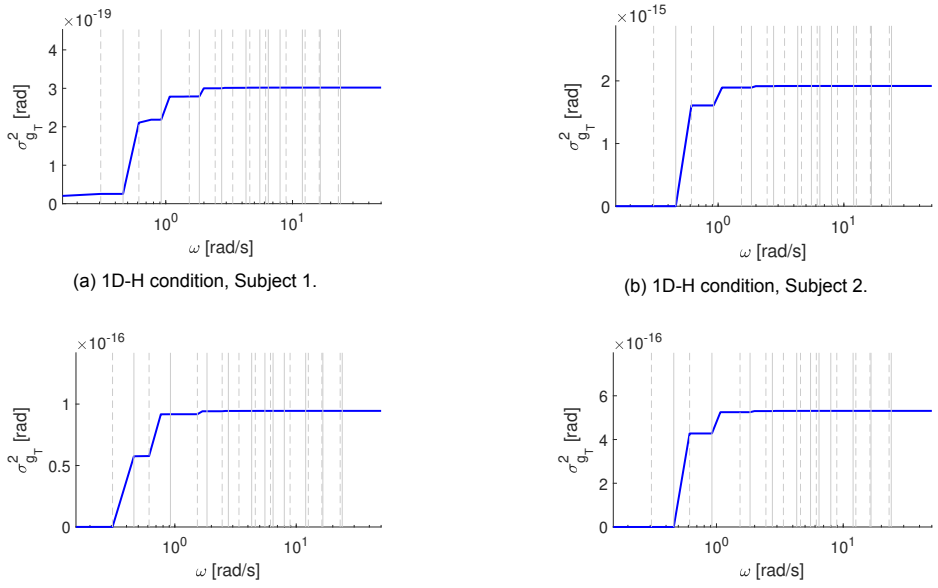

(a) 1D-H condition, Subject 1.

(b) 1D-H condition, Subject 2.

(c) 2D condition, Subject 1.

(d) 2D condition, Subject 2.

Figure D.3: Examples cumulative performance at each frequency for both subjects in both conditions.

E

Right gaze

In this part of the appendix, some tables and figures are shown for the right gaze, whereas the left gaze was shown in the paper from Part I. This section includes the performance, natural frequency values, relative remnant and VAF scores.

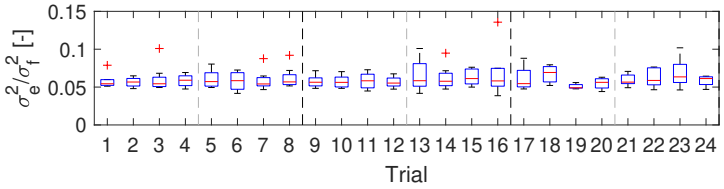

(a) Horizontal performance in 1D-H condition.

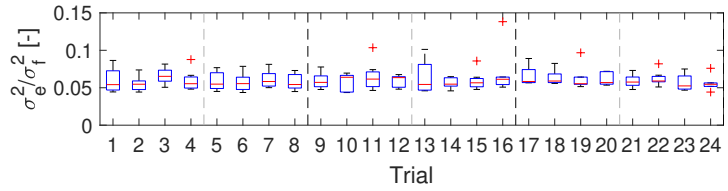

(b) Horizontal performance in 2D condition.

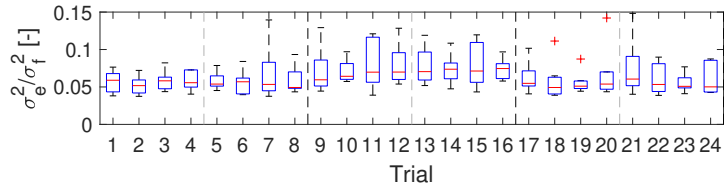

(c) Vertical performance in 1D-V condition.

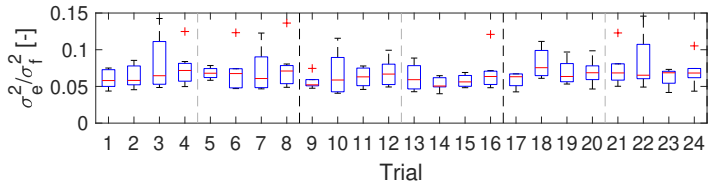

(d) Vertical performance in 2D condition.

Figure E.1: Performance (right gaze) per trial per condition; short breaks are indicated with light gray dashed lines, longer breaks are indicated with black dashed lines.

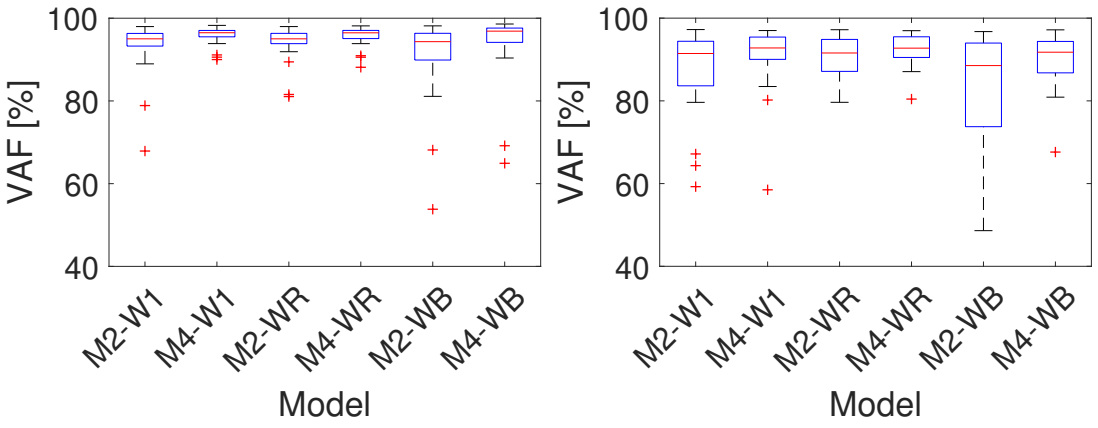

(a) $H_{g_H}(s)$, 1D-H condition.

(b) $H_{g_V}(s)$, 1D-V condition.

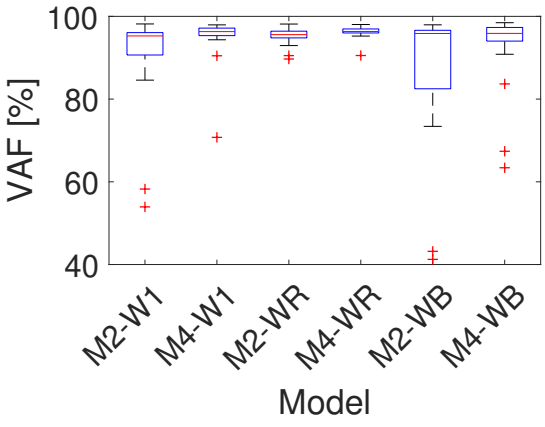

(c) $H_{g_H}(s)$, 2D condition.

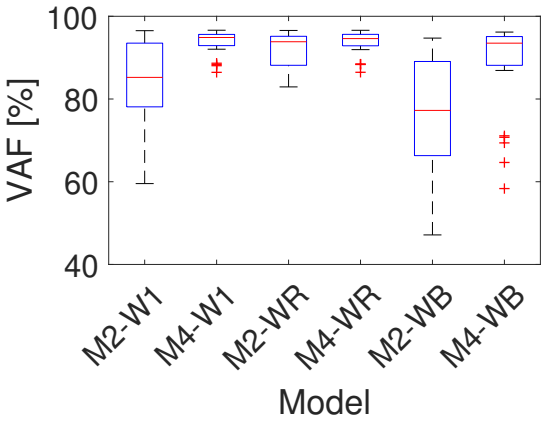

(d) $H_{g_V}(s)$, 2D condition.

Figure E.2: VAF scores of different estimated gaze models ($H_{g_{H,V}}(s)$) for each condition for the right eye.

Table E.1: ω_g statistics ($\mu \pm \sigma$ rad/s , N = 21) for the M4-models in every condition, for the right eye. For the 2D condition, the horizontal (2D(-H)) and vertical (2D(-V)) directions are separated.

Model	Condition			
	1D-H	1D-V	2D(-H)	2D(-V)
M4-W1	24.0 ± 5.4	26.5 ± 8.5	26.1 ± 7.6	21.4 ± 8.1
M4-WR	24.2 ± 5.8	29.0 ± 9.1	26.4 ± 7.7	22.0 ± 8.2
M4-WB	29.2 ± 7.0	32.7 ± 7.8	31.7 ± 7.7	34.9 ± 6.2

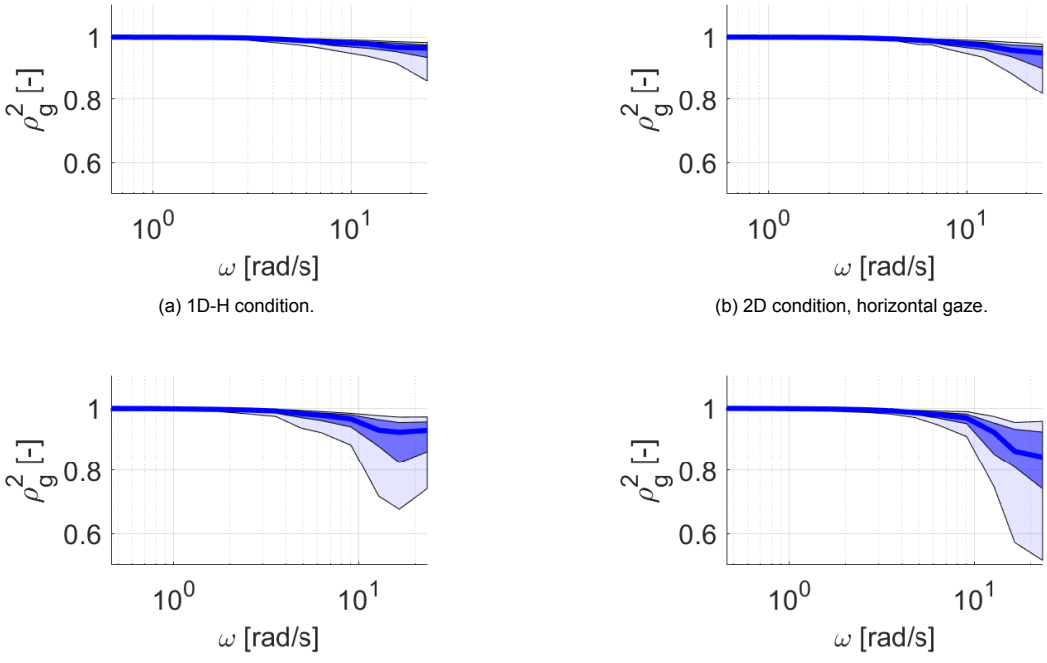

(a) 1D-H condition.

(b) 2D condition, horizontal gaze.

(c) 1D-V condition.

(d) 2D condition, vertical gaze.

Figure E.3: Relative remnant of right gaze in all conditions.

F

Saccades

The next figure shows saccade rate per trial. Hereafter, saccade polar plots are shown including its amplitude and direction, where the start of the saccade is at the center of the plot, and the end at the indicated node, implying a direction and amplitude. For each subject, trial 2, 10 and 18 are chosen from each condition if possible. The left L and right R eye and a least squares fit with angle $\alpha = \text{atan}(\frac{y_{sac}}{x_{sac}})$ are shown. The green circle represents the target stimulus size to serve as a reference for saccade amplitude. Inclination α is also summarized in Table F.1.

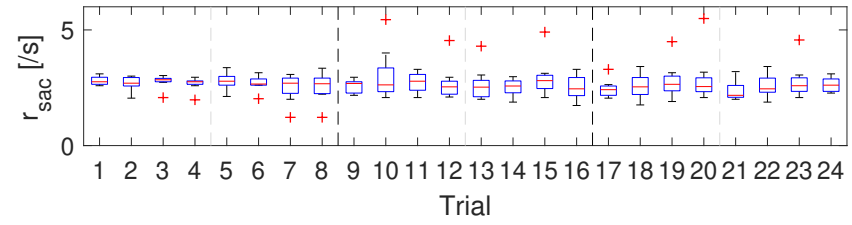

(a) 1D-H condition.

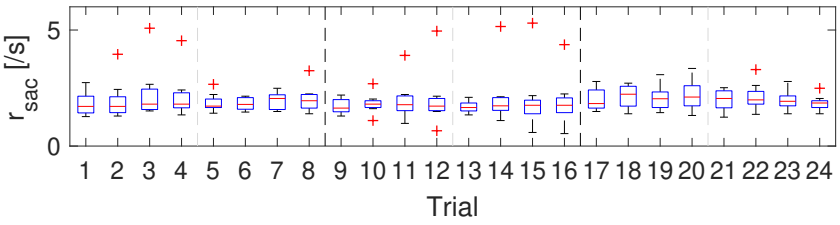

(b) 1D-V condition.

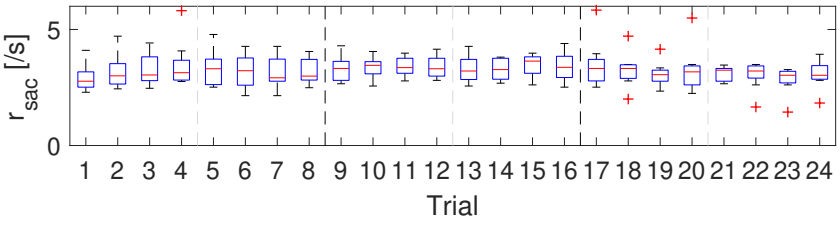

(c) 2D condition.

Figure F.1: Number of saccades per second r_{sac} per trial for the left eye.

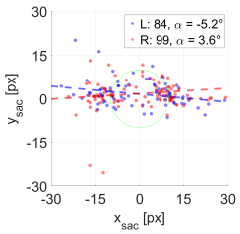

(a) 1D-H condition

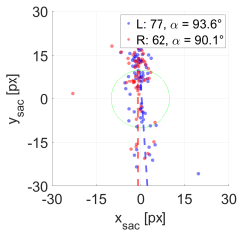

(b) 1D-V condition

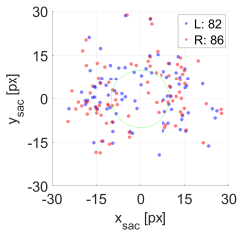

(c) 2D condition

Figure F.2: Subject 1

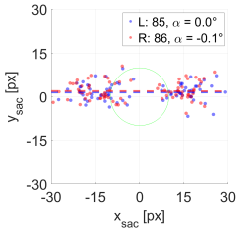

(a) 1D-H condition

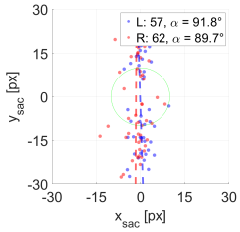

(b) 1D-V condition

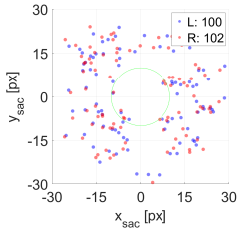

(c) 2D condition

Figure F.3: Subject 2

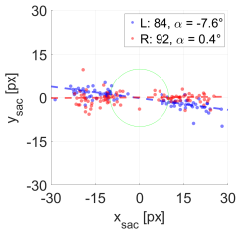

(a) 1D-H condition

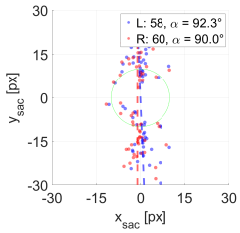

(b) 1D-V condition

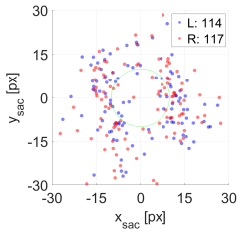

(c) 2D condition

Figure F.4: Subject 3

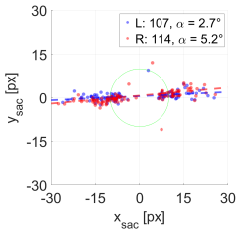

(a) 1D-H condition

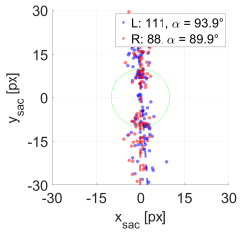

(b) 1D-V condition

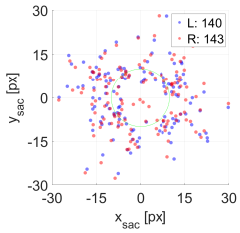

(c) 2D condition

Figure F.5: Subject 4

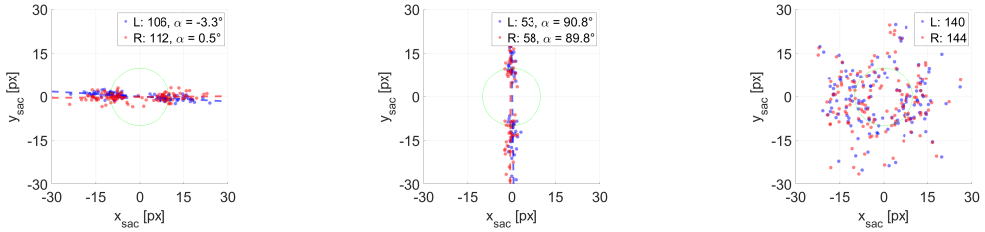

(a) 1D-H condition (b) 1D-V condition (c) 2D condition

Figure F.6: Subject 5

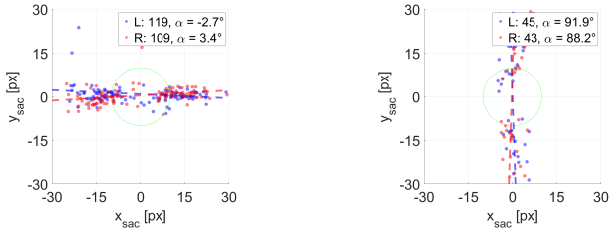

(a) 1D-H condition (b) 1D-V condition

Figure F.7: Subject 7

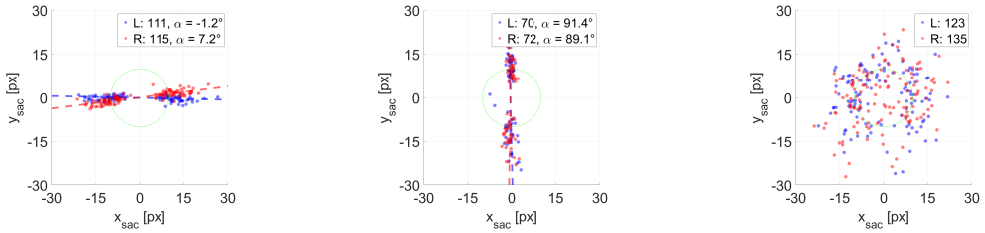

(a) 1D-H condition (b) 1D-V condition (c) 2D condition

Figure F.8: Subject 8

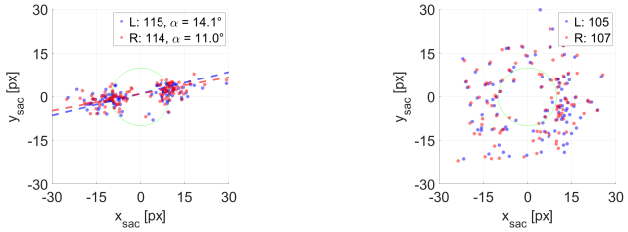

(a) 1D-H condition (b) 2D condition

Figure F.9: Subject 9

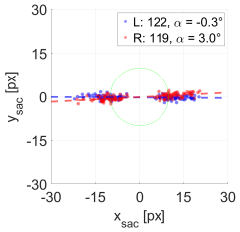

(a) 1D-H condition

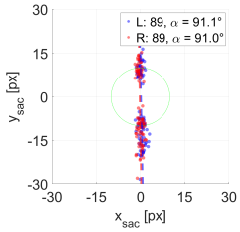

(b) 1D-V condition

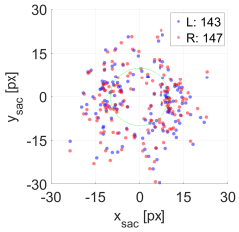

(c) 2D condition

Figure F.10: Subject 10

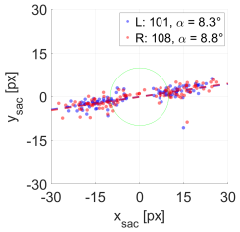

(a) 1D-H condition

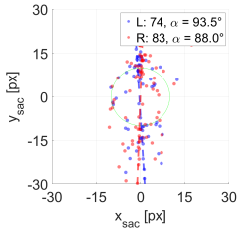

(b) 1D-V condition

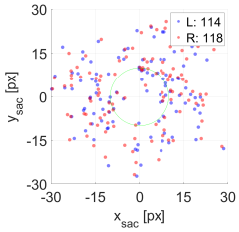

(c) 2D condition

Figure F.11: Subject 11

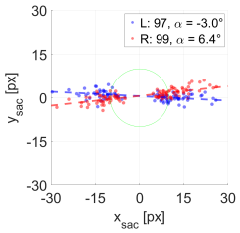

(a) 1D-H condition

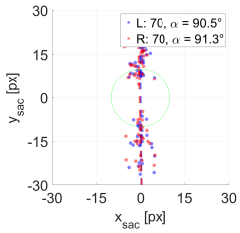

(b) 1D-V condition

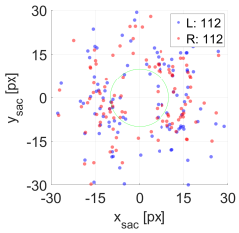

(c) 2D condition

Figure F.12: Subject 12

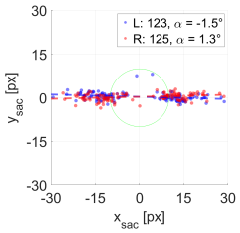

(a) 1D-H condition

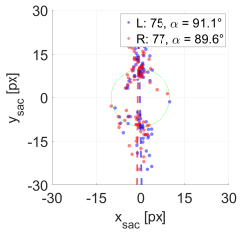

(b) 1D-V condition

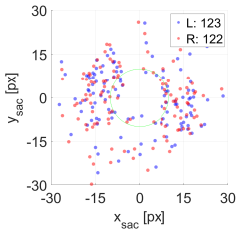

(c) 2D condition

Figure F.13: Subject 13

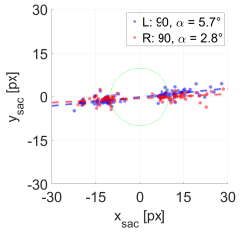

(a) 1D-H condition

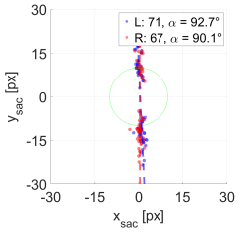

(b) 1D-V condition

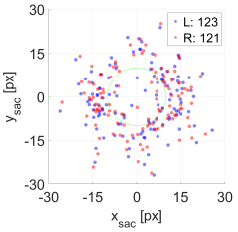

(c) 2D condition

Figure F.14: Subject 14

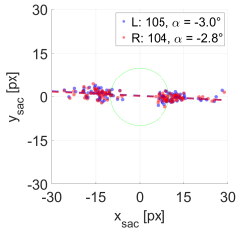

(a) 1D-H condition

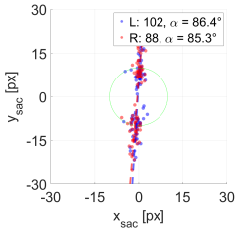

(b) 1D-V condition

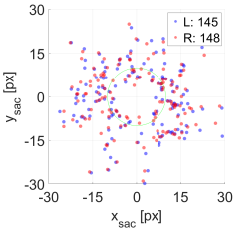

(c) 2D condition

Figure F.15: Subject 16

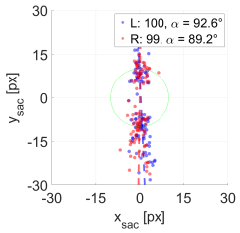

(a) 1D-H condition

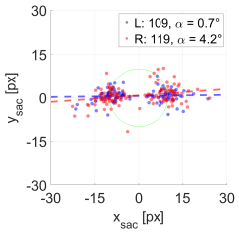

(b) 1D-V condition

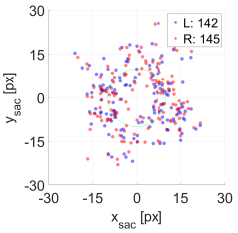

(c) 2D condition

Figure F.16: Subject 17

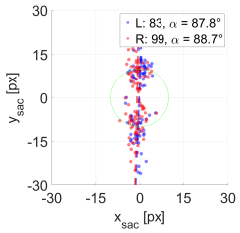

(a) 1D-H condition

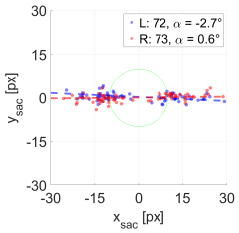

(b) 1D-V condition

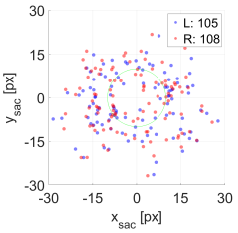

(c) 2D condition

Figure F.17: Subject 18

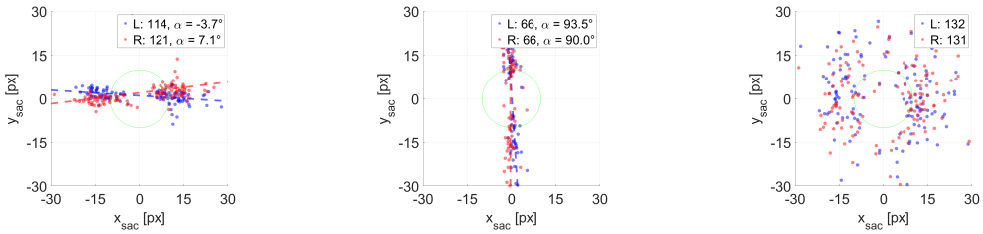

(a) 1D-H condition (b) 1D-V condition (c) 2D condition

Figure F.18: Subject 19

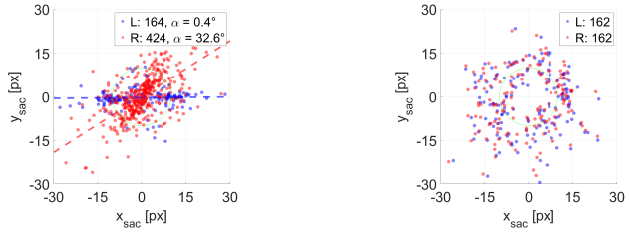

(a) (b)

Figure F.19: Subject 20

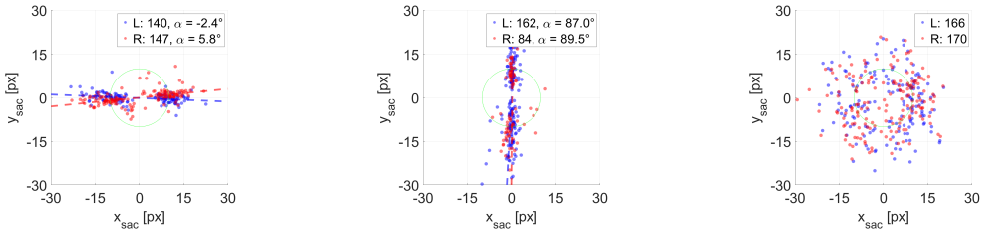

(a) 1D-H condition (b) 1D-V condition (c) 2D condition

Figure F.20: Subject 21

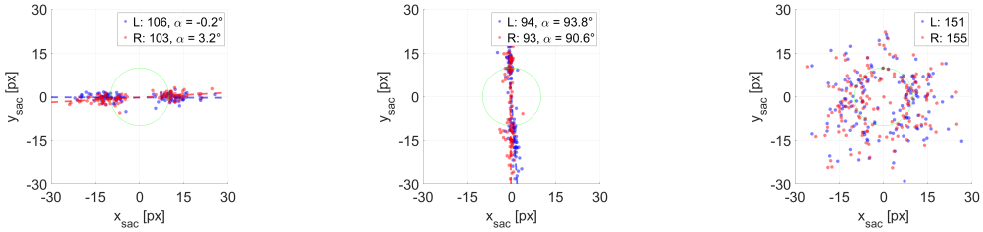

(a) 1D-H condition (b) 1D-V condition (c) 2D condition

Figure F.21: Subject 22

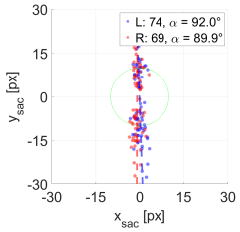

(a) 1D-H condition

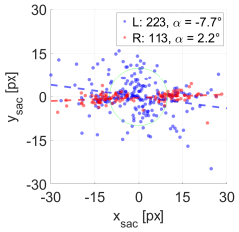

(b) 1D-V condition

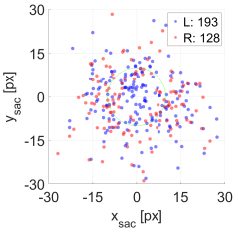

(c) 2D condition

Figure F.22: Subject 23

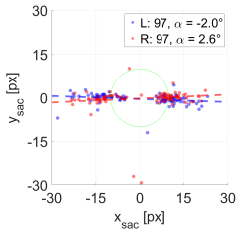

(a) 1D-H condition

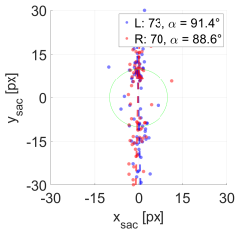

(b) 1D-V condition

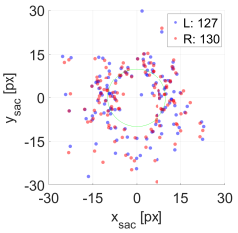

(c) 2D condition

Figure F.23: Subject 24

Table F.1: Saccade pattern inclination ($\mu + \sigma$) $\alpha = \text{atan}(\frac{y_{sac}}{x_{sac}})$ in degrees.

Subject	Condition			
	1D-H		1D-V	
	Left	Right	Left	Right
1	-3.9 ± 3.4	4.4 ± 6.0	91.5 ± 1.2	89.5 ± 1.0
2	-3.2 ± 4.0	-1.0 ± 3.5	91.4 ± 3.3	90.8 ± 3.0
3	-7.7 ± 2.0	3.5 ± 3.3	91.9 ± 1.7	89.0 ± 1.6
4	0.3 ± 1.9	3.0 ± 2.0	93.2 ± 1.4	90.6 ± 1.3
5	-3.8 ± 0.5	0.5 ± 0.7	90.1 ± 0.9	89.4 ± 0.4
7	-3.0 ± 1.3	2.8 ± 1.2	92.9 ± 1.1	90.8 ± 1.7
8	0.0 ± 0.9	7.7 ± 0.8	91.2 ± 0.4	87.6 ± 1.3
9	7.8 ± 2.5		92.2 ± 1.0	89.0 ± 1.2
10	-0.8 ± 0.7	3.2 ± 0.5	91.0 ± 0.5	91.3 ± 0.4
11	4.1 ± 4.0	4.6 ± 2.3	93.7 ± 1.4	90.1 ± 1.6
12	-1.3 ± 1.6	7.5 ± 1.4	89.2 ± 0.7	90.0 ± 1.1
13	-0.5 ± 0.7	3.1 ± 1.4	91.3 ± 0.8	89.0 ± 0.7
14	4.7 ± 0.8	2.0 ± 0.6	91.4 ± 0.5	89.2 ± 0.4
16	-3.3 ± 0.7	-4.1 ± 1.0	86.4 ± 0.7	86.0 ± 0.7
17	-0.7 ± 1.0	5.0 ± 1.7	91.7 ± 0.8	88.1 ± 1.1
18	-3.2 ± 0.7	1.4 ± 0.6	87.8 ± 0.6	88.1 ± 0.6
19	-5.8 ± 2.9	4.0 ± 1.0	93.0 ± 1.0	89.7 ± 1.3
20	2.5 ± 1.0		92.6 ± 0.4	89.3 ± 1.6
21	-2.7 ± 0.6	4.1 ± 1.2	89.9 ± 1.3	89.6 ± 1.5
22	-0.1 ± 0.3	3.7 ± 0.5	92.3 ± 1.5	89.9 ± 0.8
23	-5.4 ± 5.0	1.8 ± 0.5	89.8 ± 3.8	87.2 ± 4.6
24	-1.6 ± 0.8	2.2 ± 0.4	91.6 ± 0.7	88.9 ± 1.5

G

Model parameters

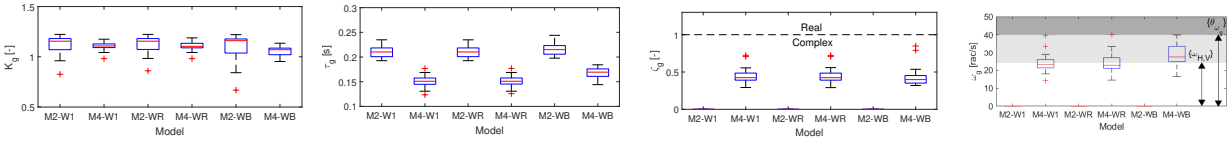

(a) Gain. (b) Time delay. (c) Damping ratio. (d) Natural frequency

Figure G.1: Fitted gaze parameter for different horizontal gaze models in the 1D-H condition, for the right eye.

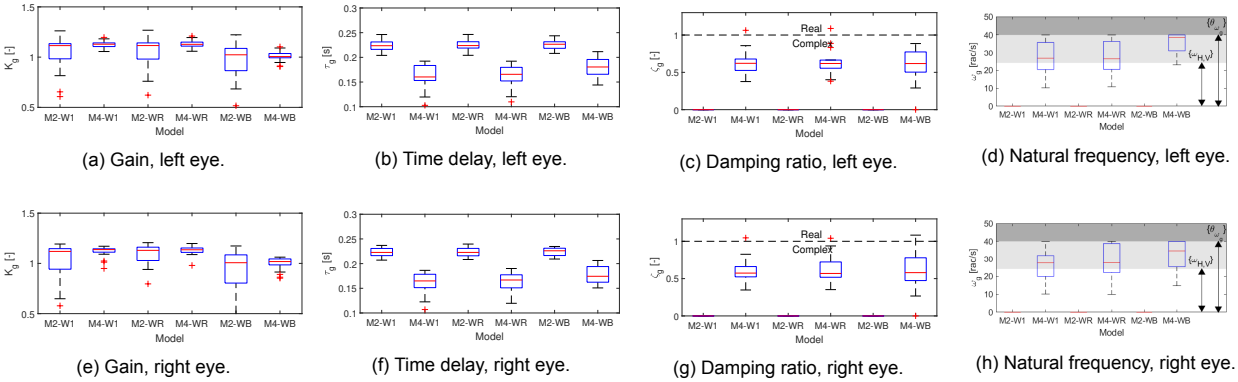

(a) Gain, left eye. (b) Time delay, left eye. (c) Damping ratio, left eye. (d) Natural frequency, left eye.

(e) Gain, right eye. (f) Time delay, right eye. (g) Damping ratio, right eye. (h) Natural frequency, right eye.

Figure G.2: Fitted gaze parameter for different vertical gaze models in the 1D-V condition, for both left and right eye.

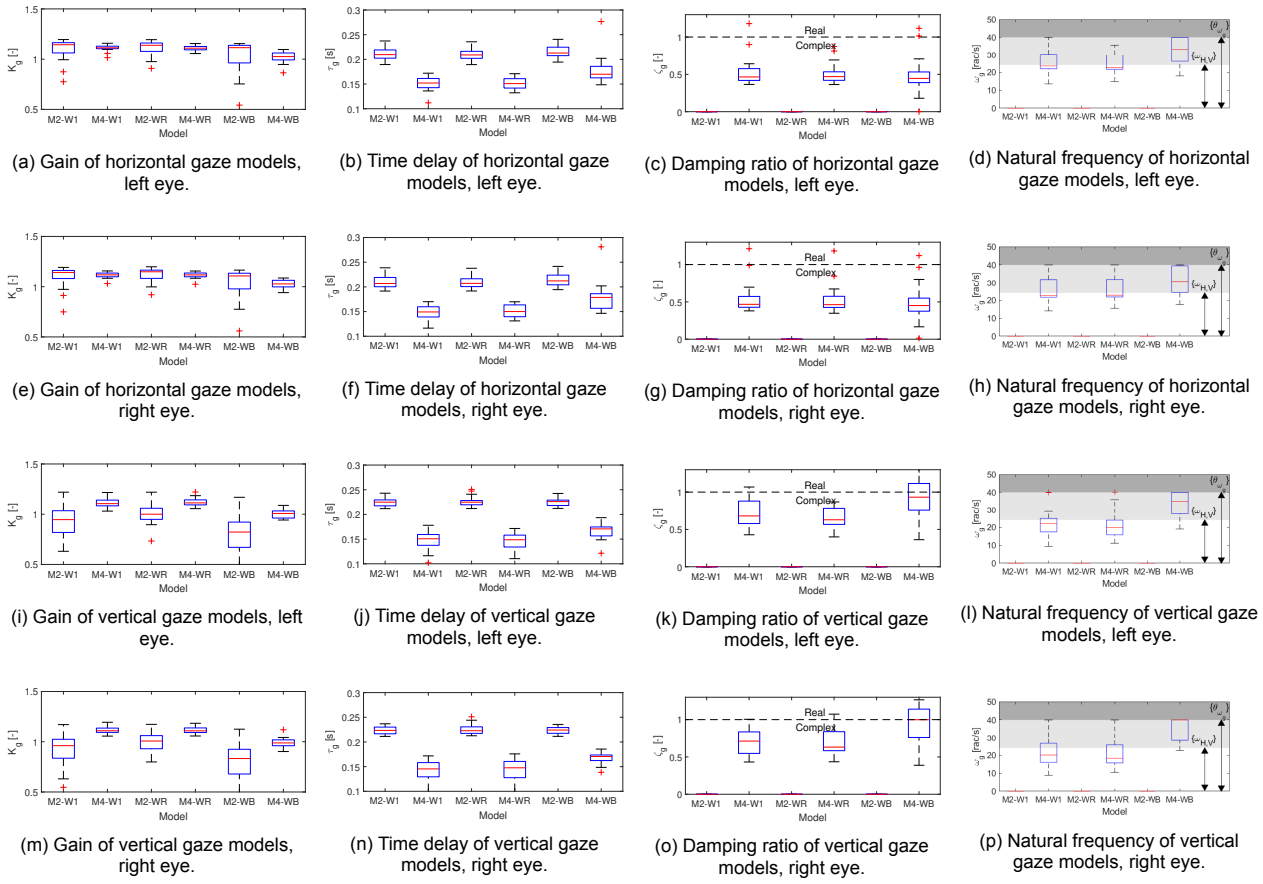

(a) Gain of horizontal gaze models, left eye.

(b) Time delay of horizontal gaze models, left eye.

(c) Damping ratio of horizontal gaze models, left eye.

(d) Natural frequency of horizontal gaze models, left eye.

(e) Gain of horizontal gaze models, right eye.

(f) Time delay of horizontal gaze models, right eye.

(g) Damping ratio of horizontal gaze models, right eye.

(h) Natural frequency of horizontal gaze models, right eye.

(i) Gain of vertical gaze models, left eye.

(j) Time delay of vertical gaze models, left eye.

(k) Damping ratio of vertical gaze models, left eye.

(l) Natural frequency of vertical gaze models, left eye.

(m) Gain of vertical gaze models, right eye.

(n) Time delay of vertical gaze models, right eye.

(o) Damping ratio of vertical gaze models, right eye.

(p) Natural frequency of vertical gaze models, right eye.

Figure G.3: Fitted gaze parameters for horizontal and vertical gaze models for the 2D condition, for both left and right eye.

H

Bode plots

In this appendix the Bode plots are shown with fitted frequency response functions of all subject in every condition. For each subject, the median of the fitted parameters are taken, and the median of the estimated gaze dynamics is taken as well. Model M2-W1, M4-W1, M2-WR, M4-WR, M2-WB and M4-WB are indicated with a green solid line, green dashed line, red solid line, red dashed line, blue solid line and blue dashed line, respectively. The estimated gaze dynamics are indicated with black dots. Occasionally within subjects, all trials of a particular condition were removed, which explains why some figures appears to be missing.

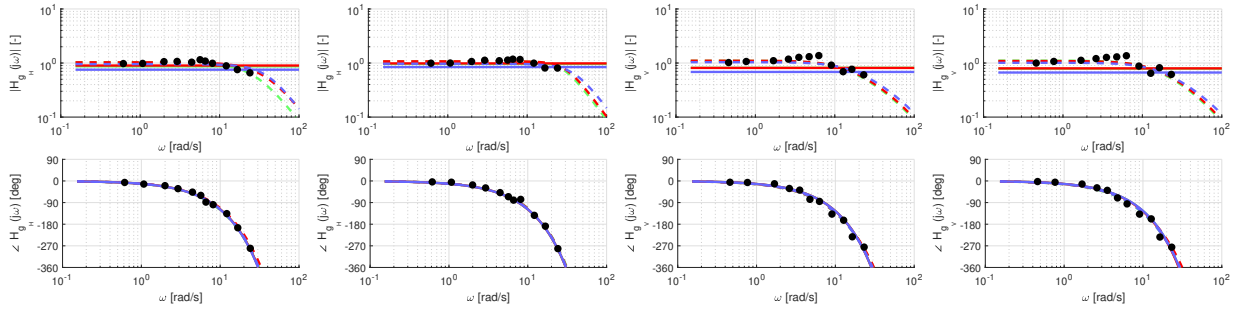

(a) 1D-H, left eye. (b) 1D-H, right eye. (c) 1D-V, left eye. (d) 1D-V, right eye.

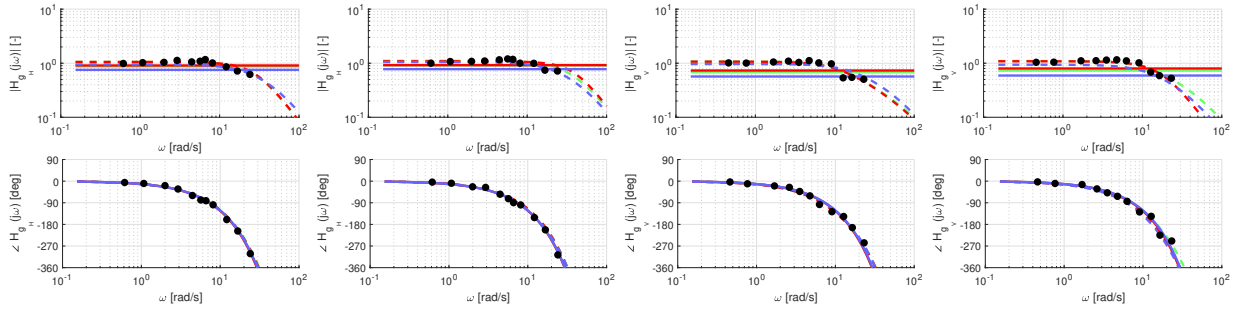

(e) 2D(-H), left eye. (f) 2D(-H), right eye. (g) 2D(-V), left eye. (h) 2D(-V), right eye.

Figure H.1: Subject 1

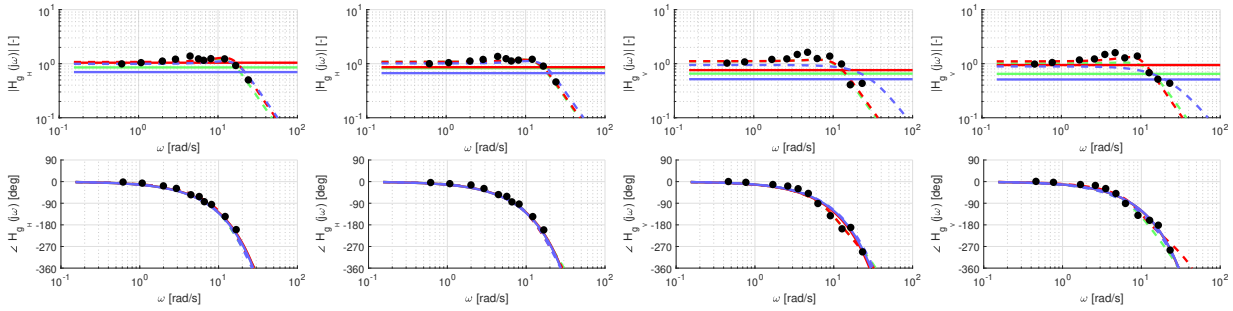

(a) 1D-H, left eye. (b) 1D-H, right eye. (c) 1D-V, left eye. (d) 1D-V, right eye.

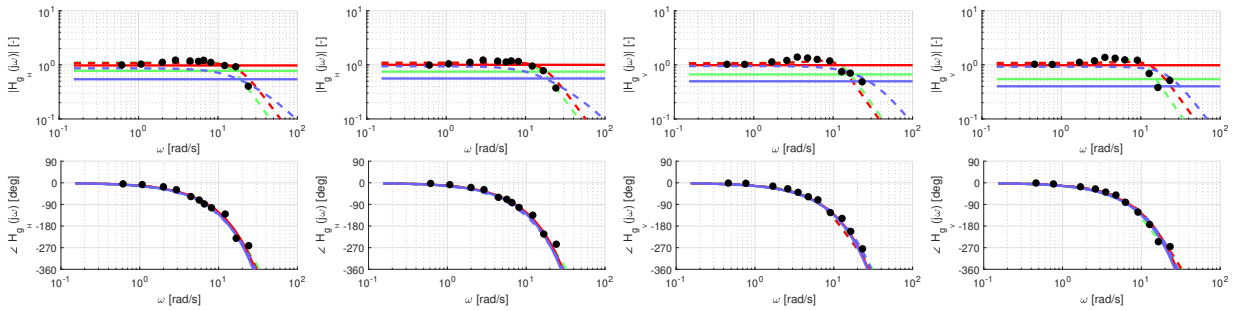

(e) 2D(-H), left eye. (f) 2D(-H), right eye. (g) 2D(-V), left eye. (h) 2D(-V), right eye.

Figure H.2: Subject 2

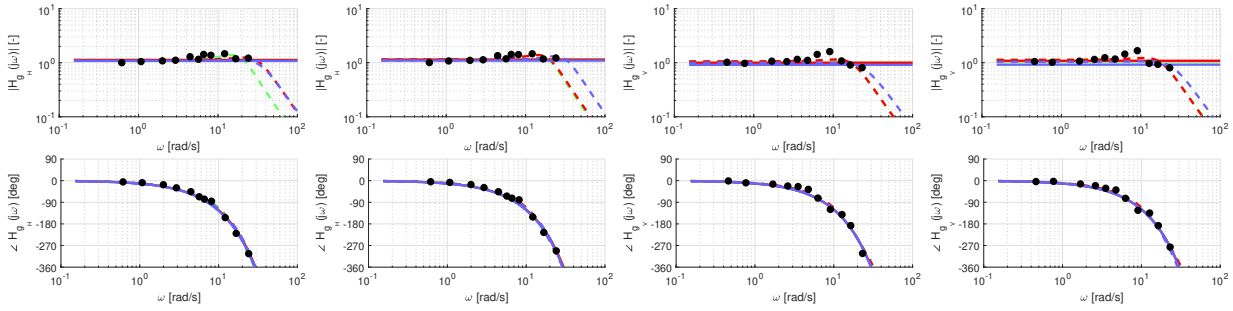

(a) 1D-H, left eye. (b) 1D-H, right eye. (c) 1D-V, left eye. (d) 1D-V, right eye.

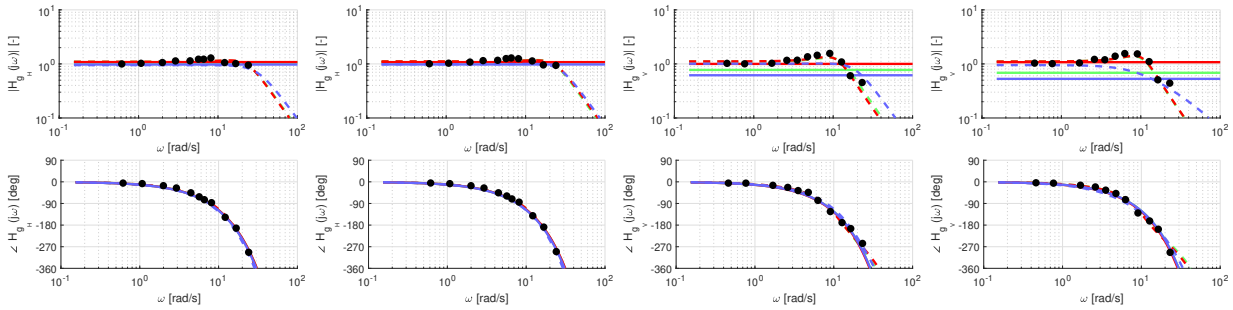

(e) 2D(-H), left eye. (f) 2D(-H), right eye. (g) 2D(-V), left eye. (h) 2D(-V), right eye.

Figure H.3: Subject 3

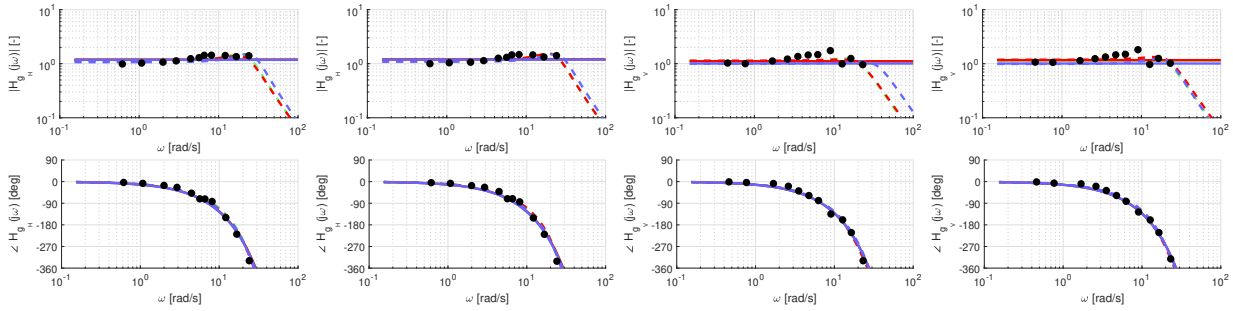

(a) 1D-H, left eye. (b) 1D-H, right eye. (c) 1D-V, left eye. (d) 1D-V, right eye.

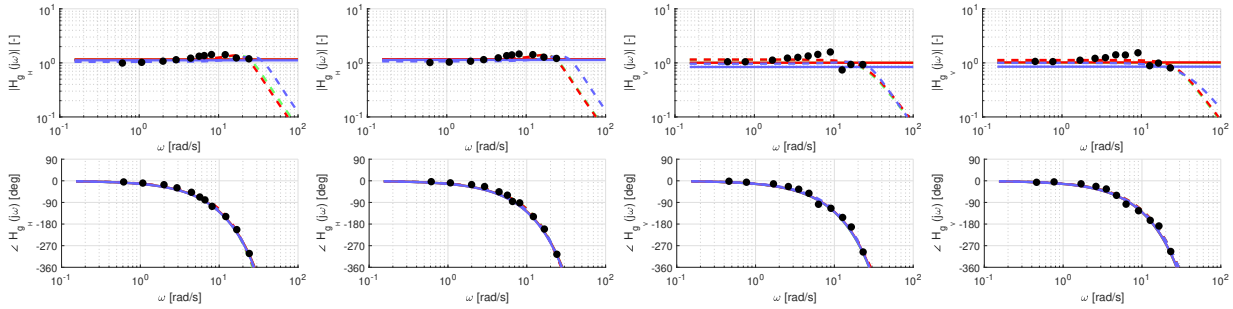

(e) 2D(-H), left eye. (f) 2D(-H), right eye. (g) 2D(-V), left eye. (h) 2D(-V), right eye.

Figure H.4: Subject 4

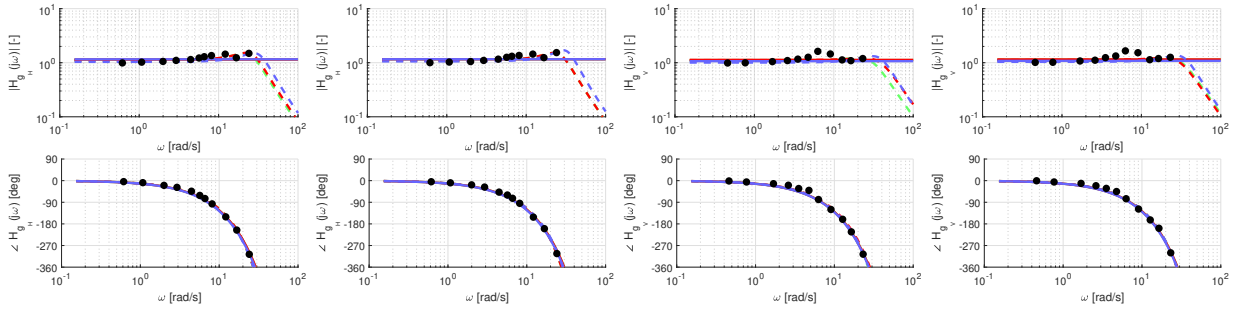

(a) 1D-H, left eye. (b) 1D-H, right eye. (c) 1D-V, left eye. (d) 1D-V, right eye.

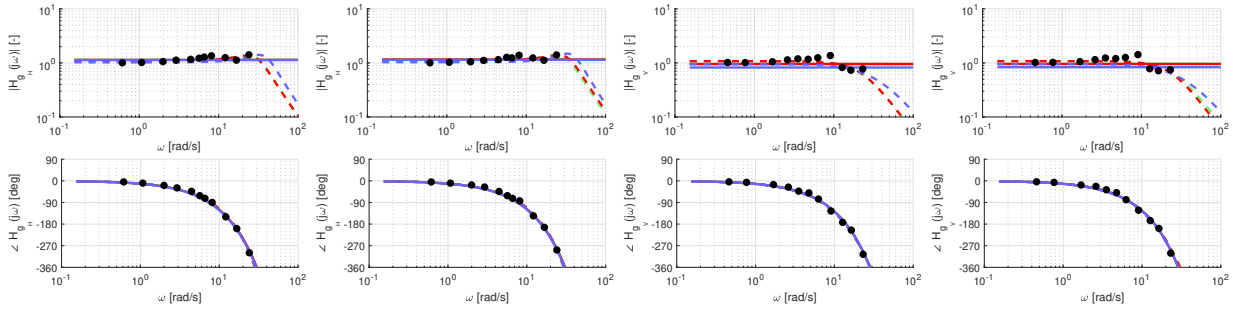

(e) 2D(-H), left eye. (f) 2D(-H), right eye. (g) 2D(-V), left eye. (h) 2D(-V), right eye.

Figure H.5: Subject 5

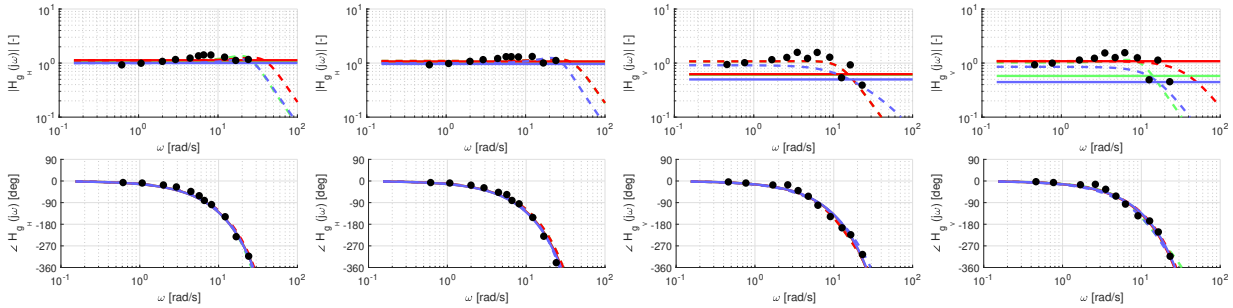

(a) 1D-H, left eye. (b) 1D-H, right eye. (c) 1D-V, left eye. (d) 1D-V, right eye.

Figure H.6: Subject 7

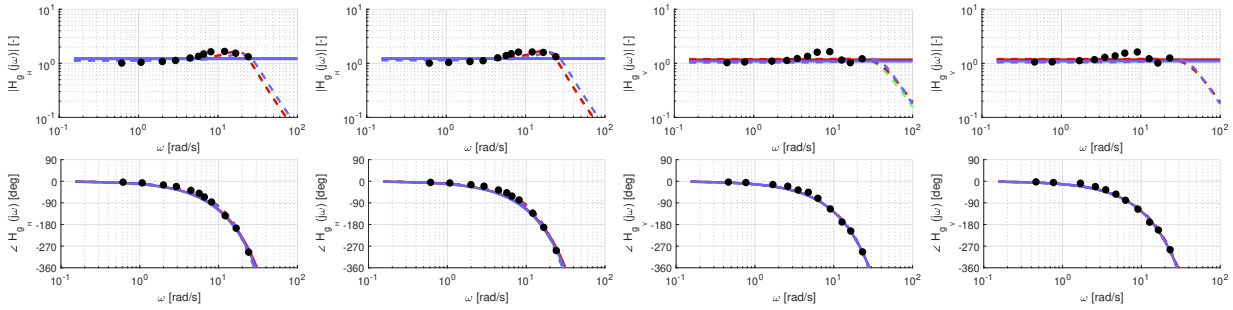

(a) 1D-H, left eye. (b) 1D-H, right eye. (c) 1D-V, left eye. (d) 1D-V, right eye.

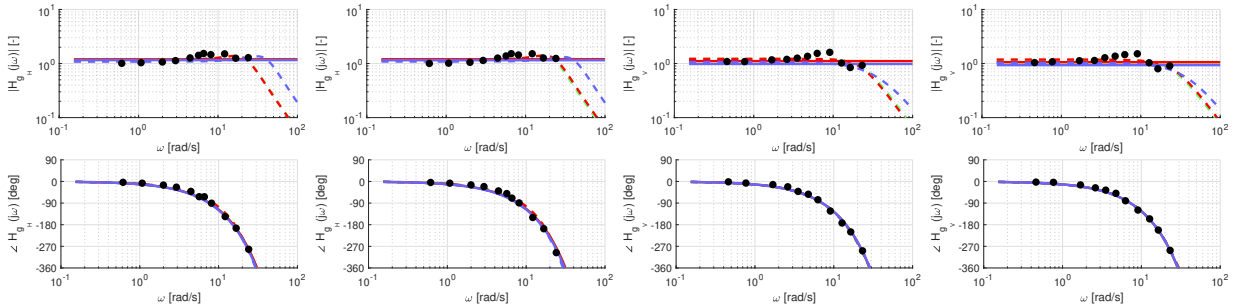

(e) 2D(-H), left eye. (f) 2D(-H), right eye. (g) 2D(-V), left eye. (h) 2D(-V), right eye.

Figure H.7: Subject 8

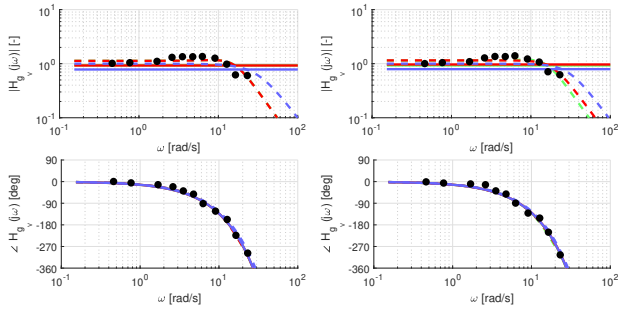

(a) 1D-V, left eye.

(b) 1D-V, right eye.

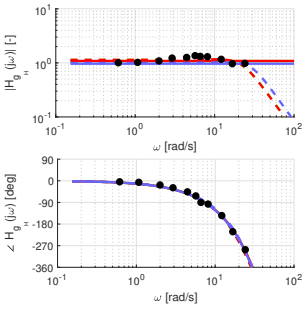

(c) 2D(-H), left eye.

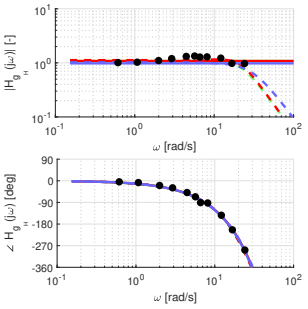

(d) 2D(-H), right eye.

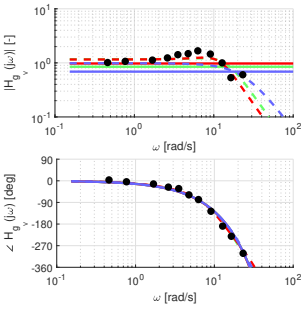

(e) 2D(-V), left eye.

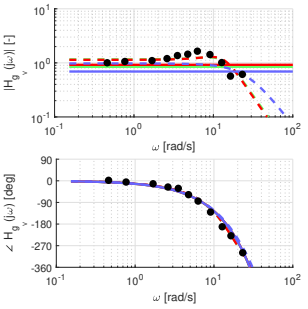

(f) 2D(-V), right eye.

Figure H.8: Subject 9

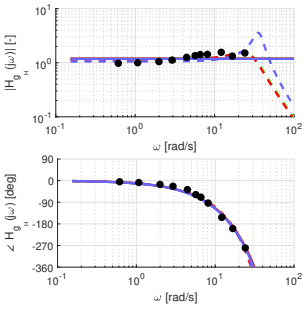

(a) 1D-H, left eye.

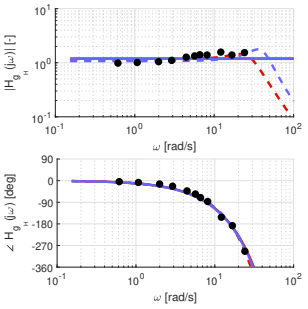

(b) 1D-H, right eye.

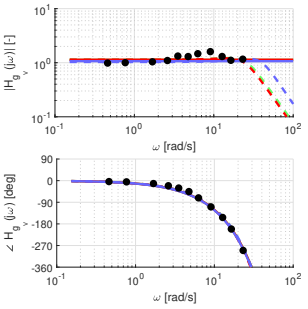

(c) 1D-V, left eye.

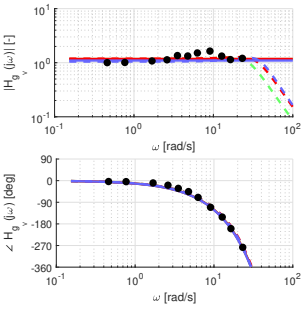

(d) 1D-V, right eye.

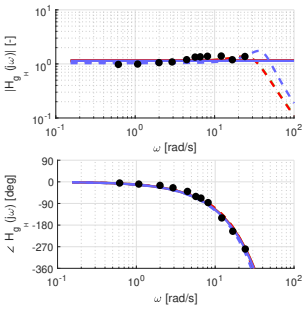

(e) 2D(-H), left eye.

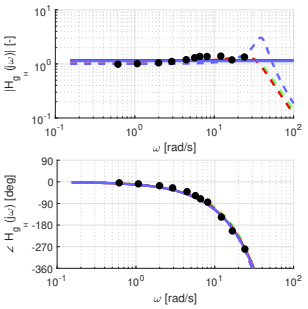

(f) 2D(-H), right eye.

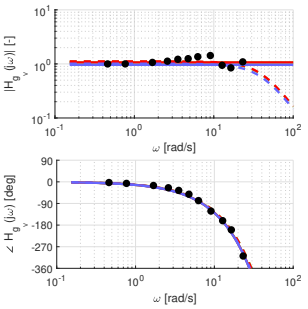

(g) 2D(-V), left eye.

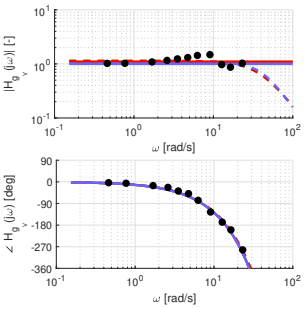

(h) 2D(-V), right eye.

Figure H.9: Subject 10

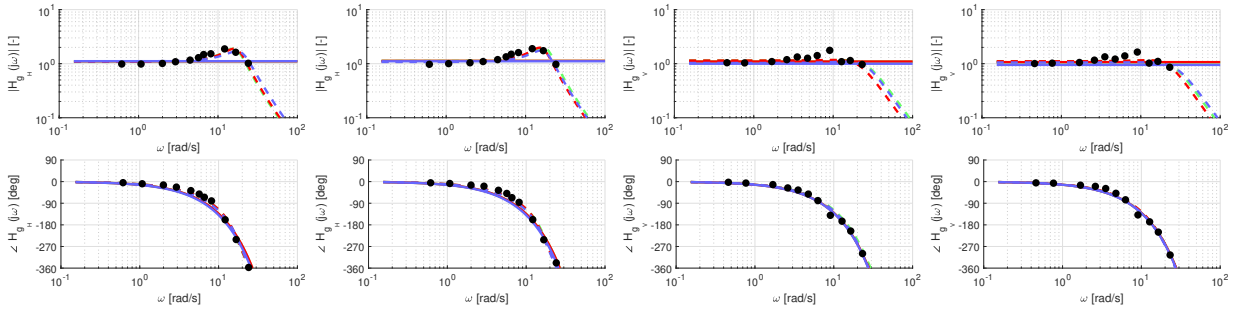

(a) 1D-H, left eye. (b) 1D-H, right eye. (c) 1D-V, left eye. (d) 1D-V, right eye.

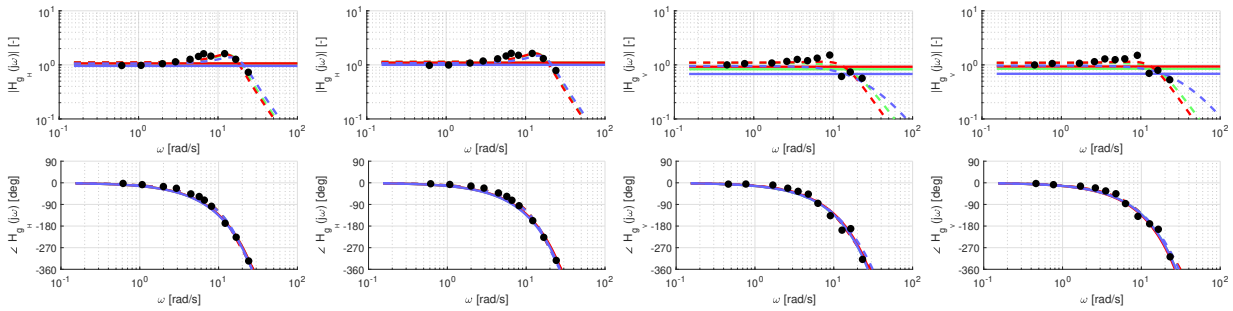

(e) 2D(-H), left eye. (f) 2D(-H), right eye. (g) 2D(-V), left eye. (h) 2D(-V), right eye.

Figure H.10: Subject 11

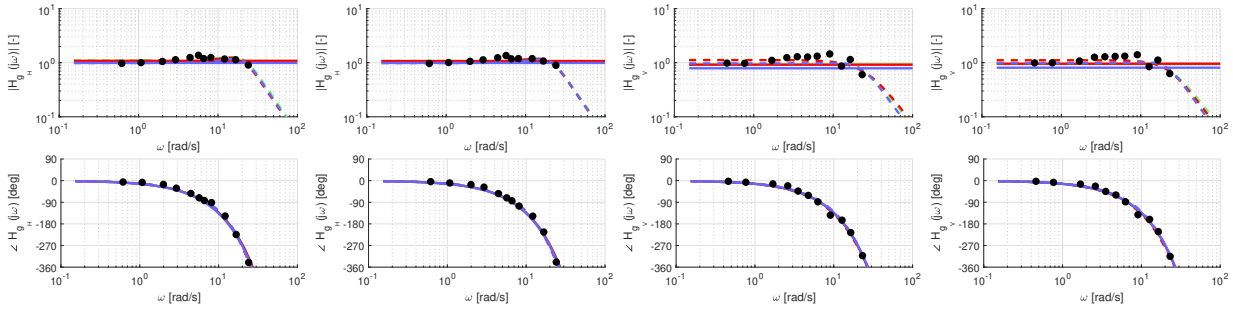

(a) 1D-H, left eye. (b) 1D-H, right eye. (c) 1D-V, left eye. (d) 1D-V, right eye.

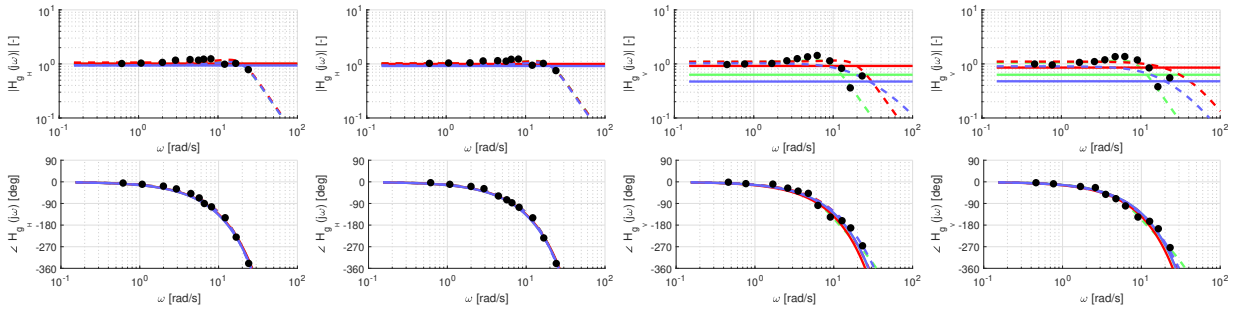

(e) 2D(-H), left eye. (f) 2D(-H), right eye. (g) 2D(-V), left eye. (h) 2D(-V), right eye.

Figure H.11: Subject 12

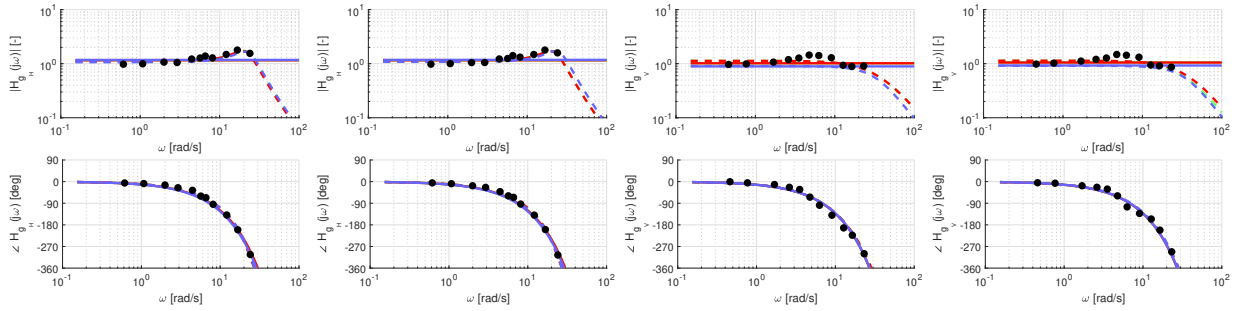

(a) 1D-H, left eye. (b) 1D-H, right eye. (c) 1D-V, left eye. (d) 1D-V, right eye.

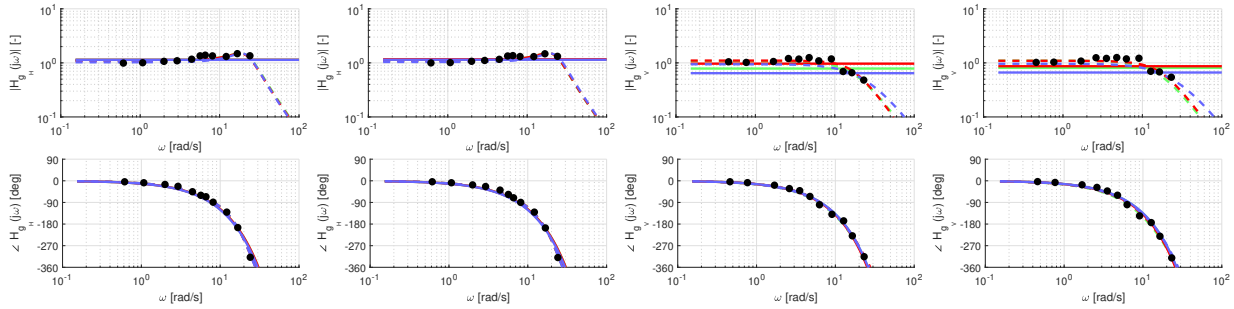

(e) 2D(-H), left eye. (f) 2D(-H), right eye. (g) 2D(-V), left eye. (h) 2D(-V), right eye.

Figure H.12: Subject 13

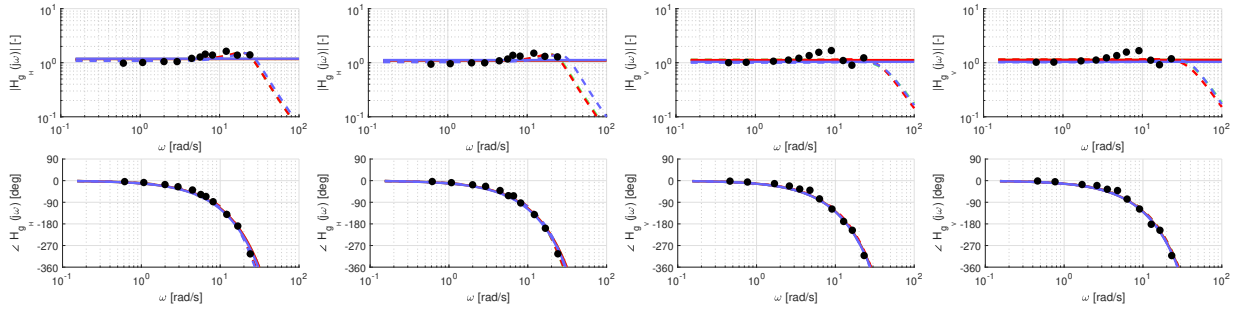

(a) 1D-H, left eye. (b) 1D-H, right eye. (c) 1D-V, left eye. (d) 1D-V, right eye.

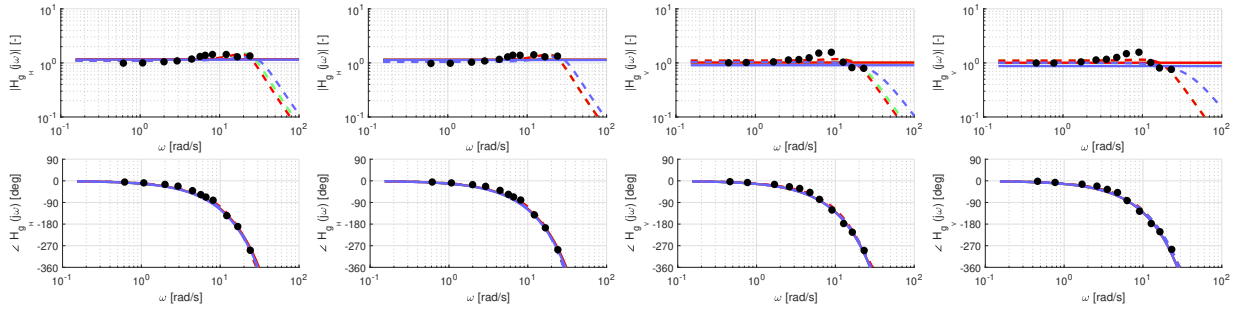

(e) 2D(-H), left eye. (f) 2D(-H), right eye. (g) 2D(-V), left eye. (h) 2D(-V), right eye.

Figure H.13: Subject 14

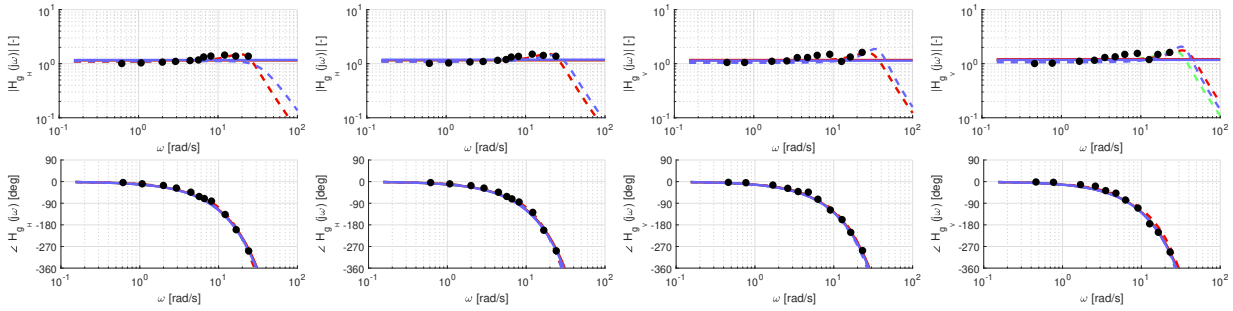

(a) 1D-H, left eye. (b) 1D-H, right eye. (c) 1D-V, left eye. (d) 1D-V, right eye.

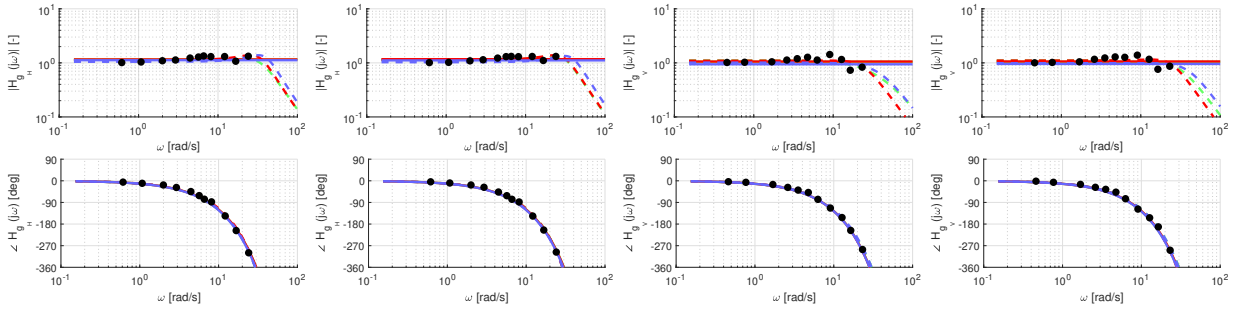

(e) 2D(-H), left eye. (f) 2D(-H), right eye. (g) 2D(-V), left eye. (h) 2D(-V), right eye.

Figure H.14: Subject 16

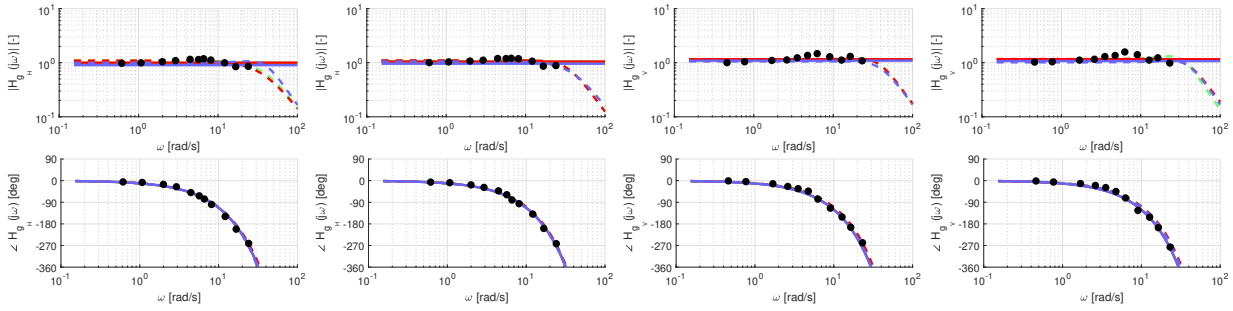

(a) 1D-H, left eye. (b) 1D-H, right eye. (c) 1D-V, left eye. (d) 1D-V, right eye.

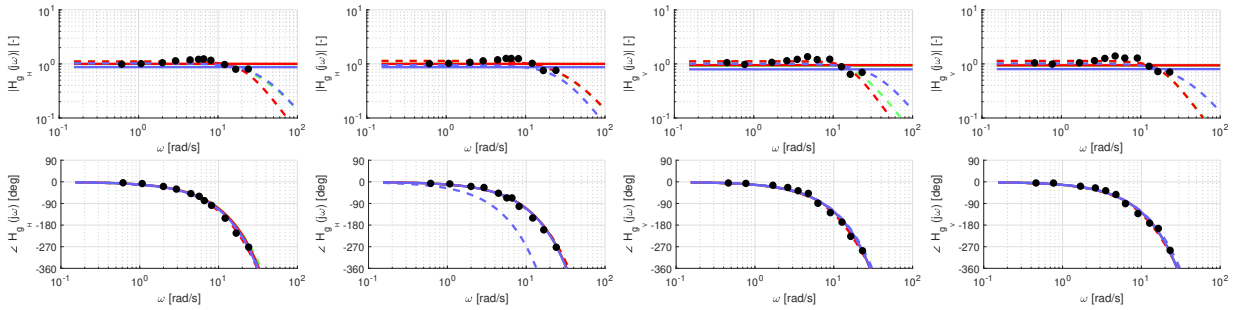

(e) 2D(-H), left eye. (f) 2D(-H), right eye. (g) 2D(-V), left eye. (h) 2D(-V), right eye.

Figure H.15: Subject 17

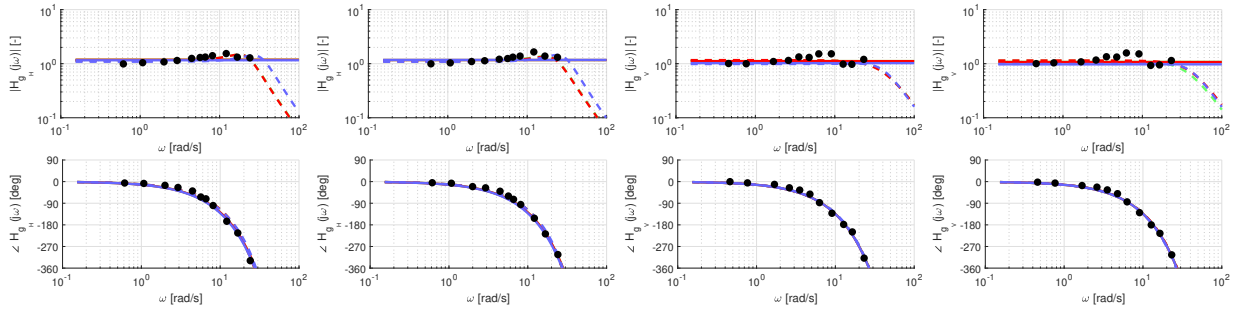

(a) 1D-H, left eye. (b) 1D-H, right eye. (c) 1D-V, left eye. (d) 1D-V, right eye.

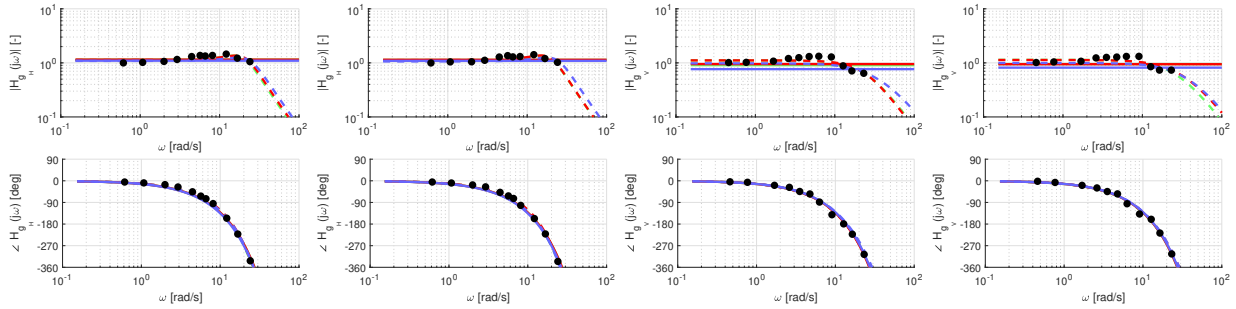

(e) 2D(-H), left eye. (f) 2D(-H), right eye. (g) 2D(-V), left eye. (h) 2D(-V), right eye.

Figure H.16: Subject 18

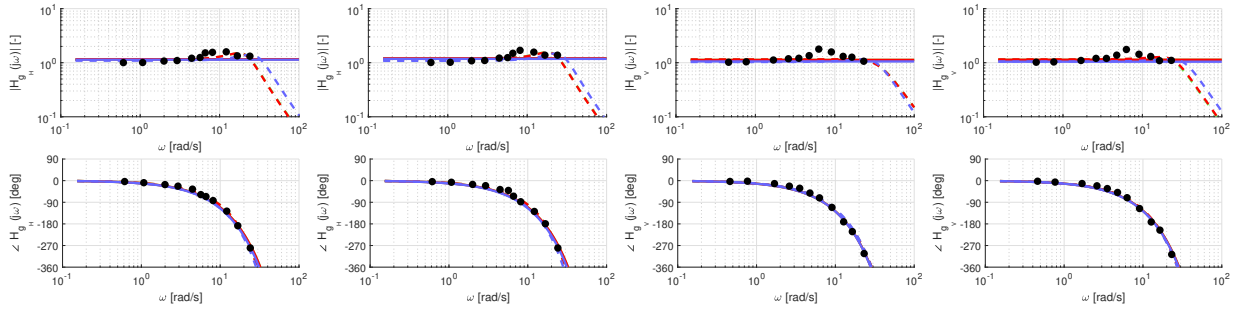

(a) 1D-H, left eye. (b) 1D-H, right eye. (c) 1D-V, left eye. (d) 1D-V, right eye.

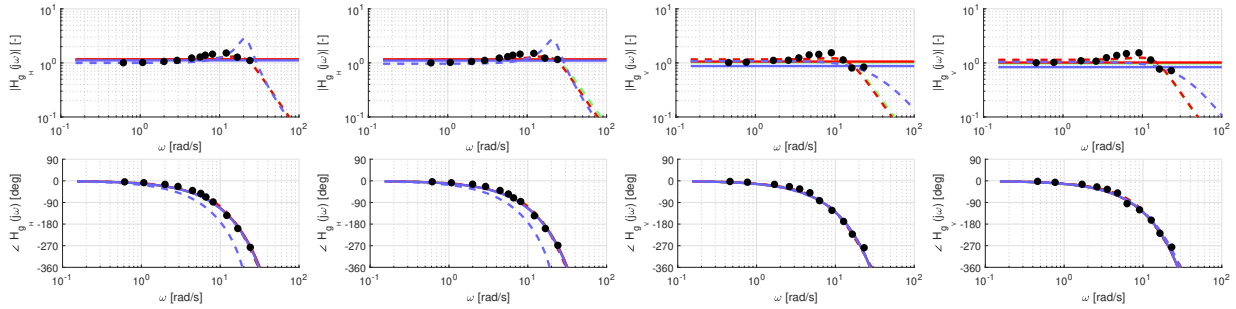

(e) 2D(-H), left eye. (f) 2D(-H), right eye. (g) 2D(-V), left eye. (h) 2D(-V), right eye.

Figure H.17: Subject 19

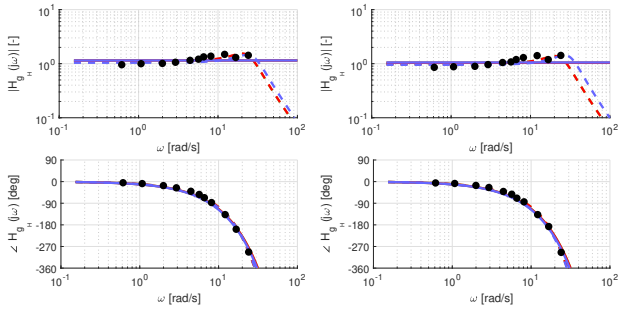

(a) 1D-H, left eye.

(b) 1D-H, right eye.

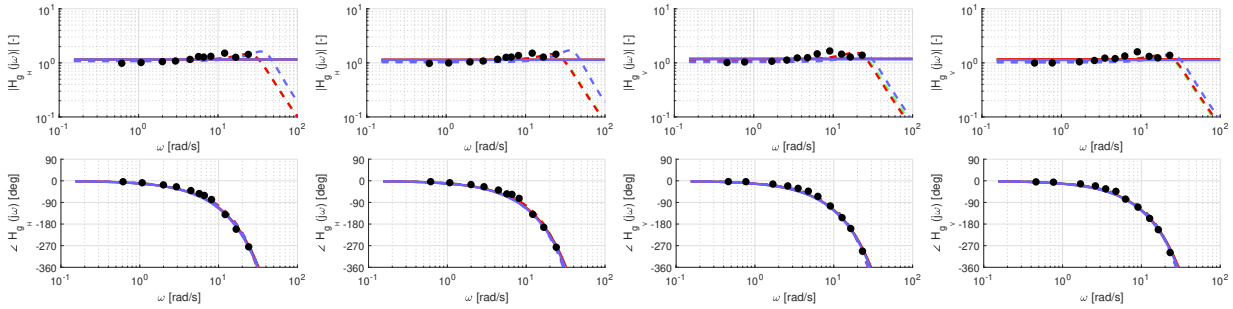

(c) 2D(-H), left eye. (d) 2D(-H), right eye. (e) 2D(-V), left eye. (f) 2D(-V), right eye.

Figure H.18: Subject 20

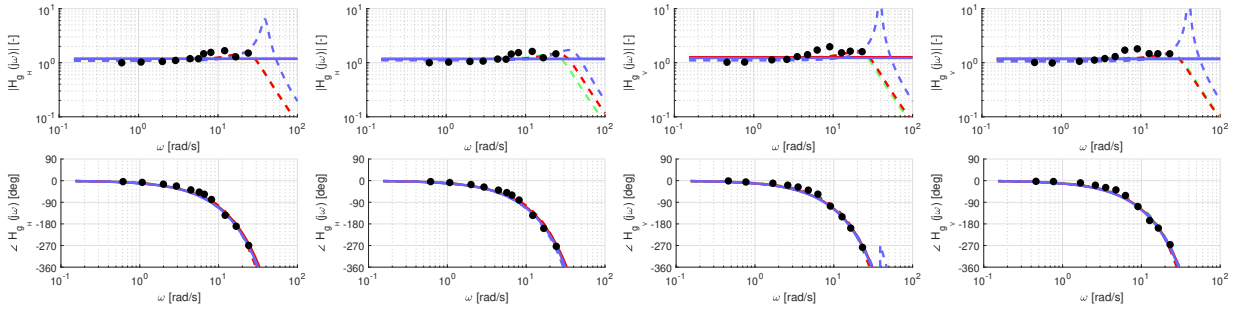

(a) 1D-H, left eye. (b) 1D-H, right eye. (c) 1D-V, left eye. (d) 1D-V, right eye.

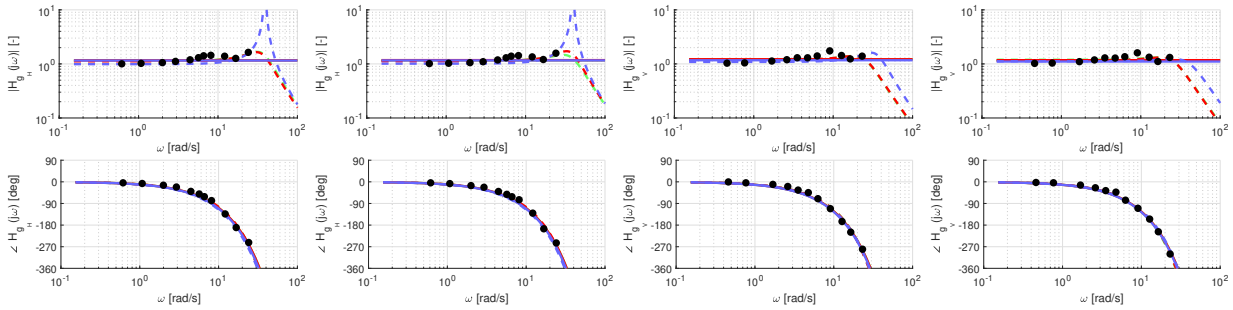

(e) 2D(-H), left eye. (f) 2D(-H), right eye. (g) 2D(-V), left eye. (h) 2D(-V), right eye.

Figure H.19: Subject 21

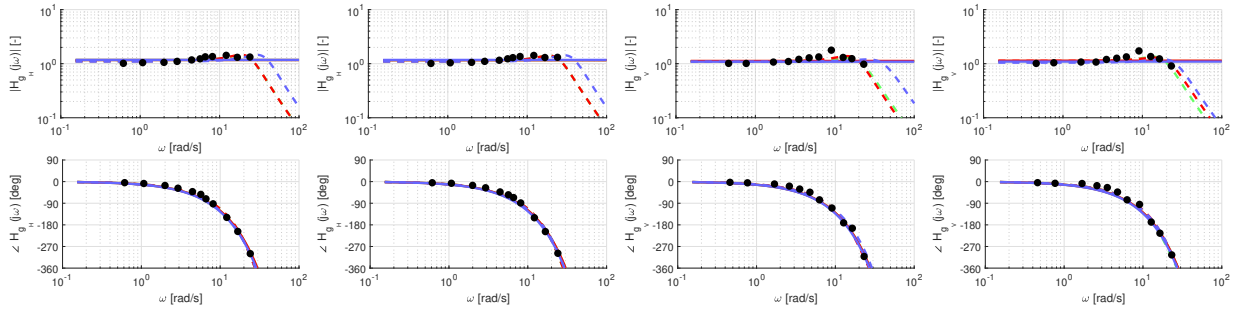

(a) 1D-H, left eye. (b) 1D-H, right eye. (c) 1D-V, left eye. (d) 1D-V, right eye.

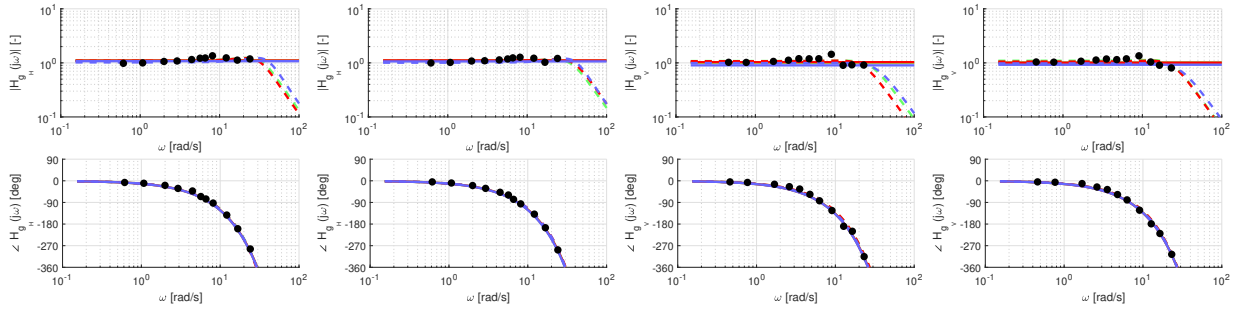

(e) 2D(-H), left eye. (f) 2D(-H), right eye. (g) 2D(-V), left eye. (h) 2D(-V), right eye.

Figure H.20: Subject 22

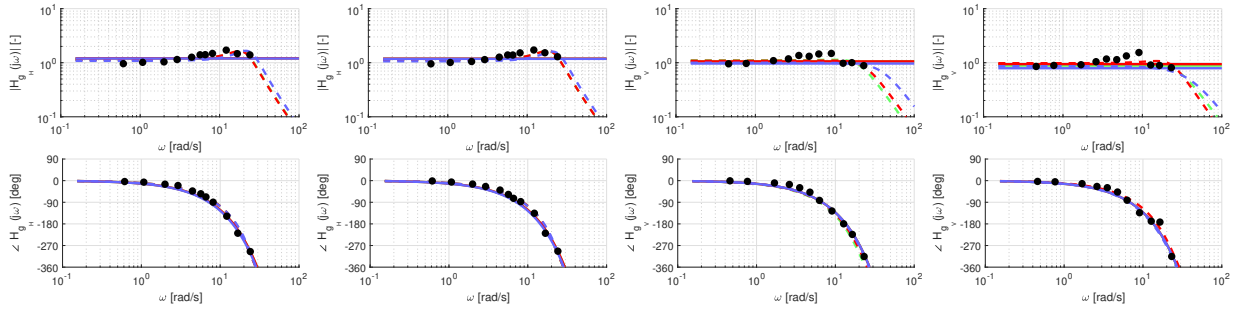

(a) 1D-H, left eye. (b) 1D-H, right eye. (c) 1D-V, left eye. (d) 1D-V, right eye.

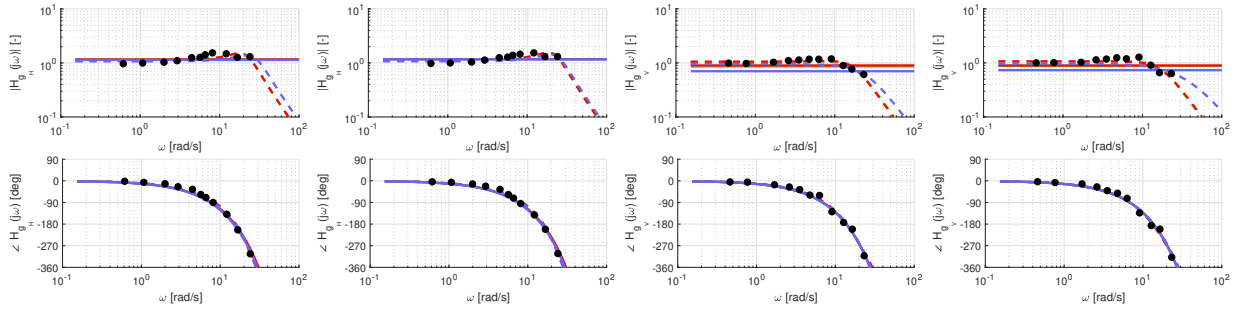

(e) 2D(-H), left eye. (f) 2D(-H), right eye. (g) 2D(-V), left eye. (h) 2D(-V), right eye.

Figure H.21: Subject 23

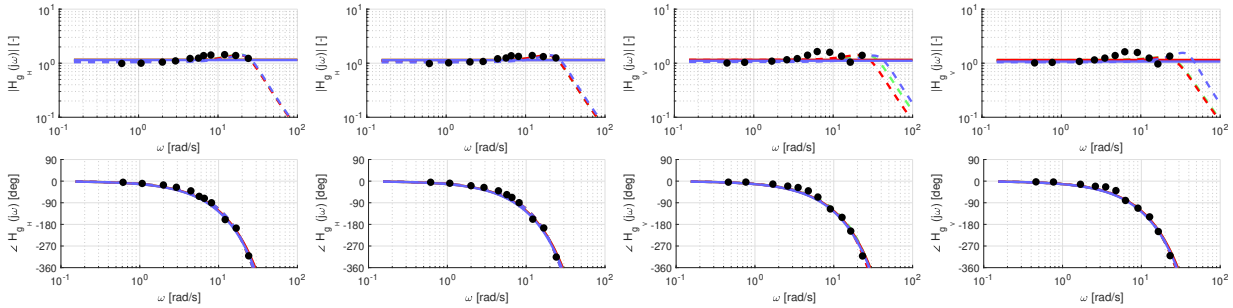

(a) 1D-H, left eye.

(b) 1D-H, right eye.

(c) 1D-V, left eye.

(d) 1D-V, right eye.

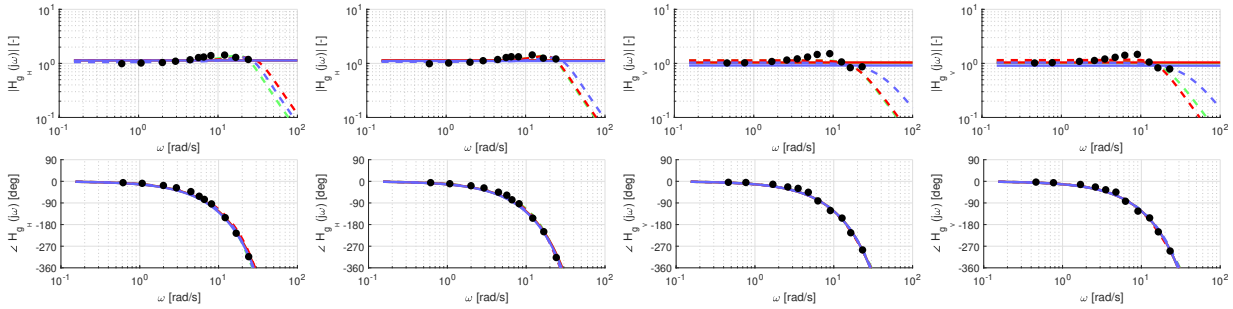

(e) 2D(-H), left eye.

(f) 2D(-H), right eye.

(g) 2D(-V), left eye.

(h) 2D(-V), right eye.

Figure H.22: Subject 24

Error compositions

The error decomposition for each condition is shown in this part, where the error in horizontal and vertical direction is shown, e_H and e_V respectively, for both left L and right R eye. The error consists of a blue, red and yellow part, which are the error at ω_H, ω_V and ω_N respectively, where ω_N are all frequencies but $\omega_{H,V}$. For each subject, the means of these are shown per condition, with the minimum and maximum of the e(ω_N) indicated as well with the error bar. Some subjects appear to miss some conditions, but this is because all trials were discarded for this particular condition.

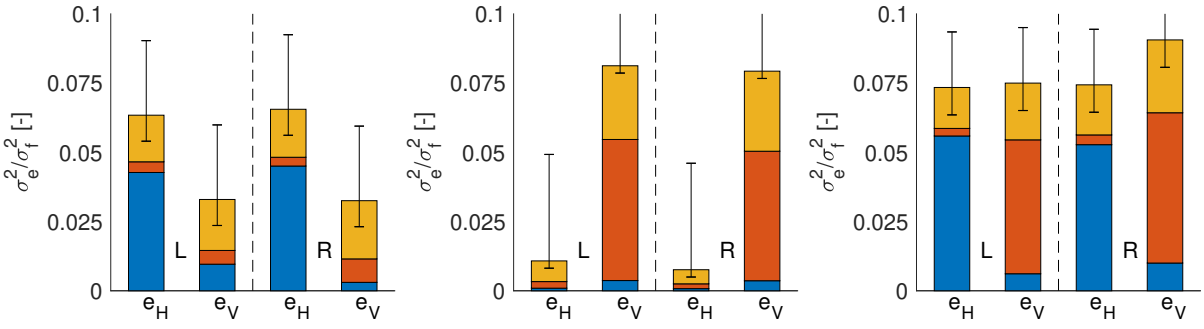

(a) 1D-H condition. (b) 1D-V condition. (c) 2D condition.

Figure I.1: Subject 1

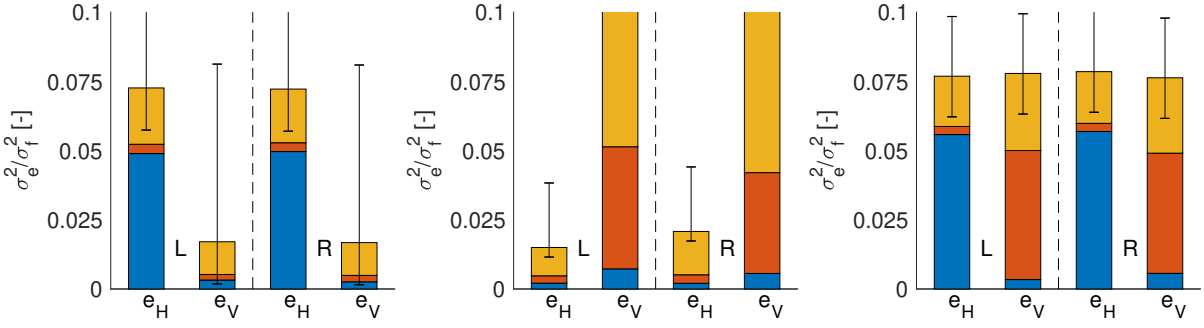

(a) 1D-H condition. (b) 1D-V condition. (c) 2D condition.

Figure I.2: Subject 2

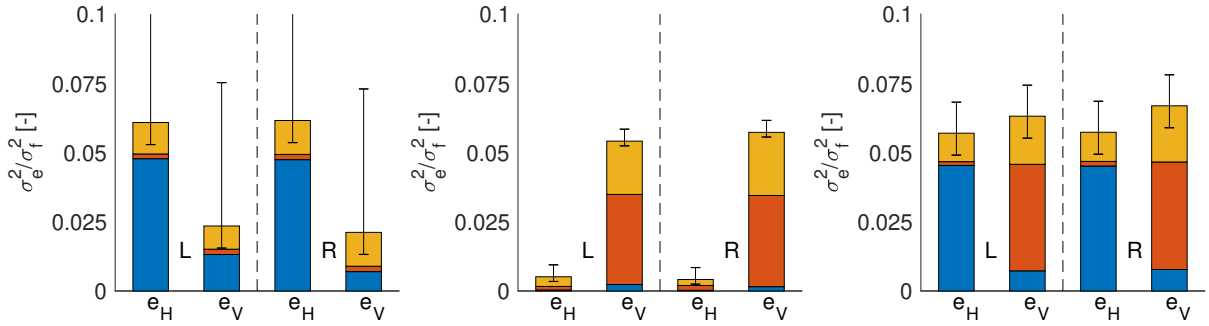

(a) 1D-H condition. (b) 1D-V condition. (c) 2D condition.

Figure I.3: Subject 3

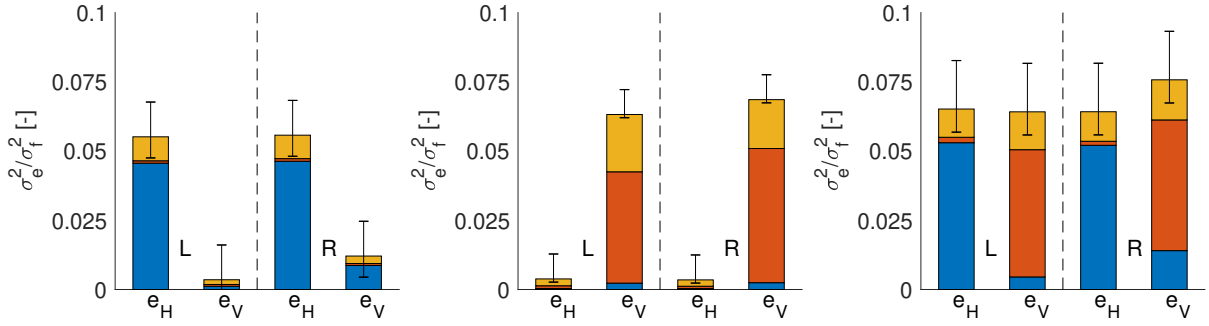

(a) 1D-H condition. (b) 1D-V condition. (c) 2D condition.

Figure I.4: Subject 4

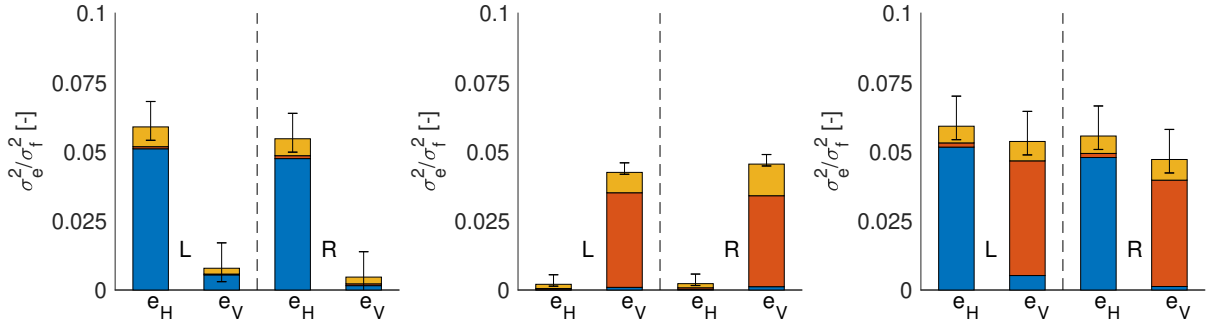

(a) 1D-H condition. (b) 1D-V condition. (c) 2D condition.

Figure I.5: Subject 5

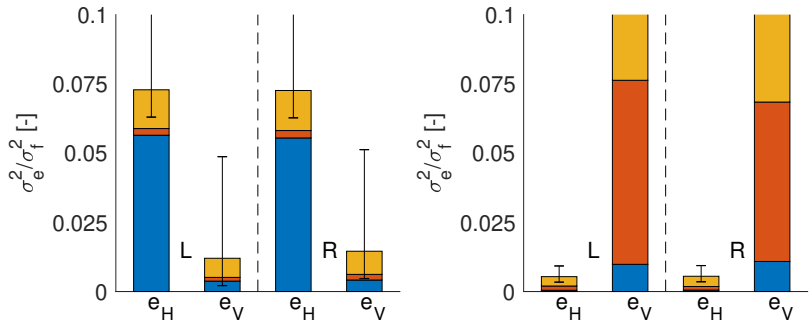

(a) 1D-H condition. (b) 1D-V condition.

Figure I.6: Subject 7

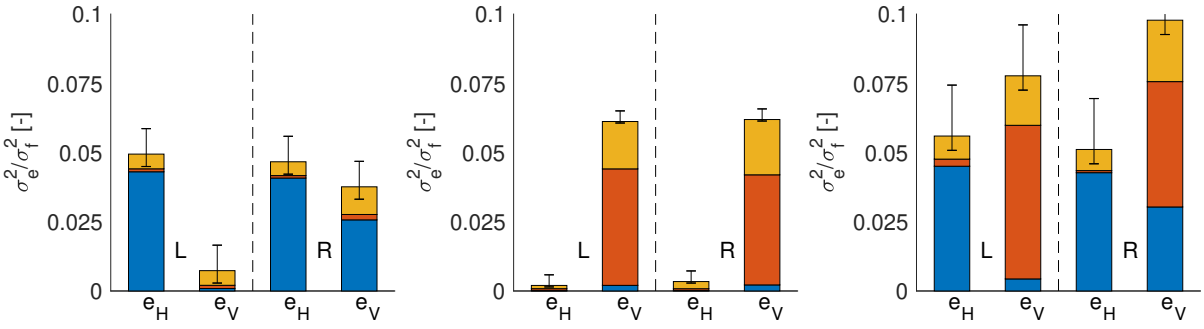

(a) 1D-H condition. (b) 1D-V condition. (c) 2D condition.

Figure I.7: Subject 8

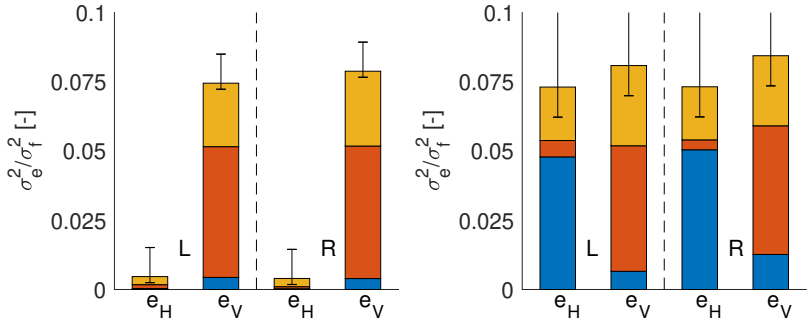

(a) 1D-H condition. (b) 2D condition.

Figure I.8: Subject 9

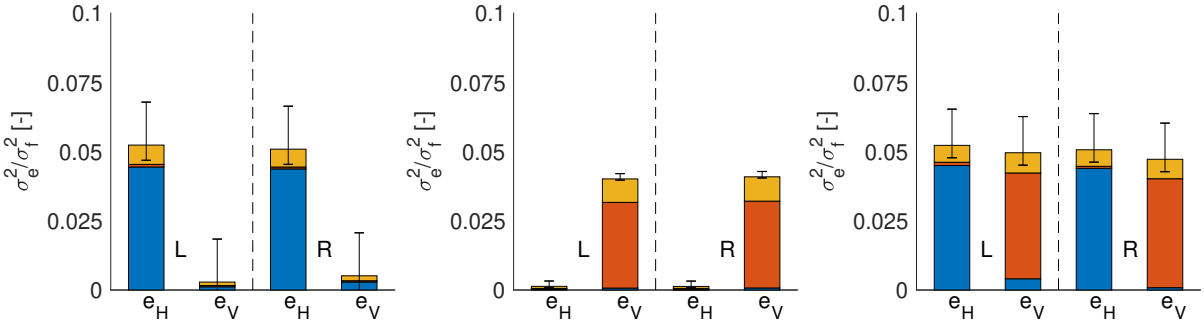

(a) 1D-H condition. (b) 1D-V condition. (c) 2D condition.

Figure I.9: Subject 10

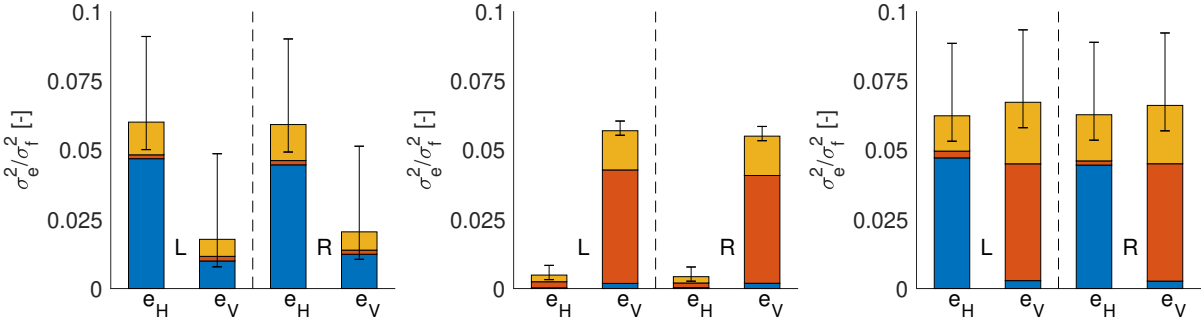

(a) 1D-H condition. (b) 1D-V condition. (c) 2D condition.

Figure I.10: Subject 11

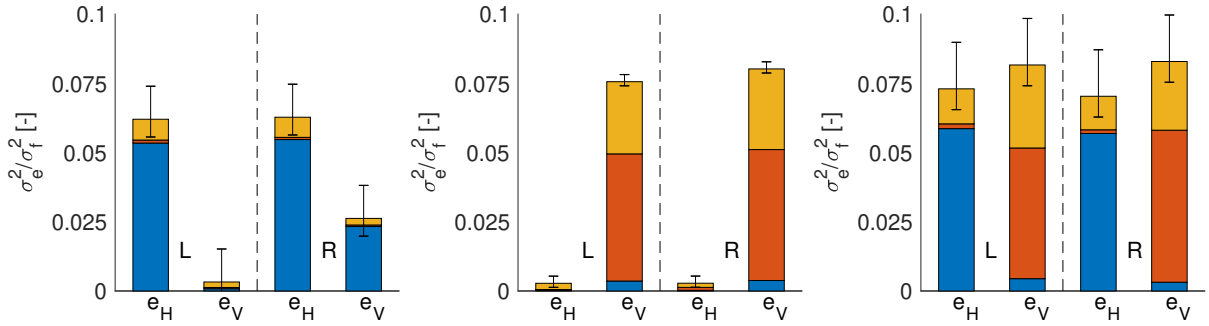

(a) 1D-H condition. (b) 1D-V condition. (c) 2D condition.

Figure I.11: Subject 12

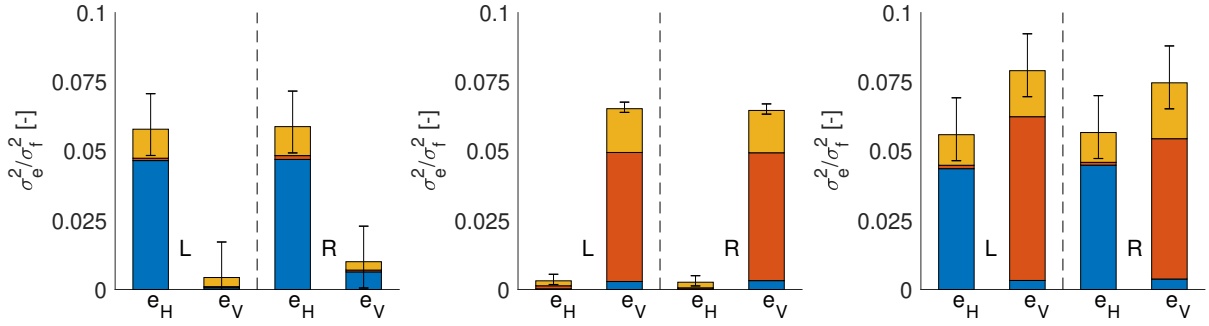

(a) 1D-H condition. (b) 1D-V condition. (c) 2D condition.

Figure I.12: Subject 13

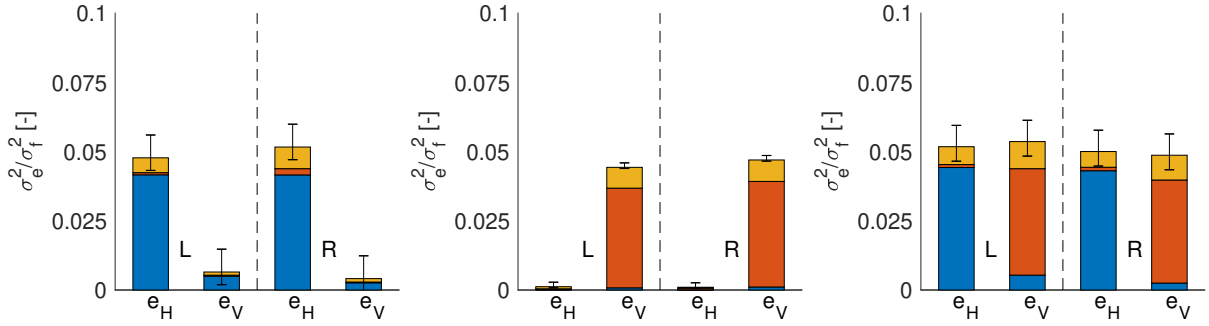

(a) 1D-H condition. (b) 1D-V condition. (c) 2D condition.

Figure I.13: Subject 14

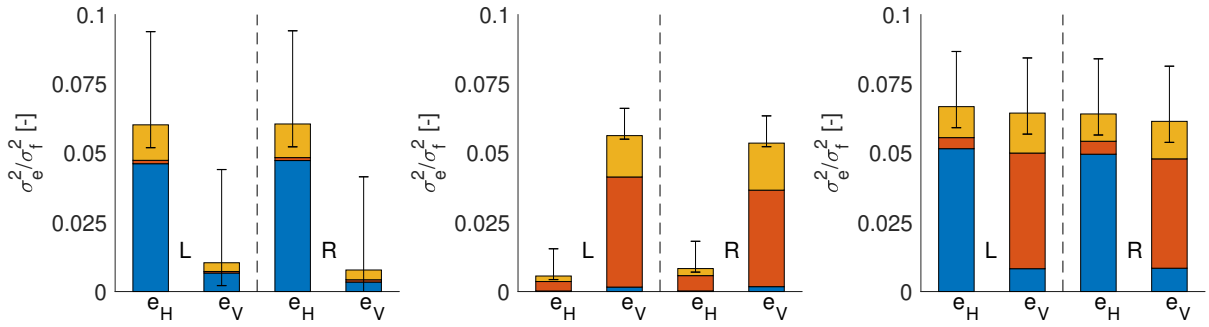

(a) 1D-H condition. (b) 1D-V condition. (c) 2D condition.

Figure I.14: Subject 16

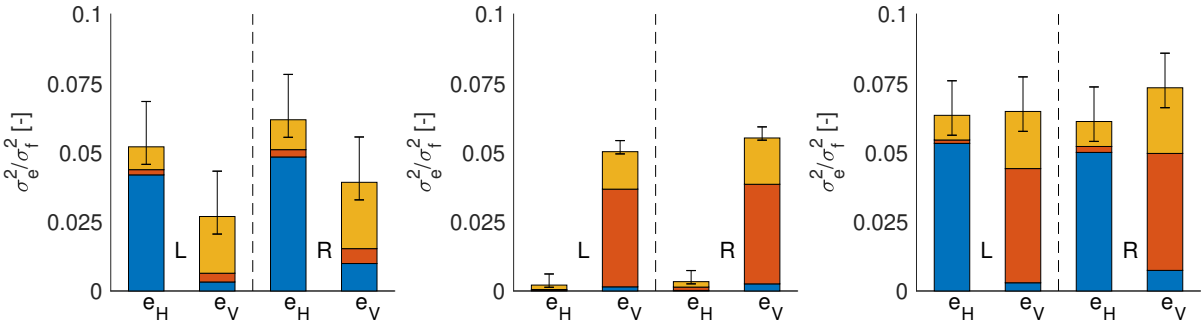

(a) 1D-H condition. (b) 1D-V condition. (c) 2D condition.

Figure I.15: Subject 17

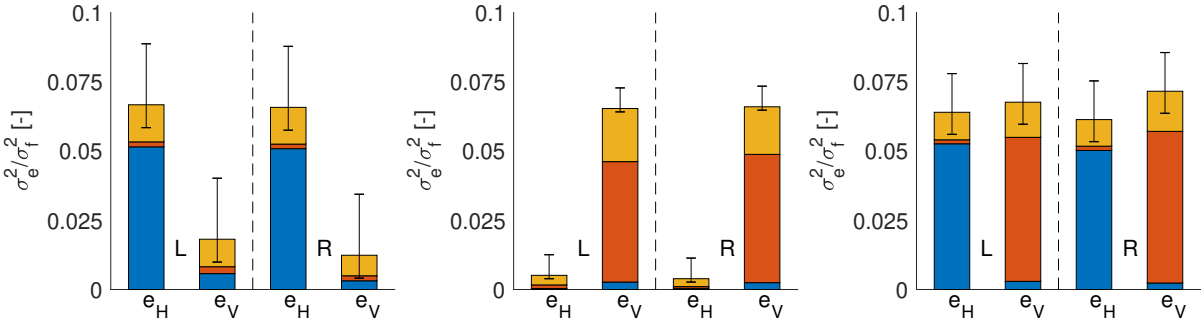

(a) 1D-H condition. (b) 1D-V condition. (c) 2D condition.

Figure I.16: Subject 18

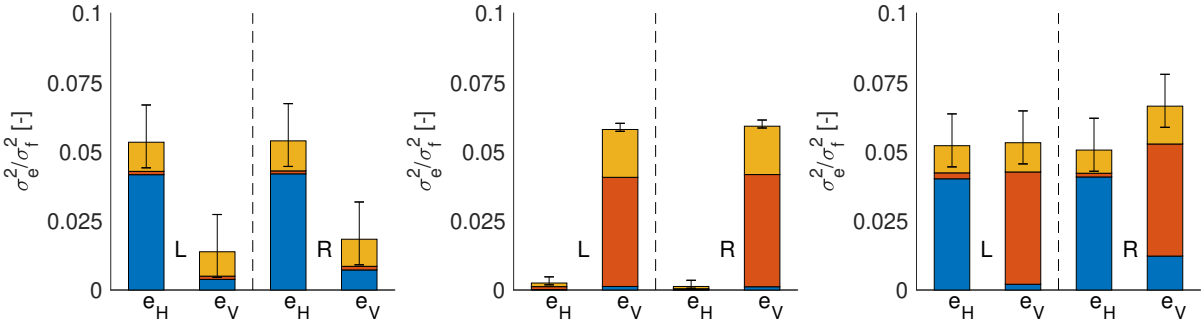

(a) 1D-H condition. (b) 1D-V condition. (c) 2D condition.

Figure I.17: Subject 19

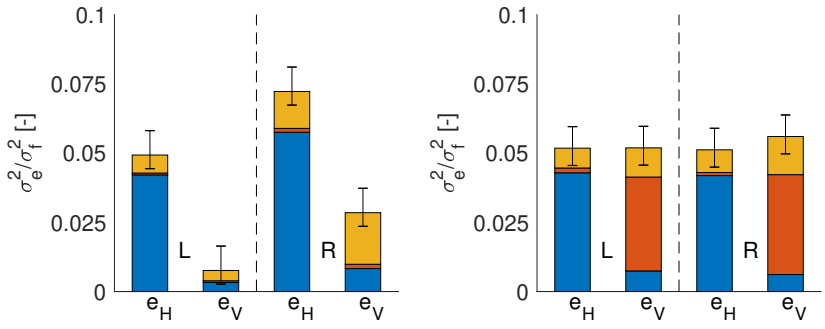

(a) 1D-V condition. (b) 2D condition.

Figure I.18: Subject 20

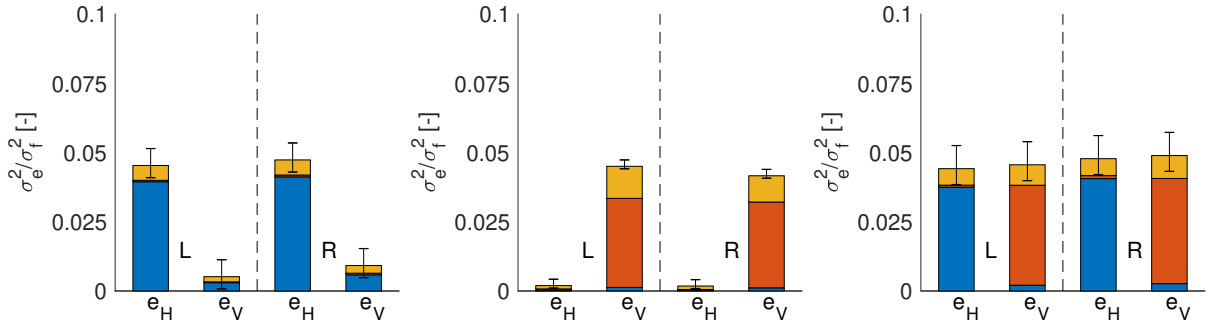

(a) 1D-H condition. (b) 1D-V condition. (c) 2D condition.

Figure I.19: Subject 21

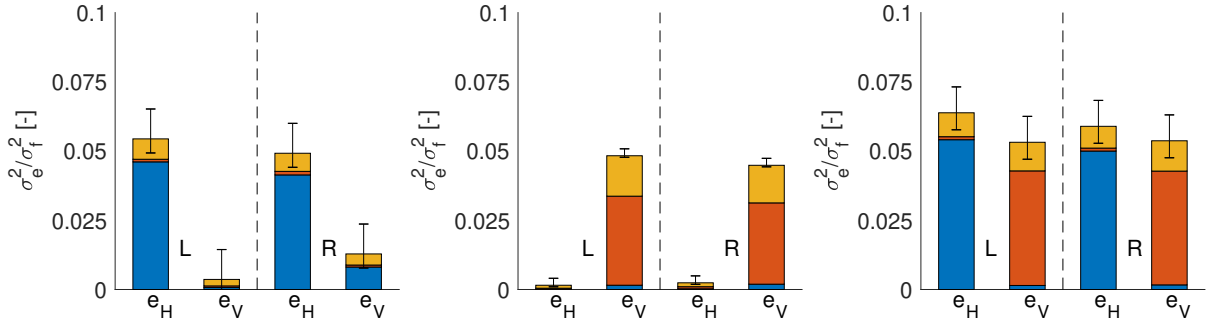

(a) 1D-H condition. (b) 1D-V condition. (c) 2D condition.

Figure I.20: Subject 22

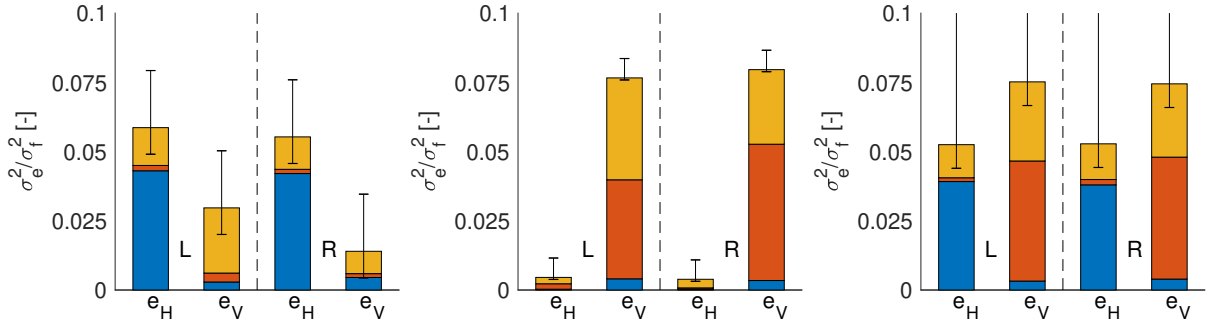

(a) 1D-H condition. (b) 1D-V condition. (c) 2D condition.

Figure I.21: Subject 23

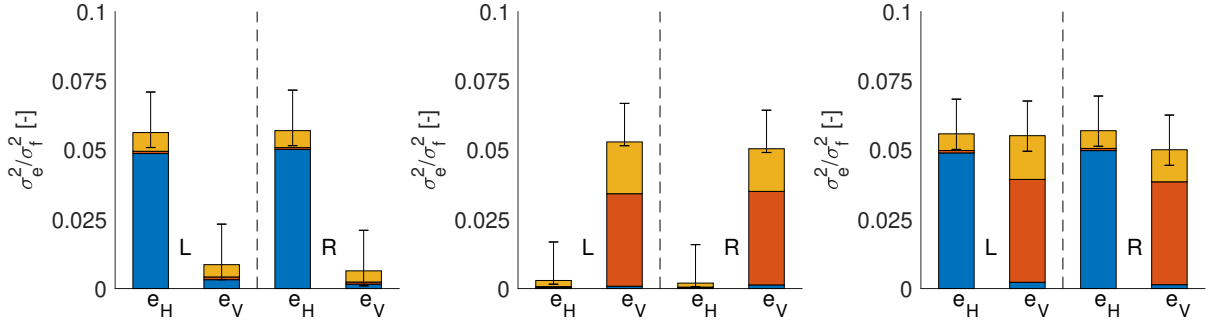

(a) 1D-H condition. (b) 1D-V condition. (c) 2D condition.

Figure I.22: Subject 24

Bibliography

1&1 IONOS Products (2017), 'What is parallax scrolling?', [online] Available at https://www.ionos.com/digitalguide/websites/web-design/parallax-websites-scrolling-with-3d-effect/. [Accessed on 18 June 2019].

Barendswaard, S., Pool, D. M. & Mulder, M. (2016), 'Human crossfeed in dual-axis manual control with motion feedback.', *IFAC-PapersOnLine* **49**(19). 13th IFAC Symposium on Analysis, Design, and Evaluation of Human-Machine Systems.

Bargary, G., Bosten, J. M., Goodbourn, P. T., Lawrance-Owen, A. J. & Mollon, J. D. (2017), 'Individual differences in human eye movements: An oculomotor signature?', *Vision Research* **141**, pp. 157 – 169.

Barnes, G., Grealy, M. & Collins, S. (1997), 'Volitional control of anticipatory ocular smooth pursuit after viewing, but not pursuing, a moving target: evidence for a re-afferent velocity store', *Experimental Brain Research* **116**(3), pp. 445–455.

Barrett, R. (2016), 'Importance and relevance of eye dominance', [online] Available at https://www.aop.org.uk/ot/cet/2016/06/20/the-importance-and-relevance-of-eye-dominance-part-1/article. [Accessed on 10 April 2019].

Bishop, C. M. (2006), *Pattern Recognition and Machine Learning*, Springer Science + Business Media, LLC, 233 Spring Street, New York, NY 10013, USA.

Blehm, C., Vishnu, S., Khattak, A., Mitra, S. & Yee, R. W. (2005), 'Computer vision syndrome: A review', *Survey of Opthalmology* **50**, pp. 253 – 262.

Büskens, J. (2018), Quantifying ageing effect on gaze dynamics, Master's thesis, Technical University of Delft.

Büskens, J., Pel, J. J. M. & Pool, D. M. (2019), Effects of multisine signal bandwidth on eye movement dynamics, *in* 'In Proceedings of the 14th IFAC/IFIP/IFORS/IEA Symposium on Analysis, Design, and Evaluation of Human-Machine Systems, Tallinn, Estonia'.

Castillo, X., Castro-Obregón, S., Gutiérrez-Becker, B., Gutiérrez-Ospina, G., Karalis, N., Khalil, A. A., Lopez-Noguerola, J. S., Lozano Rodríguez, L., Martínez-Martínez, E., Perez-Cruz, C., Pérez-Velázquez, J., Pinã, A. L., Rubio, K., Salazar García, H. P., Syeda, T., Vanoye-Carlo, A., Villringer, A., Winek, K. & Zille, M. (2019), 'Re-thinking the etiological framework of neurodegeneration', *Frontiers in Neuroscience* .

Chronos Vision (2017), 'Scleral search coils 2d/3d', [online] Available at http://www.chronos-vision.de/downloads/CV_Product_SSC.pdf. [Accessed on 20 June 2019].

Colagiogio, P., Colnaghi, S., Versino, M. & Ramat, S. (2013), 'A new tool for investigating the functional testing of the vor', *Frontiers in Neurology* **4**(165).

Dai, W., Selesnick, I., Rizzo, J., Rucker, J. & Hudson, T. (2017), 'A nonlinear generalization of the savitzky-golay filter and the quantitative analysis of saccades', *Journal of Vision* **17**(9).

De Boer, C. (2015), Visuomotor integration in neurodegenerative brains, PhD thesis, Graduate School Neurosciences Amsterdam Rotterdam (ONWAR).

De Vries, R. J. (2016), A tracking task for quantifying loss of motor skills due to parkinson's disease, Master's thesis, Technical University of Delft.

Duchowski, A. T. (2017), *Eye Tracking Methodology; Theory and Practice*, 3rd edn, Springer International Publishing AG, Gewerbestrasse 11, 6330 Cham, Switzerland.

Enderle, J. D. (2002), 'Neural control of saccades', *Progress in Brain Research* **140**, pp. 21–49.

Enderle, J. D. & Zhou, W. (2010), *Models of Horizontal Eye Movements, Part II: A Third Order Linear Saccade Model*, Morgan & Claypool. DOI:10.2200/S00264ED1V01Y201003BME035.

Erkelens, C. J. (2006), 'Coordination of smooth pursuit and saccades', *Vision Research* **46**.

EyeSeeTec GmbH (2016), 'EyeSeeCam Sci User Manual'. Obtained from EyeSeeCam Sci software package.

EyeSeeTec GmbH (2017), 'EyeSeeCam Sci', Brochure.
URL: *https://www.eyeseetec.de/wp-content/uploads/2017/02/EyeSeeCamSci-Brochure.pdf*

Fukushima, K., Fukushima, J., Warabi, T. & Barnes, G. R. (2013), 'Cognitive processes involved in smooth pursuit eye movements: behavioral evidence, neural substrate and clinical correlation', *Frontiers in Systems Neuroscience* **7**(4), pp. 1–28.

Goodman, T. M., Bergen, T., Blattner, P., Ohno, Y., Schanda, J. & Uchida, T. (2016), 'The use of terms and units in photometry -– implementation of the CIE system for mesopic photometry'.

Haartsen, Y. (2017), Quantifying loss of motor skills after cerebellar stroke, Master's thesis, Technical University of Delft.

Harting, J. K. & Updyke, B. V. (2006), 'Oculomotor-related pathways of the basal ganglia', *Progress in Brain Research* **151**, pp. 441–460.

Hess, R. A. (1981), 'Pursuit tracking and higher levels of skill development in the human pilot', *IEEE Transactions on Systems, Man, and Cybernetics* **SMC-11**(4), pp. 262–273.

Hunt, R. W. G. (2004), *The Reproduction of Colour*, 6th edn, John Wiley & Sons, Chichester, West Sussex, England.

Kandel, E. R., Schwarts, J. H. & Jessell, T. M. (2000), *Principles of Neural Science*, 4th edn, McGraw-Hill Companies.

Katsanis, J., Iacono, W. G. & Harris, M. (1998), 'Development of oculomotor functioning in preadolescence, adolescence, and adulthood', *Psychophysiology* **35**(1), pp. 64–72.

Komogortsev, O. V. & Karpov, A. (2013), 'Automated classification and scoring of smooth pursuit eye movements in the presence of fixations and saccades', *Behavior Research Methods* **43**, pp. 203–215.

Krauzlis, R. J. (2005), 'The control of voluntary eye movements: New perspectives', *The Neuroscientist* **11**(2), pp. 124 – 137.

Krauzlis, R. J., Goffart, L. & Hafed, Z. M. (2016), 'Neural control of fixation and fixational eye movements', *Phil. Trans. R. Soc. B* **372**. http://dx.doi.org/10.1098/rstb.2016.0205.

Leigh, R. J. & Zee, D. S. (2006), *The Neurology of Eye Movements*, 4th edn, Oxford University Press.

Levison, W. H., Baron, S. & Kleinman, D. L. (1969), 'A model for human controller remnant', *IEEE Transactions on Man-Machine Systems* **MMS-10**(4), pp. 101 – 108.

McCamy, M. B., Jazi, A. N., Otero-Millan, J., Macknik, S. L. & Martinez-Conde, S. (2013), 'The effects of fixation target size and luminance on microsaccades and square-wave jerks'. DOI: 10.7717/peerj.9.

McRuer, D. T., Graham, D., Krendel, E. & Reisener, W. (1965), Human pilot dynamics in compensatory systems; theory, models, and experiments with controlled element and forcing function variations, Technical report, Systems Technology, Inc.; The Franklin Institute.

McRuer, D. T. & Jex, H. R. (1967), 'A review of quasi-linear pilot models', *IEEE Transactions on human factors in electronics* **8**(3), pp. 231–249.

Metz, L. D. (1982), 'A time-varying approach to the modeling of human control dynamics', *IEEE Transactions on Systems, Man, and Cybernetics* **SMC-12**(1), pp. 24 – 35.

Mind Media (2019), 'Eog', [online] Available at `https://www.mindmedia.com/en/solutions/research/eog/`. [Accessed on 20 June 2019].

Missal, M. & Heinen, S. J. (2017), 'Stopping smooth pursuit', *Philosophical Transactions of the Royal Society B* **372**. http://dx.doi.org/10.1098/rstb.2016.0200.

Mulder, M., Pool, D. M., Abbink, D. A., Boer, E. R., Zaal, P. M., Drop, F. M., van der El, K. & van Paassen, M. M. (2017), 'Manual control cybernatics: Start-of-the-art and current trends', *IEEE Transacations on Human-Machine Systems* **48**(5), pp. 1–12.

Munoz, D. P. (2002), 'Commentary: Saccadic eye movements: overview of neural circuitry', *Progress in Brain Research* **140**, pp. 89–96.

Munoz, D. P. & Fecteau, J. H. (2002), 'Vying for dominance: dynamic interactions control visual fixation and saccadic initiation in the superior colliculus', *Progress in Brain Research* **140**, pp. 3–19.

Przedborski, S., Vila, M. & Jackson-Lewis, V. (2003), 'Neurodegeneration: What is it and where are we?', *Journal of Clinical Investigation* **111**.

Purves, D., Augustine, G. J., Fitzpatrick, D., Hall, W. C., LaMantia, A., McNamara, J. O. & Williams, S. M. (2004), *Neuroscience*, 3rd edn, Sinauer Associates, Inc.

Remington, L. A. (2012), *Clinical Anatomy and Physiology of the Visual System*, 3rd edn, Butterworth-Heinemann. Chapter 12.

Richardson, D. C. & Spivey, M. J. (2008), 'Eye-tracking: Characteristics and methods'.

Sammaknejad, N., Pouretemad, H., Eslahchi, C., Salahirad, A. & Alinejad, A. (2017), 'Gender classification based on eye movements: A processing effect during passive face viewing', *Adv Cogn Psychol* **13**(3).

Schneor, E. & Hochstein, S. (2005), 'Effects of eye dominance in visual perception', *International Congress Series 1282* pp. pp. 719–723.

Sharpe, L. T., Stockman, A., Jagla, W. & Jägle, H. (2005), 'A luminous efficiency function, v*(λ), for daylight adaptation', *Journal of Vision* **5**, pp. 948–968.

Squire, L., Berg, D., Bloom, F., du Lac, S., Ghosh, A. & Spitzer, N. (2008), *Fundamental Neuroscience*, 3rd edn, Academic Press.

Steinman, R. M. (1965), 'Effect of target size, luminance, and color on monocular fixation*', *Journal of the Optical Society of America* **55**(9), pp. 1158–1165.

Thaler, L., Schütz, A. C., Goodale, M. A. & Gegenfurthner, K. R. (2013), 'What is the best fixation target? the effect of target shape on stability of fixational eye movements', *Vision Research* **76**, pp. 31–42.

The National Eye Institute (2015*a*), 'Facts about cataract', [online] Available at `https://nei.nih.gov/health/cataract/cataract_facts`. [Accessed on 9 April 2019].

The National Eye Institute (2015*b*), 'Facts about color blindness', [online] Available at `https://nei.nih.gov/health/color_blindness/facts_about`. [Accessed on 9 April 2019].

Theodoridis, S. & Koutroumbas, K. (2006), *Pattern Recognition*, 3rd edn, Elsevier Inc. https://doi.org/10.1016/B978-0-12-369531-4.X5000-8.

Tobii AB (2019), 'Tobii pro x3-120', [online] Available at `https://www.tobiipro.com/product-listing/tobii-pro-x3-120/`. [Accessed on 22 May 2019].

Van der El, K. (2018), How humans use preview information in manual control, PhD thesis, Delft University of Technology.

Versteeg, R. (2019), 'Classifying human control behaviour by artificial intelligence'. Preliminary master's thesis, Technical University of Delft.

Voogd, J. & Barmack, N. H. (2006), 'Oculomotor cerebellum', *Progress in Brain Research* **151**, pp. 231–268.

Vos, J. J. (1979), 'Colorimetric and photometric properties of a 2deg fundamental observer', *Color Research & Application* **3**(3), pp. 125–128.

Welch, G. & Bishop, G. (2004), An introduction to the kalman filter, Technical report, Department of Computer Science, University of North Carolina at Chapel Hill.

Young, L. R. & Sheena, D. (1975), 'Survey of eye movement recording methods', *Behavior Research Methods & Instruments* **7**(5), pp. 397–429.

Zaal, P. M. T., Pool, D. M., de Bruin, J., Mulder, M. & van Paassen, M. M. (2009), 'Use of pitch and heave motion cues in a pitch control task', *Journal of Guidance, Control and Dynamics* **32**(2), pp. 366–377.

Zambarbieri, D. (2002), 'The latency of saccades toward auditory targets in humans', *Progress in Brain Research* **140**, pp. 51–59.